

## Combustion and Combustors for MGT Applications

**R. Tuccillo and M.C. Cameretti**

Dipartimento di Ingegneria Meccanica per l'Energetica (D.I.M.E.)  
Università di Napoli "Federico II"  
via Claudio 21  
80125 Napoli  
ITALY

[tuccillo@unina.it](mailto:tuccillo@unina.it) / [mc.cameretti@unina.it](mailto:mc.cameretti@unina.it)

### **ABSTRACT**

*An introductory overview of the micro and small-scale devices for the combustion in micro-gas turbines is presented at the beginning of this paper in order to identify and select the main topics to be discussed in the following. The wide variety of combustion systems for this particular application, together with the different strategies and design concepts that are proposed for setting up efficient MGT combustors, suggests the opportunity of outlining the several levels of approach to the studies on this subject. Therefore, the paper proceeds with a general thermo-kinetic analysis of the combustion conditions which are expected for both different fuel supplies and variable MGT load levels. The successive step is the comparison of different combustor concepts for a small-scale turbine of the 100 kW range, and the CFD analysis gives indications on the behaviour of the several combustion systems. The same computational tool is finally employed for an exhaustive analysis of a lean-premixed combustor also when operated with low BTU fuels or under part-load conditions.*

### **1. FOREWORDS**

This lecture aims at a discussion of the main characteristics that the combustion chamber within a micro-gas turbine should present consistently with the requirements of a small-size energy conversion system. Many authors have been dealing in recent years with the problems related with both micro-combustion and micro-combustors and their studies, combined with the manufacturers' experience, contributed to the practical applications which can be already be found within actually operating systems.

Defining a commonly recognized "size scale" for the micro-combustors is not properly straightforward, since the examples which can be found in technical and scientific literature start from some demonstration devices on a real micro-scale, with power outputs of the order of magnitude of a few Watts, coming up to micro (or mini) gas turbines in the 10 – 300 kW range. The first cases are developed with the main purpose of demonstrating the possibility of rising up the power density of ultra-compact energy systems, while the second ones correspond to really employable MGT based plants addressed either to the single electric power generation or to the combined production of power and electricity. In these latter cases, the reliability of the combustion system is a fundamental requirement to be complied with, and different strategies can be followed by the manufacturers in order to set up efficient MGT combustors, say:

- Proceeding with a combustor design expressly accounting for the particular operating conditions of the MGT;
- Adapting, in some sense, the well consolidated experience in the field of combustion chambers for industrial gas turbines to this novel application.

The first procedure is of course the most challenging, although the most appropriate, one as it aims at the best fit of the combustor size with the dimensions of the whole system and it must overcome the major problems related with the micro-combustion development.

The second one may often consist either of the scaling of combustors for medium range gas turbines or, in some cases, of the adoption of a single tubular combustor instead of the multiple tubular chambers which often equip a higher output gas turbine. Also this strategy, although simpler than the previous one, must however deal with the relevant changes in combustor fluid-dynamics which take place under the MGT operating conditions.

The literature which is referred to at the end of this paper [1-73] offers a wide variety of examples on all the topics concerning the MGT combustion, so on both micro and mini scale devices and with the different strategies described above. Therefore, this lecture starts with an overview of the state of art of the studies in these fields, so exploring the typical configuration of gas turbine combustors and their modifications to the MGT case as well. The same overview includes the description of the typical operating conditions occurring for the MGT combustors.

The paper proceeds with the authors' contribution to the studies of combustor and combustion for this particular application, so dealing with some topics like:

- The employment of both conventional fuels and of those derived from the gasification of bio-masse or solid wastes;
- The definition of the typical operating conditions for the MGT combustor, also under variable electrical or thermal load;
- The preliminary prediction, on a thermo-kinetic basis, of the dependence of the nitric oxide production on the residence time and operating conditions;
- The comparison of combustors originating from different design concepts;
- A number of CFD based applications addressed to the combustor analysis under the several point of view listed above.

The general purpose of the paper being an overview of the different possible approaches to the MGT combustion, the final objective, rather than a definite solution, is the assessment of the several problems which are presently left open for a complete compliance of the combustion chamber features with the micro-combustion requirements.

## **2. STATE OF THE ART**

### **2.1 Overview of Gas Turbine Combustor Configurations**

The proliferation of micro devices creates a strong demand for small-scale power sources. These power sources commonly convert chemical energy stored in fuels into electrical and mechanical power by combustion in sub-centimeter packages.

The problems connected to combustion and emissions are present in micro-gas turbines and in conventional gas turbines as well: an overview on combustion systems [26] is presented in the following in order to better understand which methods are used to comply with these problems, also considering those due in particular to the microscale combustion.

The basic objective is always that of achieving an easy ignition, a wide ignition range, high combustion efficiency and minimum soot and polluting gas formation. Since some of these requirements may conflict,

the end result is inevitably a compromise solution. As it is well known, for example, the formation trends of smoke and nitric oxides are directly opposite to those of carbon monoxide and unburned hydrocarbons.

Many strategies have to be considered in order to meet the emission regulation requirements, including exhaust after-treatment (i.e. SCR) and newer combustion processes (e.g. catalytic combustion and, surface stabilized combustion). The newer combustion strategies aim at reducing reaction temperatures in an effort to minimize thermal NO<sub>x</sub>, but also lead to inherently low CO due to the relatively large residence times and minimal cooling air requirements.

A method is to use a somewhat **variable geometry** to adjust the amount of air entering the primary combustion zone: at high pressures, large quantities of air are employed to minimize soot and nitric oxide formation; at low pressures the primary airflow is partially introduced, raising the fuel/air ratio and reducing the emissions of CO and HC.

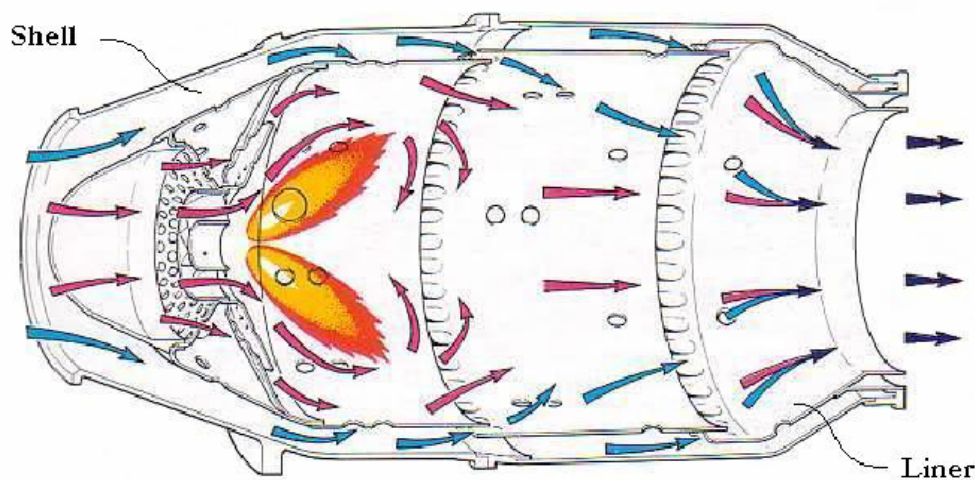


Figure 2.1: Typical Fuel and Air Flows in a Tubular, Diffusive Combustor.

Another approach is using combustion separated zones, each designed specifically to optimize the combustion performance with its own separate supply of well-mixed fuel and air. A typical “**staged**” combustor (fig. 2.2) has a lightly loaded primary zone, operating at an equivalence ratio around 0.8, to achieve high combustion efficiency and minimize the production of CO and HC. The primary zone provides all temperature rise needed at low power and acts as a pilot source of heat for the main combustion zone downstream, which is supplied with a premixed fuel-air mixture. At full-load operation, both zones would be supplied with fuel with a low equivalence ratio (0.6) to minimize the NO and smoke emissions. Therefore, fuel and air must be staged for effective emissions reduction to obtain a primary zone temperature as in fig. 2.3 to meet the limits of permissible temperature range for reducing all four pollutants simultaneously (i.e., NO<sub>x</sub>, CO, HC, smoke) (fig. 2.4). With a staged combustion it is necessary to optimize the fuel distribution while with variable geometry the air distribution is highlighted.

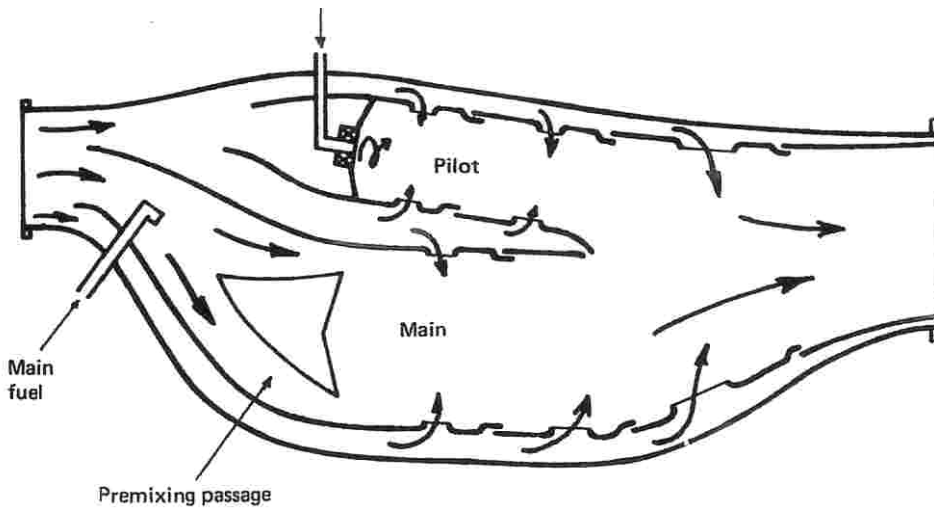


Figure 2.2: Two Staged Annular Combustor (from ref. [26]).

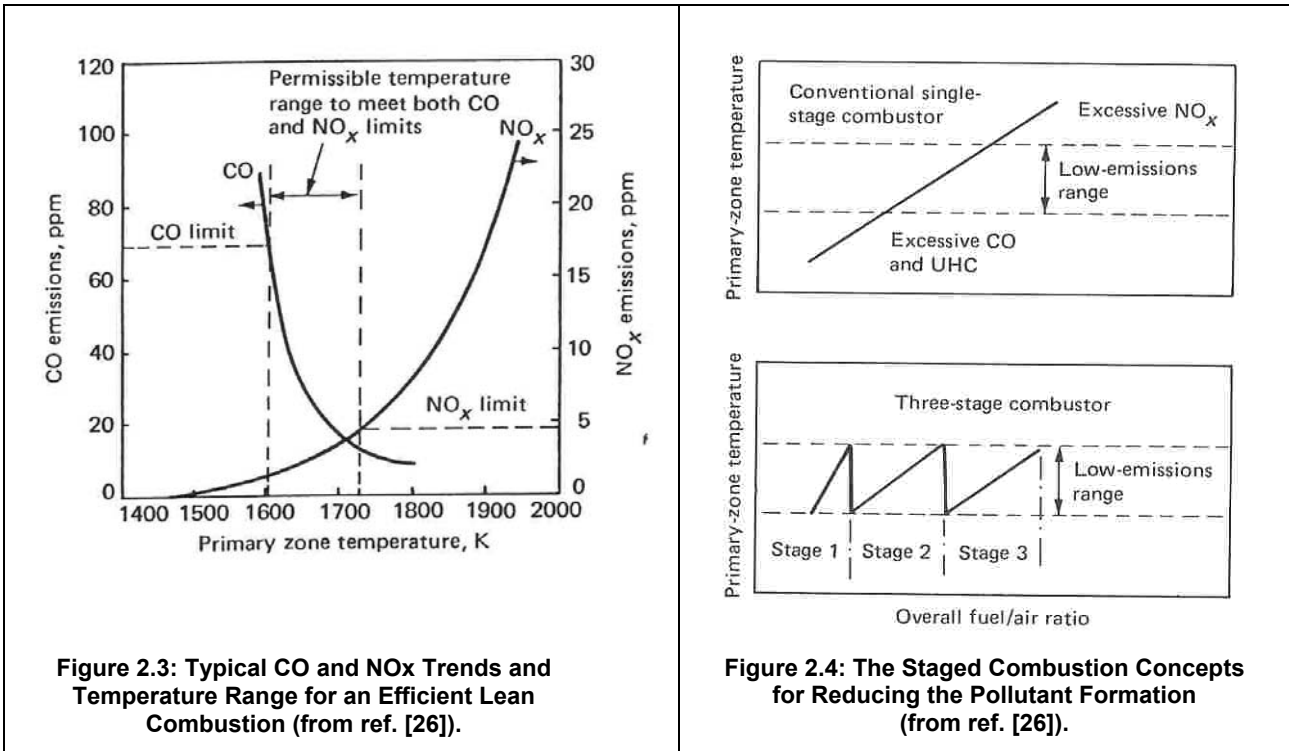


Figure 2.3: Typical CO and NOx Trends and Temperature Range for an Efficient Lean Combustion (from ref. [26]).

Figure 2.4: The Staged Combustion Concepts for Reducing the Pollutant Formation (from ref. [26]).

The **catalytic combustor** is another important concept to have low NO emissions. In this system the fuel is prevaporized and premixed with air at a very low equivalence ratio and then the mixture is passed through a catalytic reactor bed. The result is a very lean mixture combustion that normally is outside the limits of flammability. Of consequence, the temperature is very low with low formation of NOx.

In addition, also the engine size is considered in combustor design: in small engine with high shaft speed, the combustor is usually short of **annular reverse-flow** type (fig. 2.5). This combustor has the characteristic that the first two film-cooling slots in the liner dome discharge air in upstream direction. The main advantages are high efficient utilization of the combustion volume and easy maintenance. In general, different concepts and philosophies of novel combustors for small engine are developed by industry in

the area of low-emissions combustor design (*vortex* combustor, staged-premix combustor, prechamber combustor).

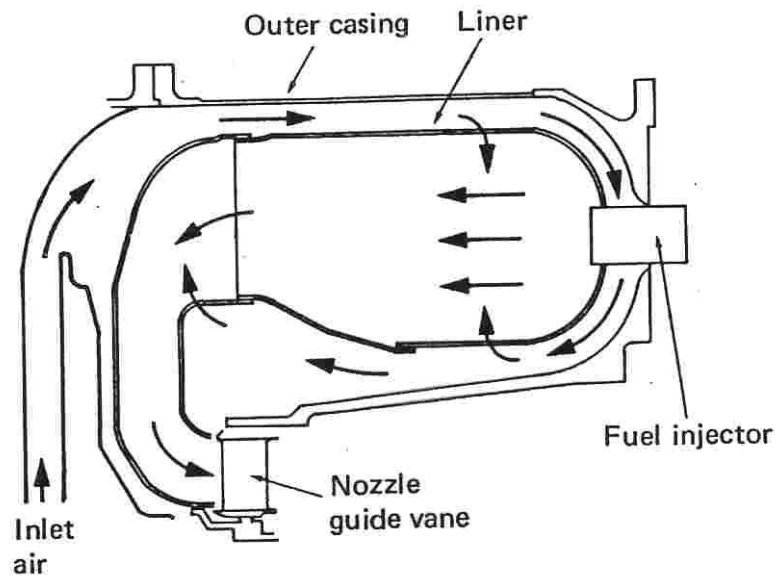


Figure 2.5: A Reverse-Flow Combustor for Small Engines (from ref. [26]).

In a **Lean Premixed-Prevaporized (LPP)** combustor the fuel has a complete evaporation (if liquid) and a mixing with air before combustion. The primary zone operates at a lean fuel/air ratio with low reaction temperature and elimination of hot spots, reducing NO<sub>x</sub> emissions. To be fully effective the LPP system should operate in conjunction with variable geometry to avoid the weak-extinction limit case. Sometimes it is necessary a piloting device to facilitate ignition and sustain combustion at difficult operating conditions. Moreover, an autoignition or flashback at the high inlet temperatures could occur before combustion zone. Figure 2.6 recalls the typical LPP combustion concept, but it should be reminded that the lean-premixed solution is nowadays usual also for gas-fuelled combustors of the *DLN* type. The flame temperature reduction may result in an inefficient combustion at part load conditions so that a pilot-assisted combustion is needed at reduced load operation (fig. 2.7).

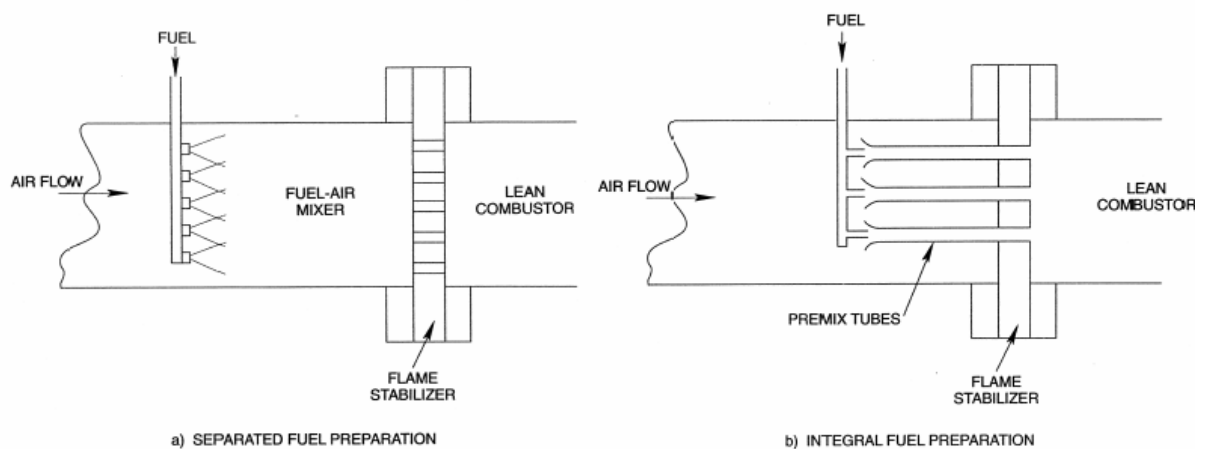


Figure 2.6: The LPP Combustor Concept (from ref. [67]).

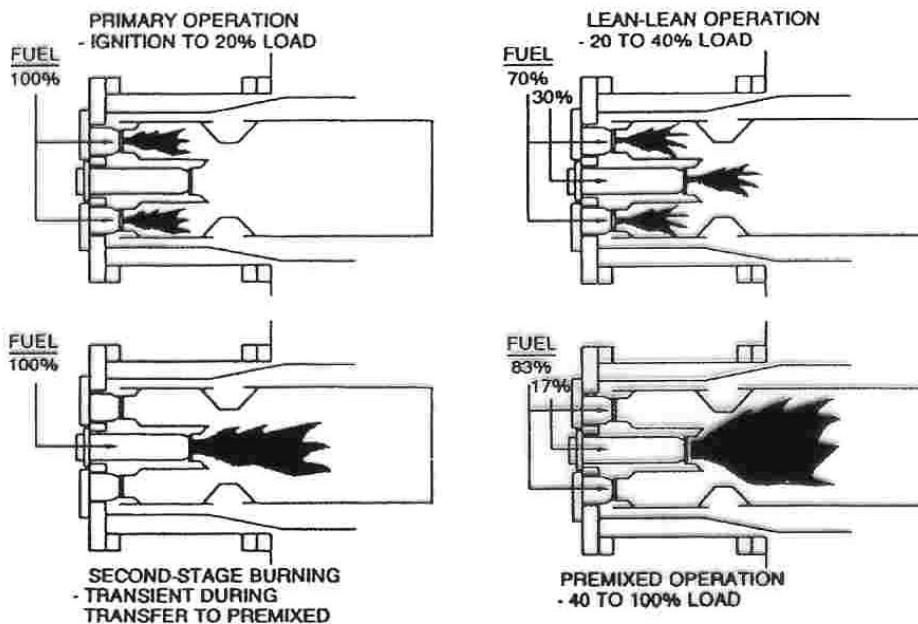


Figure 2.7: Transient Operation of a DLN (Dry-Low-NO<sub>x</sub>) Premixed Combustor (from ref. [26]).

The practice to design primary zones for a *lean mixture* (with addition of air) is addressed to reduce the flame temperatures and decrease the NO<sub>x</sub> production. In this way, an increase of CO and HC emissions is induced. On the other hand, also the excess fuel, as well as excess air, produces low flame temperatures avoiding ‘hot spots’ and moreover simultaneously low oxygen availability to reduce NO<sub>x</sub> formation. By using the latter approach, several low-NO<sub>x</sub> combustors have been developed. The problem is searching to shift from fuel-rich to fuel-lean products for correct turbine inlet conditions. In this transfer rate, the limitation is to create the sufficient long time for the oxidation of CO and HC species. The **RQL** (Rich burn- quick mix-lean burn) combustor (figs. 2.8 and 2.9) is really based on the technique of burning the fuel far above the stoichiometric conditions in a first stage of the combustor (*rich zone*), in order to avoid the production of thermal NO<sub>x</sub>, following the criteria described above. The CO and unburned hydrocarbons generated in the rich zone will be oxidized at low temperatures in the lean zone. The transition from “fuel-rich” to “fuel-lean” combustion is obtained through the introduction of air jets which dilute the mixture in the second region (*quick mix* or *quench zone*). In this way, the combustor operation is strongly influenced by the effectiveness of the dilution jet penetration at the quench stage and it is necessary to optimize the mixing pattern downstream of this zone by an optimized design.

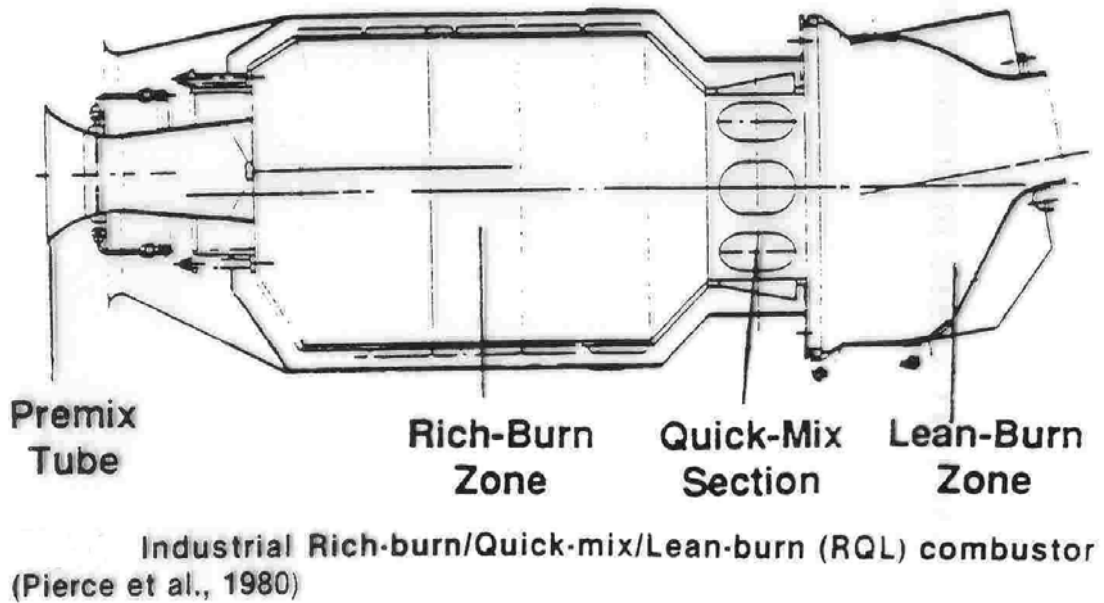


Figure 2.8: Layout of a RQL Combustor (from ref. [26]).

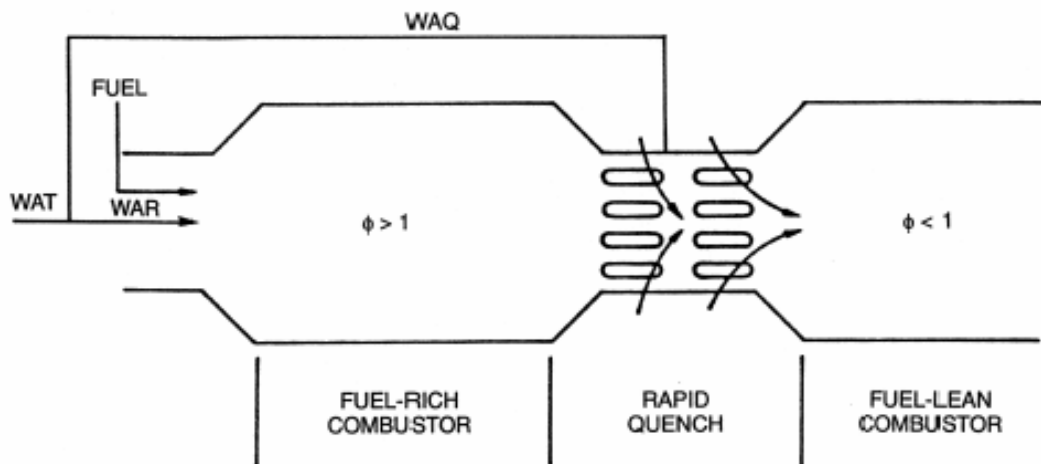


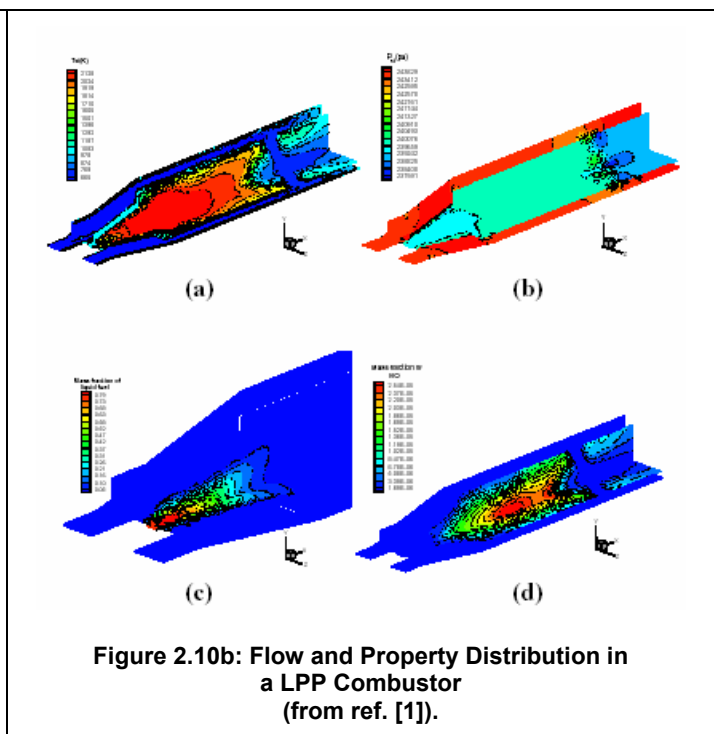
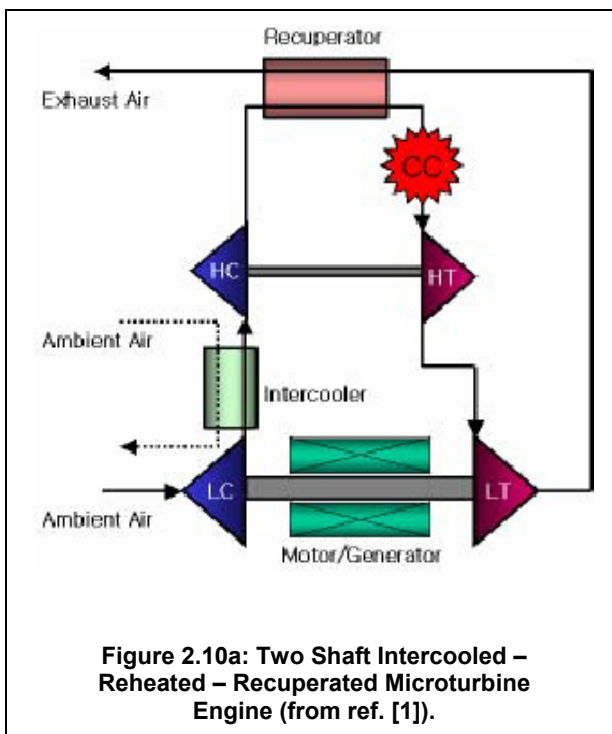
Figure 2.9: Air and Fuel Distribution in a RQL Combustor (from ref. [67]).

## 2.2 Specific Studies on MGT Combustors

Many authors have been dealing, in recent years, with the combustor concept and fluid-dynamics in micro gas turbines. The studies that can be found in technical literature are oriented to the solution of typical problems related with the MGT operation, like the pollutant reduction, the employment of different fuels, the combustion efficiency under the typical conditions imposed by the thermal cycle.

Jeong Jung Yoon and HeonSeok Lee [1] have studied a microturbine lean burn premixed combustion technology to reduce NO<sub>x</sub> emissions. They performed the study under different conditions of high temperature and high pressure with equivalent ratios between 0.10 and 0.16 in the lean region. They found a NO<sub>x</sub> increase traded-off by a CO reduction when inlet air temperature and pressure increase. An inverse

trend is found for NO<sub>x</sub> and CO production when increasing the mass flow of inlet air. Through a numerical approach with an appropriate combustion model, a complicated swirling flow pattern was predicted, and numerical values of NO<sub>x</sub> and CO emission were calculated and compared with experiments. As air to fuel ratio decreased from designed equivalence ratio, red flame increased. The flame had stable structures up to the design equivalence ratio because of the strong swirl in premix chamber. Through a three dimensional flow analysis in the LPP combustor, it was possible to predict the characteristics of swirl in premix chamber, the recirculation position in primary zone, the role of dilution holes, and the existence of jet flow, etc. As a result of this study, NO<sub>x</sub> can be reduced up to less than 42ppm at 15% of oxygen when the 20kW class microturbine examined is operated at design condition. In the following figure 2.10b, the temperature, pressure profiles and NO<sub>x</sub> in the combustor are shown.



Satoshi Dodo and other authors [2] have studied a prototype machine for a next generation microturbine system applying a simple humid air turbine system with a low NO<sub>x</sub> combustor which employs a lean-lean zone combustion concept. Low NO<sub>x</sub> emission of 7.6 p.p.m. and high combustion efficiency of 95.6 % for the power conversion system were achieved at the part-load tests.

O. Ibrahim et al. [3] compared the predicted and measured performance of the microturbine system and discussed the change in NO<sub>x</sub> emissions resulting from overfiring the combustor when reducing the air preheating temperature in by-pass mode. The goal of this research was to quantify to which extent variable heat output is possible using an existing microturbine design and it was shown that the full benefit of variable heat output can only be gained with a modified combustor design. As an example a lean-lean staged combustor concept is proposed by the authors. A modified combustor concept is in fact necessary in order to take full advantage of the operational benefit of variable heat output while maintaining low emissions. In particular, a staged concept appears to be the most promising for this purpose (figure 2.11).

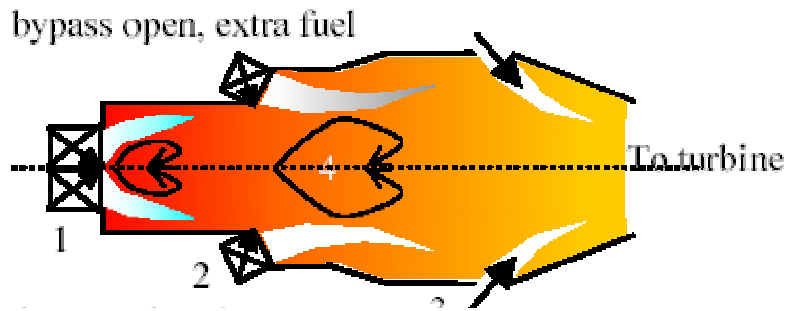


Figure 2.11: Concept of a Lean-Lean Staged Combustor (from ref. [3]).

Other authors in [4] have described a reduced NO<sub>x</sub> and CO, partially premixed flame combustor that has been developed for the 175 kW Advanced Integrated Microturbine System (AIMS) recuperated cycle gas micro-turbine (fig. 2.12a). The AIMS turbine is equipped with a recuperated silo combustor (fig. 2.12b). This new, reduced emissions combustor retains key features of the conventional Dry Low NO<sub>x</sub> (DLN) combustors. The authors [4] showed that with natural gas fuel, without water or steam injection, NO<sub>x</sub> and CO emissions from the new combustor are in the single-digit range at full-speed, full-load conditions. The CO emissions are strongly influenced by the pressure effect, so increasing at base load (when compared to similar conditions in commercial combustors running at higher pressures).

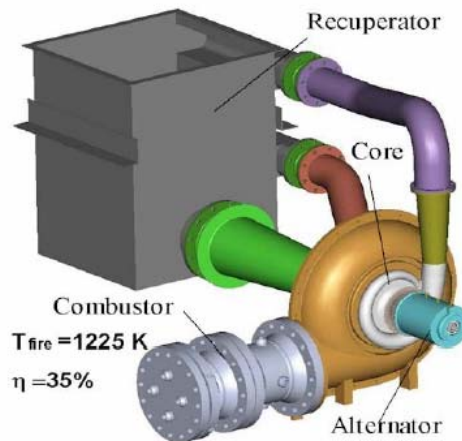


Figure 2.12a: The Advanced Integrated Microturbine System (from ref. [4]).

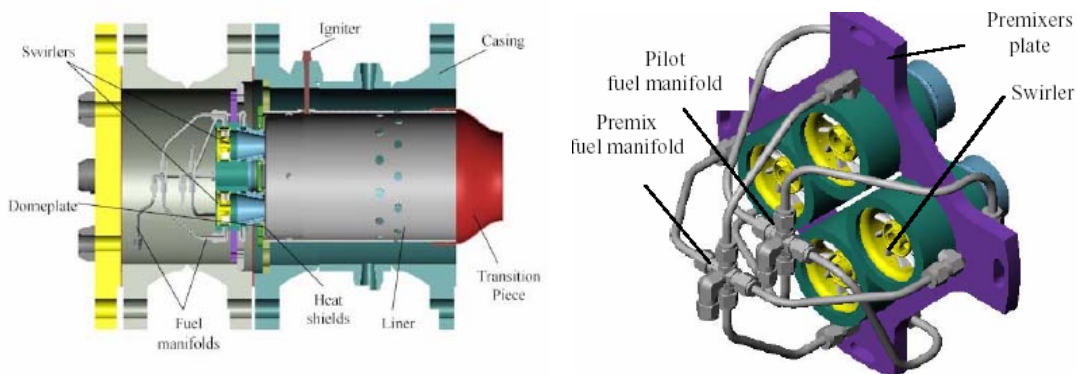
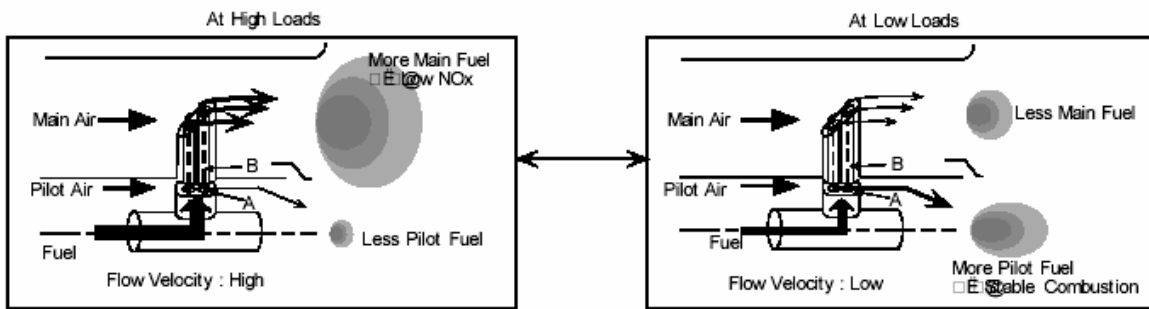


Figure 2.12b: The AIMS Turbine Combustor and the Fuel Nozzle Assembly (from ref. [4]).

Tsutomu Wakabayashi et al. [10] studied the performance of a dry low-NO<sub>x</sub> gas turbine combustor designed with a new fuel supply concept. This concept uses automatic fuel distribution achieved by an interaction between the fuel jet and the airflow. At high loads, most of the fuel is supplied to the lean premixed combustion region for low-NO<sub>x</sub>, while at low loads, it is supplied to the pilot combustion region for stable combustion. They used a numerical simulation to estimate the equivalence ratio in the fuel supply unit and measured NO<sub>x</sub> emissions through the pressurized combustion experiments on the combustor with this fuel supply unit using natural gas as fuel. The NO<sub>x</sub> were reduced and stable combustion was achieved over a wide equivalence ratio range. Two figures below (fig. 2.13) show the fuel supply scheme.



**Figure 2.13: Diagram of the Innovative Fuel Supply Concept (from ref. [10]).**

The same authors in ref. [5] described the combustion performance of a dry low-NO<sub>x</sub> gas turbine combustor designed with the innovative fuel supply concept using gaseous fuel (fig. 2.14). In any case, NO<sub>x</sub> emissions was not low enough at high loads, and combustion efficiency was not high at medium and low loads. Furthermore, the pressure loss of the combustor was high. Therefore, the prototype combustor was improved from the viewpoint of NO<sub>x</sub> emission, combustion efficiency and combustor pressure loss. In particular, they conducted two modifications: the first modification was to divide the main region into two parts in the radial direction by a cylindrical ring, and to provide fuel-distributing modules with different fuel distribution in each main region with a different gap; the second one was to provide an inward flow at the exit of the fuel supply unit. The combustion efficiency of the combustor with both modifications became higher, not adversely affecting NO<sub>x</sub> at high loads.

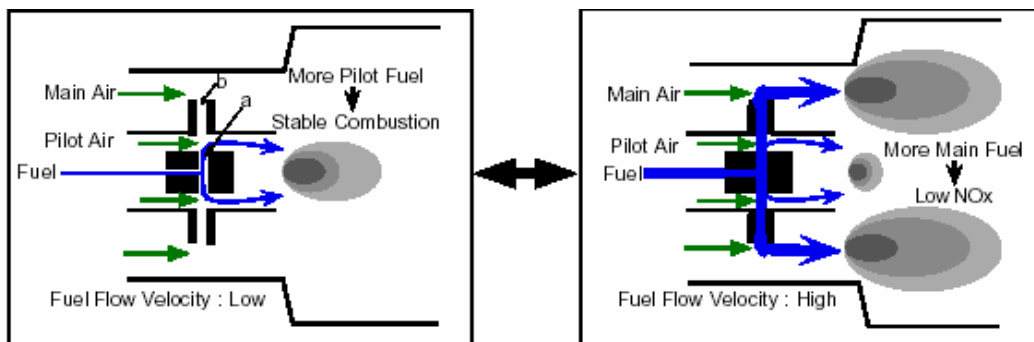


**Figure 2.14a: Diagram of the Innovative Fuel Supply Concept (from ref. [5]).**

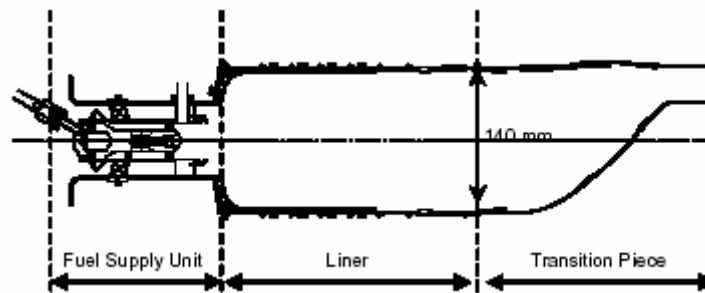


Figure 2.14b: Structure of the Combustor (from ref. [5]).

A newly designed micro gas turbine combustor for a 100-kWe, MGT based power plant is under development at the Ansaldo Ricerche facilities [6, 57]. The authors themselves are presently contributing to the analysis of this combustion chamber. The design starts from a single silo chamber shape with two fuel lines, and is associated with a radial swirler flame stabiliser (fig. 2.15). They adopted a lean premix technique to control both flame temperature and NO<sub>x</sub> production. Combustor design process is based on two major steps: the diagnostics-focussed design for methane only and experimentally validated design optimisation with suitable burner adaptation to non-standard fuels. In particular in [6], the authors focus on the first step of the combustor development and i.e., on the main design criteria for both burner and liner cooling system development. The design process control invoked both 2D and 3D CFD analysis by using two turbulence models,  $k-\epsilon$  and Reynolds Stress Model (RSM). It was possible to observe that the results of the standard  $k-\epsilon$  model turbulence model differ considerably from RSM results, especially when the central vortex and the penetration of the dilution flow jet are to be described. Of course, experimental testing should allow assessing the most suitable model for the CFD analysis of this type of MGT combustors.

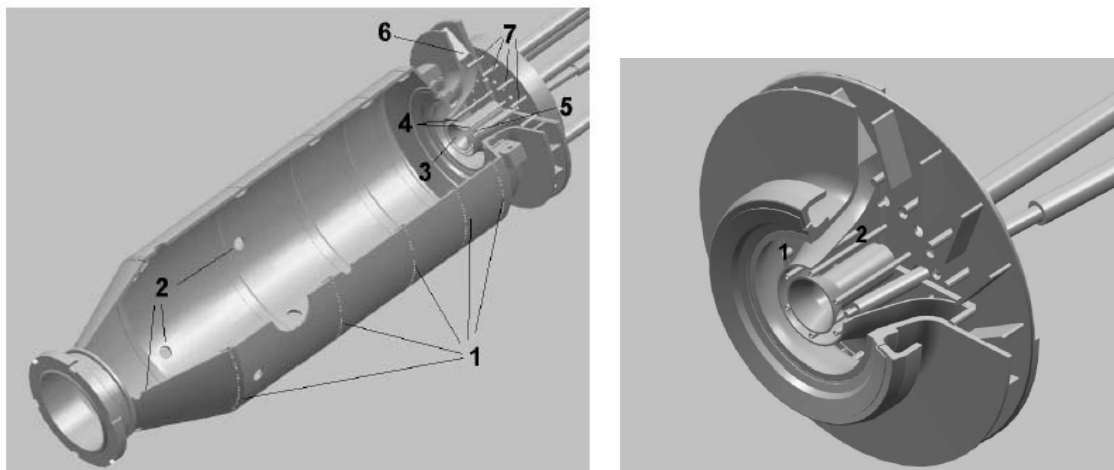
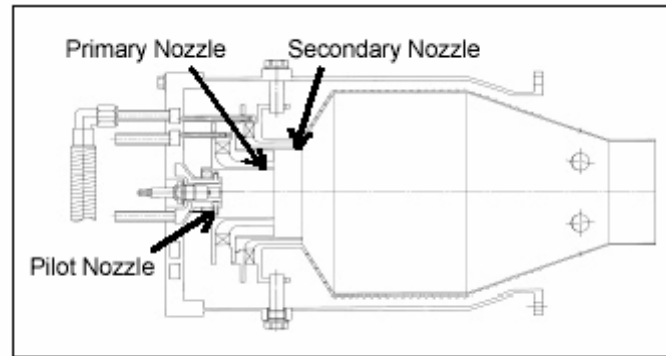


Figure 2.15: The ARI 100 Prototype Combustor and Details of the Inlet Channels (from ref. [6]).

Yoichiro Ohkubo et al. [7] developed a 300 kWe class gas turbine with two-shaft and simple-cycle to apply to cogeneration systems. The gas turbine engine is operated in the range of about 30% partial load to 100% load. The gas turbine combustor requires a wide range of stable operations and low NO<sub>x</sub> characteristics. A double staged lean premixed combustor (fig. 2.16), which has a primary combustion duct made of Si<sub>3</sub>N<sub>4</sub> ceramics, was developed to meet NO<sub>x</sub> regulations of less than 80 p.p.m. (corrected at 0% oxygen). The gas turbine with this combustor has demonstrated superior low-emission performance of nearly 40 p.p.m. of NO<sub>x</sub>, and more than 99.5% of combustion efficiency between 30% and 100% of

engine load. Many test cases have demonstrated stable high combustion performance varying the compressor inlet air temperature range between 5 C and 35 C. The output power decreases while increasing the compressor inlet air temperature, in order to keep a constant temperature at the turbine inlet. The NO<sub>x</sub> decreases when the temperature is more than 15 C and it increases in the temperature range of less than 15 C, when the output power was kept a constant maximum power. As a result, the NO<sub>x</sub> emission presents a peak value of 40 p.p.m. at 15 C.



**Figure 2.16: Pilot-Assisted, Double Staged Combustor (from ref. [7]).**

Also M.C. Mkpadi et al. [9] studied the turbine combustion to reduce the NO<sub>x</sub> formation: a two-stage lean/lean primary zone at simulated atmospheric pressure gas turbine combustion conditions was shown to give low NO<sub>x</sub> emissions at atmospheric pressure and 600K inlet temperature. All the combustion air was admitted to the first lean stage, where very lean <5ppm low NO<sub>x</sub> combustion occurred. A 40mm outlet diameter radial swirler with radial vane passage fuel injection was used in the first stage. After completion of this first stage lean combustion, second stage of fuel injection with no associated air occurred 320mm downstream of the primary swirler outlet, using 76mm radially inward wall injection. This was followed by a dump flow expansion to a 140mm diameter combustor. This provided an expansion shear layer and associated turbulence to mix the second stage fuel with the outlet products from the primary swirl combustion. The use of the second stage fuel was shown to reduce the NO<sub>x</sub> emissions by 50% compared with injecting all of the fuel into the first stage radial swirler. Emission levels of NO<sub>x</sub> at a first stage swirler equivalence ratio of 0.4 were below 5 p.p.m. and at an overall primary zone equivalence ratio of 0.8 with the two stage fuel injection, NO<sub>x</sub> emissions were about 20 p.p.m.. The second stage NO<sub>x</sub> formation was predicted using CFD with flamelet modelling. The mole fraction profile of NO<sub>x</sub> and combustion temperatures for a range of strain rates in the second stage were predicted. NO<sub>x</sub> emissions at 0.65 equivalence ratio overall was predicted to be 23 p.p.m. at 15% oxygen compared with 16 p.p.m. measured.

In ref. [11] a numerical and experimental study on a premixed DLE gas turbine combustor has been performed. Experiments and CFD modelling have been carried out at isothermal and combustor conditions. Modelling of the combustor has been performed using a CFD code by the authors of this paper. The combustion process has been modelled using a global reaction mechanism and a Flame Generated Manifold reaction mechanism with a presumed PDF model to incorporate the effect of turbulent fluctuations. The Flame Generated Manifold method uses a flame library. Finally, the authors have compared the numerical and experimental results observing some significant differences. The CFD model is able to predict the main features of the flow and combustion process, but does not predict the recirculation length accurately. Both combustion models, presented in the paper, are able to predict the low combustion efficiency measured at the 1atm test condition. As an example, a flow field and a temperature distribution are reported (fig. 2.17).

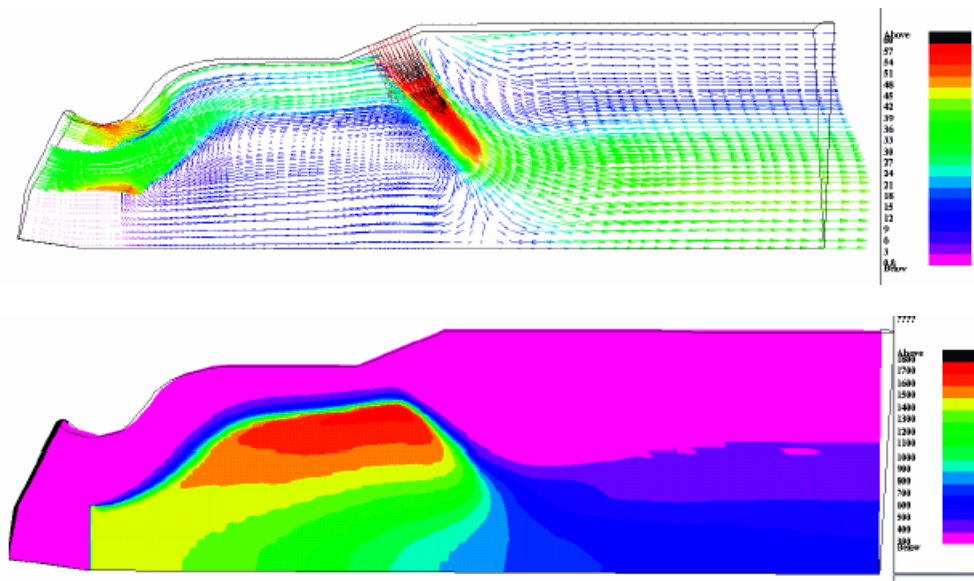


Figure 2.17: Flow Field and Temperature Distribution in a DLE Combustor (from ref. [11]).

Liedtke et al. [12] described the emission performance of a newly designed liquid fuelled micro gas turbine combustor (fig. 2.18). In order to reduce nitrogen oxides NO<sub>x</sub> lean premixed pre-vaporized combustion is utilized. Both, combustor inlet pressure and temperature are very low due to the thermodynamic cycle conditions chosen. As a consequence, the heat available for fuel spray evaporation is not sufficient. The present combustor concept therefore uses fuel film evaporation on the hot inner surface of a premix tube. To demonstrate the potential for reducing pollutant emissions overall NO<sub>x</sub> and CO concentrations of the exhaust gases have been measured and analyzed. The impact of the flame tube volume on pollutant emissions and combustion stability is considered at several operating conditions. Measured pollutant emissions indicate the great potential for pollutant reduction that is associated with the specific geometry of the combustor.

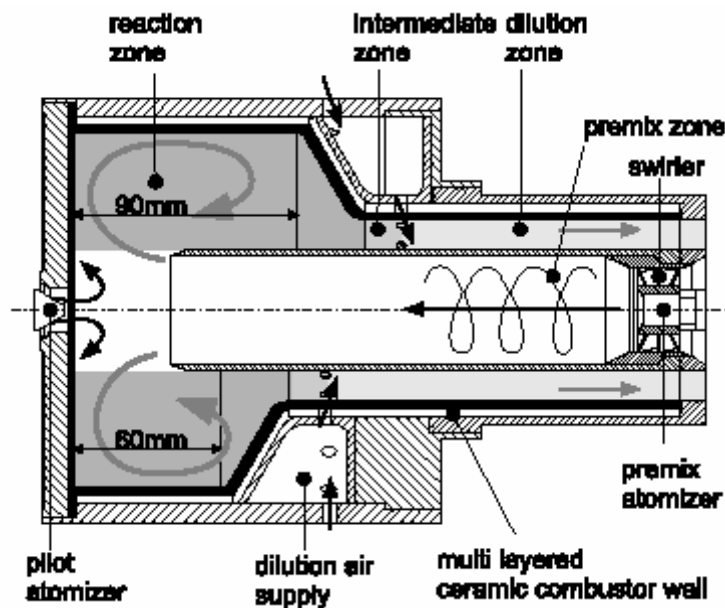
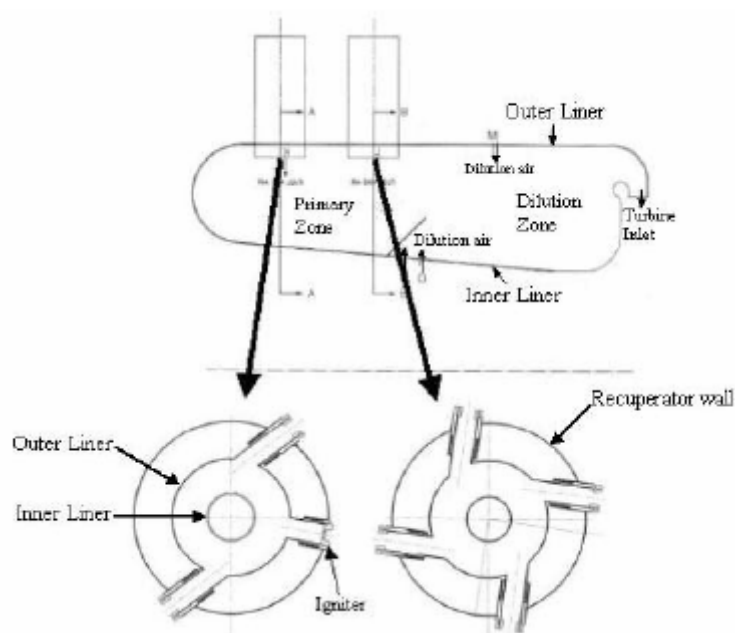


Figure 2.18: Configuration of the LPP Combustor in ref. [12].

Phi et al. [16] presented a microturbine generator which offer an attractive alternative for addressing future demand for electrical power. In the context of the stringent emission regulations, this study characterizes the exhaust emissions and mixing capability of a commercial micro-gas turbine and assesses the ability of this device to meet future emissions regulatory requirement and the extent to which mixing can be used to reduce emissions. The results obtained outline that, for this MGT, both NO<sub>x</sub> and CO are minimized for 80-100% load. The authors illustrated that NO<sub>x</sub> emissions are affected by the local equivalence ratios and that fuel staging and local quenching impact the CO emissions, by using kinetics and CFD analysis tools. A subsequent analysis using a well-stirred reactor approach has suggested that a maximum of a 10% reduction in NO<sub>x</sub> could be achieved with further improved premixing. The outline of the combustor of the 60 kW recuperated gas turbine, with cross sectional views of the fuel injection planes is shown in figure 2.19.



**Figure 2.19: Combustor Outline for a 60 kW MGT (from ref. [16]).**

Quang-Viet Nguyen [18] presents some experimental results on the correlating equivalence ratio fluctuations with combustion instabilities and NO<sub>x</sub> emissions in a jet-A fuelled lean premixed prevaporized (LPP) combustor. Real-time laser absorption measurements of equivalence ratio, together with dynamic combustor pressure, flame luminosity and fuel pressure were obtained at inlet air conditions up to 16.7 bar and 817 K. From this data, a database of real-time variables was obtained for the purposes of providing validation data for future studies of LPP combustion modelling. In addition, time and frequency space analysis of the data revealed measurable levels of acoustic coupling between all variables. Equivalence ratio and dynamic pressure cross-correlations were found to predict the level of combustion instability. The generic LPP injector used, although not optimized to have low emissions, provides some of the essential features of real injectors for the purposes of studying the relationship between fluctuations in equivalence ratios and combustion instability. In particular, the time for fuel premixing was found to have a significant and direct impact on the level of combustion instability. The results of this work support the delay concept for avoiding combustion instability when designing injector/premixers in LPP combustors.

Liedtke [19] described a new burner for a micro gas turbine utilizing the lean premixed prevaporized (LPP) combustion. This combustor design (fig. 2.20) utilizes ceramic materials for the flame tube. The objective of the new combustor concept is essentially to achieve low pollutant emissions, in particular

carbon monoxide (CO) and nitrogen oxide (NO<sub>x</sub>). The performance of the LPP concept strongly depends on the homogeneity of the air fuel mixture. Since the micro gas turbine uses liquid fuel, heat for the evaporation is required. Therefore, a homogeneous air fuel mixture is necessary for a lean combustion. To ensure complete fuel evaporation at the exit of the combustor premix tube both the droplet and the fuel film evaporation have to be investigated theoretically prior to the design process. Due to the thermodynamic cycle conditions (in the non-recuperated case) of the micro gas turbine, the combustion air temperature is too low for an intense evaporation of a liquid fuel droplet spray. The new combustor concept therefore, is based on fuel film evaporation on the hot inner surface of a premix tube. The heat required for fuel film evaporation is transferred from the hot combustion gases, flowing along the outer surface of the tube, through the tube wall. This combustor allows almost adiabatic combustion to be established. The design process of the combustor is assisted by comprehensive numerical studies of droplet and fuel film evaporation. The commercial CFD code “CFD-RC” has been utilized to investigate the isothermal flow of the combustor. The vortex flow of the burner, which provides for flame stabilization, is described in detail. Some preliminary experimental tests have been conducted. Measured pollutant concentrations of the exhaust gases meet international standards and demonstrate the great potential of the new combustor.

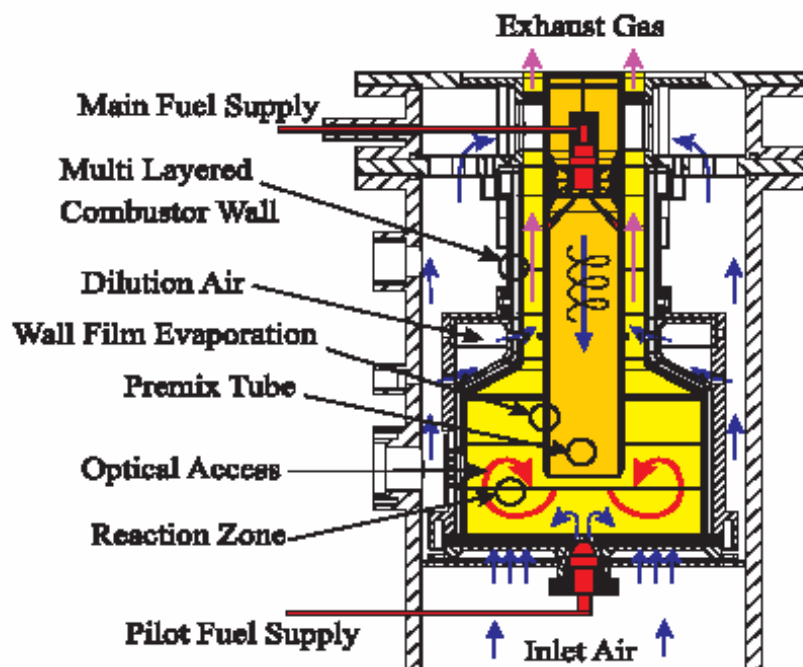


Figure 2.20: A New LPP Combustor for Micro-Gas Turbines (from ref. [19]).

In ref. [23] an aerodynamic study for the premixing device of an industrial turbine gas combustor is discussed. The work is based on a joint application of numerical CFD and experimental investigation tools in order to optimize the combustor gaseous fuel injection system (fig. 2.21). The objective is the retrofit of an old generation gas turbine combustion chamber that is carried out by both considering new targets of NO<sub>x</sub> emission and keeping the same CO emission and combustion stability. CFD has been used to compare different premixing duct configurations for improved mixing features. The use of CFD allowed a comparison of different configurations in terms of location of the holes for fuel injection and for the premixing duct geometry, in order to avoid dangerous recirculation zones. A satisfactory fuel-air mixing were pursued through improved modification of the premixing duct.

Experimental tests have been carried out in order to assess the pollutant emissions, flame stability and pattern factor characteristics of the full combustion chamber retrofitted with the modified injection system.

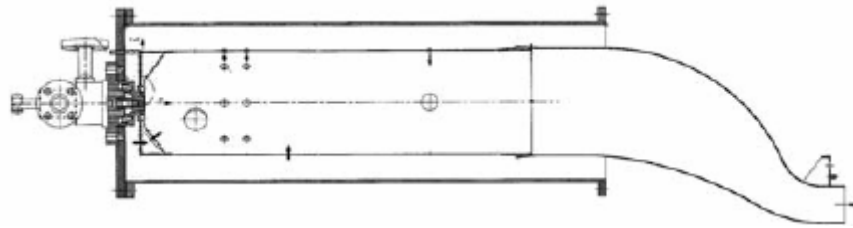


Figure 2.21: Reverse-Flow Combustion System (from ref. [23]).

The objective of the study in ref. [24] is to identify the flame structure as to establish the targets of low NO<sub>x</sub> emission, high stability and complete combustion for the micro gas turbine combustor (fig. 2.22). The concepts of the combustor are to use the circulation zone by swirl flow to ensure the flame stability and complete combustion and to induce lean premixed combustion by mixing fuel and air at the inlet of combustor to ensure low NO<sub>x</sub> emission and prevention of flashback. The micro gas turbine has been prevailing for the practical use but the flame features and its structure together with the combustor design have not been reported so far. The investigation of the flame construction and the flame characteristics related to the combustor design is needed to understand the optimum flame configuration and the ways for achieving it with respect to the combustor design. Town gas is used as the fuel. The experiments using three types of combustor design to investigate the characteristics of NO<sub>x</sub> and CO emission together with the investigation of the flame stability and visualization of the flame configuration. From the results obtained it is shown that a better premixing of the fuel and air minimize the NO<sub>x</sub> emission at 3 p.p.m. (at 0% O<sub>2</sub>) with sufficiently low CO emission.

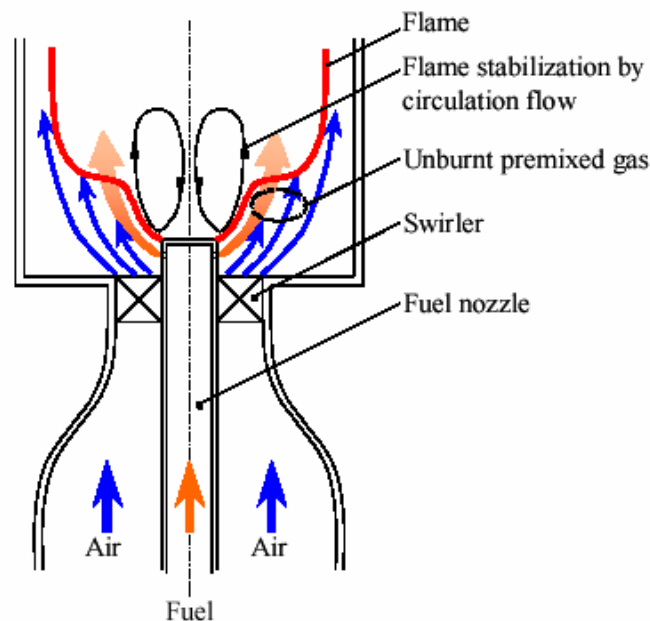


Figure 2.22: Concept of the Flame Structure of the Micro Gas Turbine Combustor (from ref. [24]).

Other kind of micro gas turbine researches are addressed to investigate the capability of the MGT to burn low-BTU biogenic fuels instead of natural gas. Actually, the energy conversion of biomass to electricity can be improved by integration of a micro gas turbine with the biogas generation process. Bohn and others [8] presented an integrated plant concept after a general overview of low-BTU fuels suitable for utilization in gas turbines. They studied the effects of biogas utilization on the characteristics of operation of a representatively modelled microturbine. For a complete study, they analyzed the effects of low-BTU fuels

on gas turbine materials and pollutant emissions. In particular, the change of emissions of nitrogen oxide and carbon monoxide was analyzed with a combustion model based on a systematically reduced 6-step reaction mechanism. This study was developed for an advanced combustor design applying ceramic materials and a transpiration cooling technology.

Spadaccini et al. [22] have presented the design, fabrication, experimental testing and modelling of the combustion system of a micro-scale gas turbine engine for power generation and micro-propulsion applications. They examined two radial inflow combustors: a single-zone arrangement and a primary and dilution-zone configuration (fig. 2.23). Both combustors were micro-machined from silicon using Deep Reactive Ion Etching (DRIE) and aligned fusion wafer bonding. The combustor volume is of  $191 \text{ mm}^3$  with an hydrogen-air and hydrocarbon-air combustion. Exit gas temperatures as high as 1800 K and power densities in excess of  $1100 \text{ MW/m}^3$  were achieved. With the same equivalence ratio and overall efficiency, the dual-zone combustor reached power densities nearly double than those of the single-zone design. Numerical simulations were used to gain insight into the fluid and combustion physics because diagnostics in micro-scale devices are difficult and highly intrusive. The performance of the micro-combustors was found to be more severely limited by heat transfer and chemical kinetics constraints by inadequate residence time for complete combustion. These studies lead to the identification of critical design trades and recommendations for micro-combustor design. In table 2.1 a comparison of operating parameters for a micro combustor and a conventional combustor is reported.

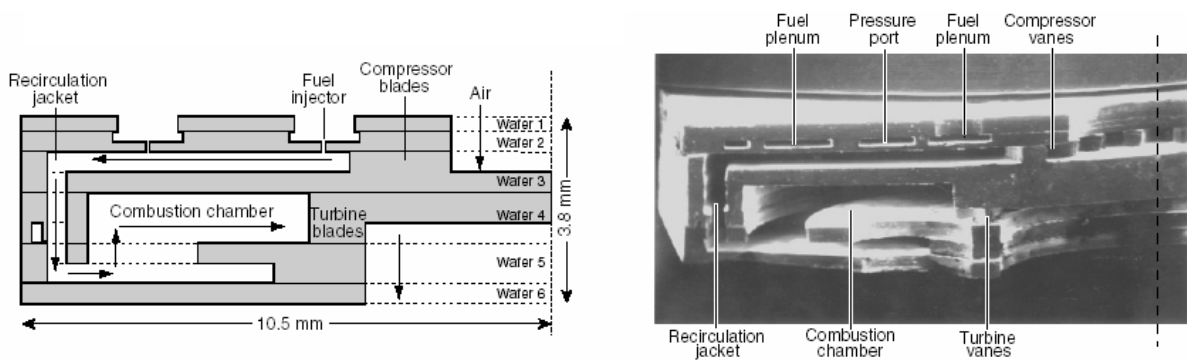


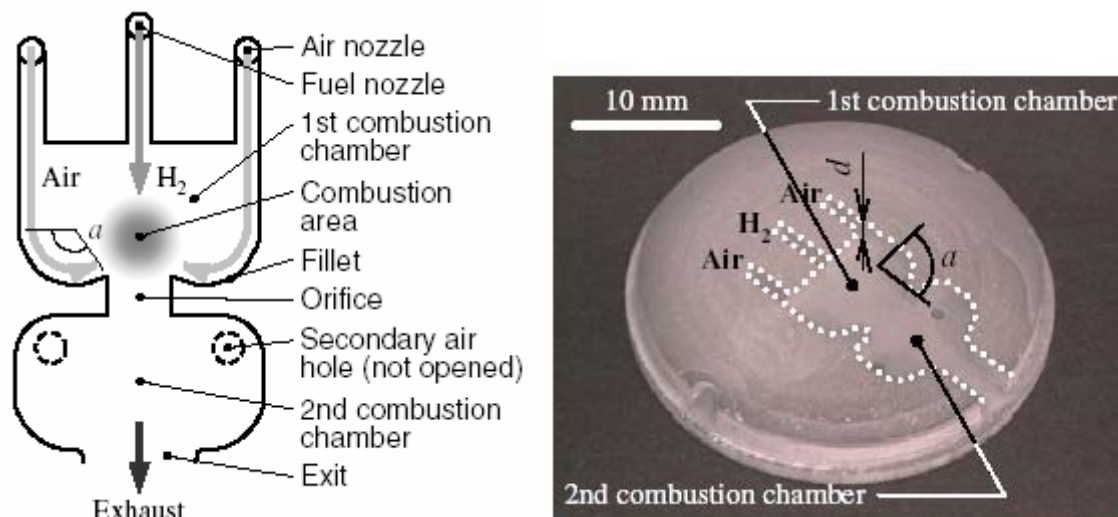
Figure 2.23: Schematics of the 6-Wafer Micro-Combustor (from ref. [22]).

Table 2.1: Comparison of the Operating Parameters for a Micro-Combustor with those for a Conventional GE90 Combustor (from ref. [22])

	Conventional Combustor	Micro-Combustor
Length	0.2 m	0.001 m
Volume	$0.073 \text{ m}^3$	$6.6 \times 10^{-8} \text{ m}^3$
Cross-sectional area	$0.36 \text{ m}^2$	$6 \times 10^{-5} \text{ m}^2$
Inlet total pressure	37.5 atm	4 atm
Inlet total temperature	870 K	500 K
Mass flow rate	140 kg/s	$1.8 \times 10^{-4} \text{ kg/s}$
Residence time	$\sim 7 \text{ ms}$	$\sim 0.5 \text{ ms}$
Efficiency	$>99\%$	$>90\%$
Pressure ratio	$>0.95$	$>0.95$
Exit temperature	1800 K	1600 K
Power Density	$1960 \text{ MW/m}^3$	$3000 \text{ MW/m}^3$

(Note: residence times are calculated using inlet pressure and an average flow temperature of 1000 K.)

A further example of real micro-combustors is offered by Tanaka et al. [28]. The micro-combustor as a two-dimensional dimensional, its depth ranging from 1 to 3 mm, and it ensures a stable combustion both for lean and fairly rich mixtures. Problems still exist in terms of combustion completion but the prototypes (fig. 2.24) let however foresee an efficient process with a rate of heat release of nearly 300 W, with firing temperatures up to 1500 °C.



**Figure 2.24: Schematics and Photograph of a Silicon-Ceramic Based 2D Micro-Combustor (from ref. [28]).**

Finally, the combustion instability is one of the most complex phenomena in engineering because of the strong complex coupling of acoustics, mixing and combustion processes. Since the acoustic behaviour is directly affected by the geometry and boundary conditions of the system, instability behaviour observed in engine applications is typically much different than in development rigs. This ambiguity has made it extremely difficult to successfully design and demonstrate the TG combustors using laboratory development test rigs and then install the combustor in service without instability problems. The combustor design must then be modified in the field which is the most expensive one. In ref. [25] a tool which will allow the combustor designer to assess designs and select a configuration which provides the least probability of instabilities and the widest operating range was described. In particular, one of the major fundamental mechanisms is the convection of fuel concentration fluctuations from the fuel injector to the reaction zone. A one-dimensional model has been developed which captures this mechanism coupled to solutions for standing acoustic waves. The model has been extended to include a parallel acoustic path and two fuel injection locations. Splitting of fuel between two injection positions is a common method to influence combustion dynamics toward a more operable system. A relatively simple model which only partially couples acoustics and heat release was applied to an axially staged combustor and the predictions are compared with the experimental behaviour. The results from this model successfully predict the overall dynamics behaviour as a function of the fuel split between the two injection locations.

After this necessary overview of the state of art in the MGT combustor studies, this paper will proceed with a comprehensive outline of the main problems to be kept in mind in order to assess the combustor concept and analysis.

### **3. COMBUSTION CHARACTERISTICS AND COMBUSTOR TYPES**

#### **3.1 General Features of the MGT Combustion**

The combustion process in a micro-gas turbine presents some typical characteristics which originate from a number of items, say:

- The thermal cycle is of the low-pressure ratio, recuperated type: compared with typical inlet air conditions in conventional gas turbine combustors, a reduced pressure and an increased temperature level are therefore expected;
- The final firing temperature is generally not above 1200 – 1250 K: thus the temperature rise throughout the combustor is limited and, consequently, a reduced fuel addition is needed: the combustor operates with a low overall equivalence ratio (defined as the actual fuel/air ratio to the stoichiometric one);
- The order of magnitude of the gas flow rate is of 0.5 – 1.0 kg/s: despite of the decreased inlet air density, the average volumetric flow rate is considerably lower than in conventional gas turbine combustors: therefore the inlet flow area will present reduced values;
- The above item meets the requirement of reducing the overall combustor size, but the length of the combustion chamber should be however properly chosen for ensuring the necessary residence time of the reactants.

Besides the general features listed above, the combustion chamber of a micro-gas turbine could frequently encounter off-design conditions induced by changes in either the MGT operation or the fuel supplied:

- Load variations may be operated either at constant or variable speed, depending on the electrical generator type: different changes are induced by the two distinct regulations in terms of inlet air conditions and overall equivalence ratio;
- In the case of combined heat and power generation with a MGT, a typical method for fulfilling increasing demand of thermal output is a partial by-pass of the internal recuperator: this produces a decrease in the inlet air temperature and consequently the fuel supply must be largely increased;
- Regarding to the adoption of non-conventional fuels, the employment of products of bio-masses or solid-waste gasification may enhance the interest toward the MGT diffusion but the fuel characteristics may considerably vary, respect to a natural gas: in some cases the hydrogen contents is relevant and a better control must be exerted on both the flammability conditions and the thermal nitric oxide production. Other fuels may be of the low LHV type and the major problems arise from the too low flame temperature and from the excess in the fuel flow rate which is needed.

In order to give a more comprehensive overview of the problems listed above, in the following we will refer to a MGT of the 100kW range, whose main operating data are recalled in table 3.1.

**Table 3.1: Data for MGT Design and Operation**

<i>MGT DATA</i>	
Mech. Arrangement	Single Shaft
Air Flow Rate	0.80 kg/s
Pressure Ratio	3.9
Compressor Exit Temp.	468 K
Combustor Inlet Temp. (Fully regenerative cycle)	905 K
Turbine Inlet Temp.	1223 K
Turbine Exit Temp.	951 K
Recuperator Exit temp. (Fully regenerative cycle)	530 K
Rated Mechanical Output	110 kW
Nominal Speed	64000 rpm
Compressor, Turbine	Radial Flow

As said before, the temperature rise for a fully recuperated cycle is slightly more than 400K, while a simple, non-recuperated cycle would require a temperature increase in the combustion chamber of nearly 750K. The following table 3.2 reports the actual fuel/air ratios needed for the combustion completion in both situations.

**Table 3.2: Natural Gas and Gaseous Fuels from Bio-Mass and Solid Waste Gasification Composition and Properties**

Fuel Composition (%, molar)	Nat. Gas (NG)	BIOM(O)	BIOM(a)	SW
<b>CH<sub>4</sub></b>	<b>92.00</b>	<b>18.00</b>	<b>9.00</b>	<b>7.00</b>
C <sub>2</sub> H <sub>6</sub>	3.70	2.00	--	7.00
C <sub>3</sub> H <sub>8</sub>	1.00	2.00	--	7.00
C <sub>4</sub> H <sub>10</sub>	0.25	2.00	--	--
N <sub>2</sub>	2.90	8.00	56.00	--
<b>H<sub>2</sub></b>	--	<b>25.00</b>	<b>9.00</b>	<b>18.00</b>
CO	--	33.00	12.00	61.00
CO <sub>2</sub>	0.15	10.00	20.00	--
H <sub>2</sub> O	--	--	--	--
<hr/>				
Mol. Mass, g/mol	17.34	21.92	28.51	23.76
<i>LHV</i> , kJ/kg	47182	19198	2798	21697
<i>h<sub>of</sub></i> , kJ/kg	-4266.9	-3720.1	-1649.5	-2923.9
<i>f<sub>st</sub></i>	0.0620	0.1680	1.257	0.1530
<i>T<sub>of</sub></i> , K	2220	2231	1571	2300
<i>f</i> , $\phi$ (fully rec. cycle)	0.0082, 0.132	0.0214, 0.127	0.191, 0.151	0.0177, 0.115
<i>f</i> , $\phi$ (no rec. cycle)	0.0181, 0.292	0.0457, 0.272	0.464, 0.369	0.0397, 0.260

The same table 3.2 reports the adiabatic flame temperatures estimated for an ideal combustion of the several gaseous fuels starting under ISO standard conditions with a stoichiometric mixture. The hydrogen

contents is fairly relevant in both the *BIOM(O)* bio-mass, oxygen-gasified, fuel and for the solid-waste derived fuel (*SW*); consequently the flame temperatures are expected to be slightly higher than in the natural gas case. Conversely, the large contents in inert species of the *BIOM(a)*, air-gasified bio-mass fuel, leads to a much lower level of the same temperature. Fig. 4.1(a) displays the actual trend of the maximum combustion temperature as a function of the combustor inlet temperature for the different fuels. The maximum temperature level must be obviously intended as the one which would be reached within a primary zone with a stoichiometric flame: the temperature is estimated at the thermo-chemical equilibrium conditions starting from air at the recuperator outlet and from the fuel compressor exit, respectively.

As explained in the lecture note on the general MGT performance estimation [73], the four situations listed in table 3.2 and in figure 3.1 refer to the employment of either the natural gas or the medium-low LHV fuel, the latter supplied without any mixture with the natural gas itself. The results in figure 3.1(a) suggest that both the *BIOM(O)* and the *SW* fuel would present a favourable behaviour in terms of flame sustenance, since some defect in calorific value, mainly due to the CO contents, is compensated by the presence of hydrogen. Problems could arise with the low LHV gas, *BIOM(a)*, which could not reach sufficiently high temperatures even in a stoichiometric core with the highest air inlet temperatures. Situations like this would suggest the employment of mixtures with natural gas in order to ensure acceptable flammability conditions.

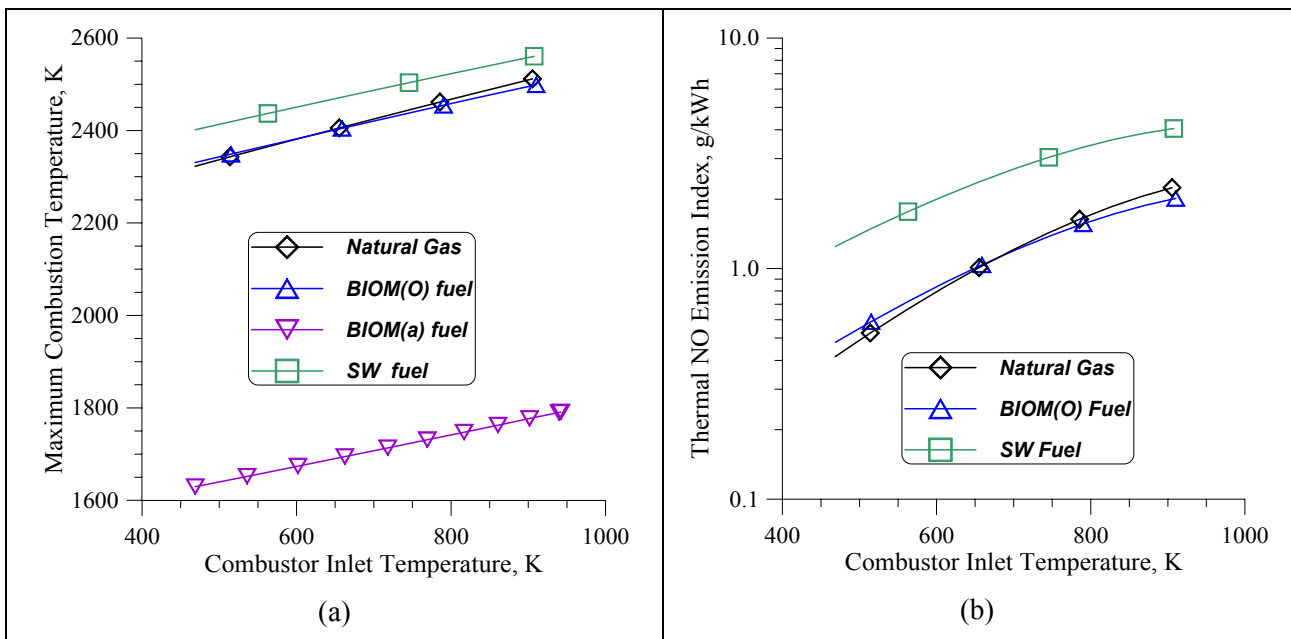
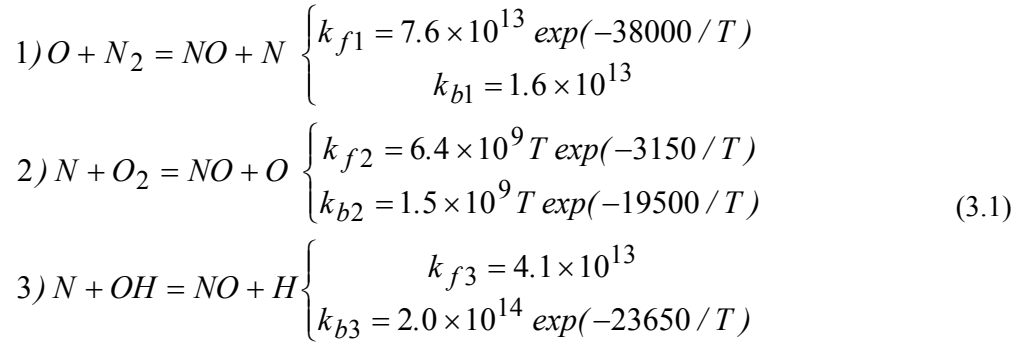


Figure 3.1: Expected Temperature Peaks and NO Emissions from Different Fuels.

On the other hand, the production of some noxious species, like the nitric oxides from the thermal formation mechanism [41], is strictly related to the same combustor inlet temperature which is responsible for the temperature peaks in fig. 3.1(a). Therefore the typical trend of the emission index of the thermal NO (fig. 3.1b) reflects the one of the maximum combustion temperature and puts into evidence that some advantages shown in terms of easy self-ignition conditions may conflict with the requirement of reducing the pollutant emissions. The results in fig. 3.1(b) are obtained by a thermo-kinetic model for the prediction of the thermal NO formation [29-32, 55], whose development is briefly outlined below:

- The computation is based on the assumption that the combustion rates are much faster than those in the extended Zel'dovich [41] mechanism:



- Therefore the thermo-chemical equilibrium is assumed for the species involved in the main reactions while those participating in the nitric oxide formation are affected by the finite rates:

$$\frac{dx_i}{dt} = \sum_{k=1}^3 \left[ k_{fk} \prod_{j=1}^7 \tilde{x}_j^{\zeta_{fk,j}} - k_{bk} \prod_{j=1}^7 \tilde{x}_j^{\zeta_{bk,j}} \right] \quad (i=1, \dots, 7) \quad (3.2)$$

where the  $\zeta_{fk,j}$ ,  $\zeta_{bk,j}$  exponents may be either 1 or 0, depending upon the presence of the  $j$ th. species in the  $k$ th. equation.

- A law is given for the air splitting between the primary, secondary and dilution regions of the combustion chamber. Similarly the whole residence time is assigned together with the time fractions pertaining to each region.
- The system of ODEs (3.2) is integrated in the time domain within the residence time interval. At each time step, the equilibrium temperature and gas composition are estimated and the local rates of the kinetic model are updated.

The results in fig. 3.1(b) are obtained under similar conditions hypothesized for the several fuels, say:

- A stoichiometric mixture is assumed in the primary region.
- The same residence time is assumed at the baseline conditions (i.e., full load, fully recuperated cycle). The actual value is then obtained by scaling the base value in accordance to the average volumetric flow rate of the reacting gases.
- The same fraction of residence time, of 5%, is assigned to the primary zone.

With the above assumptions, the nitric oxide formation related to the poor-LHV fuel, BIOM(a), is practically negligible and the results discussed in the following refer only to the other three fuels in table 3.2. Figure 3.2 displays the time evolution of the local temperatures and of the thermal NO concentrations. Both kind of profiles must be interpreted as those occurring for homogeneous mixtures of the combustion products with the air which is progressively added to the amount participating in the primary combustion. Thus the temperature and NO concentration drops after the initial peaks are due to the effect of the dilution with the air at the combustion entry conditions.

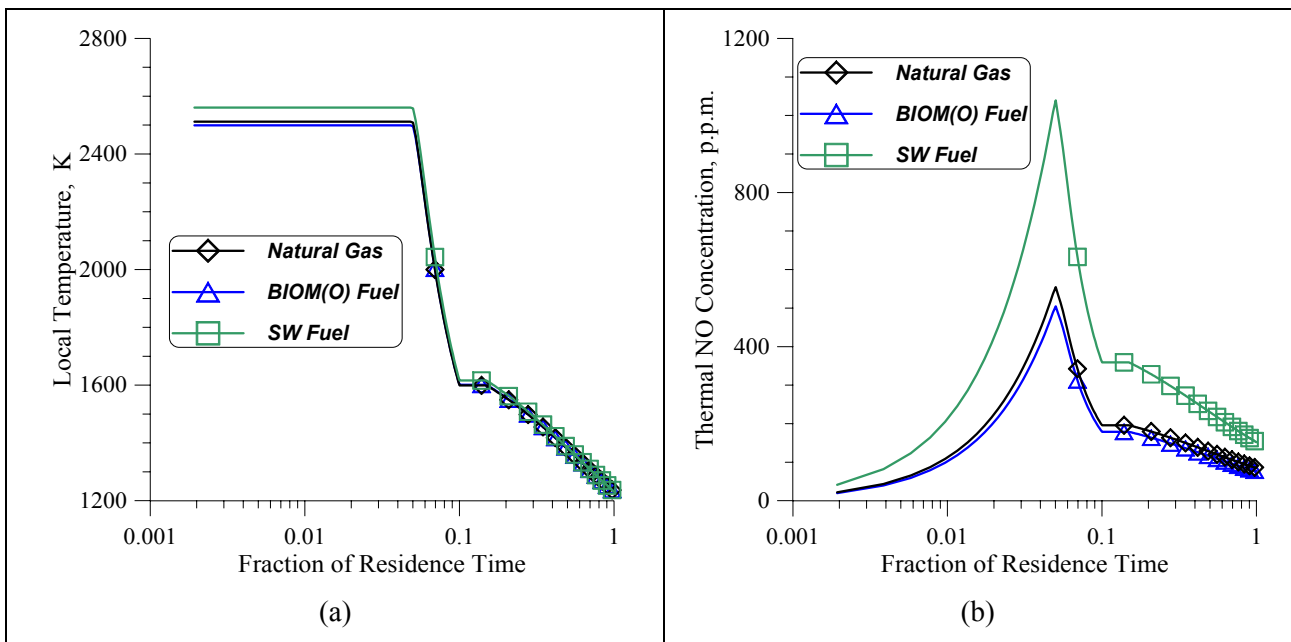
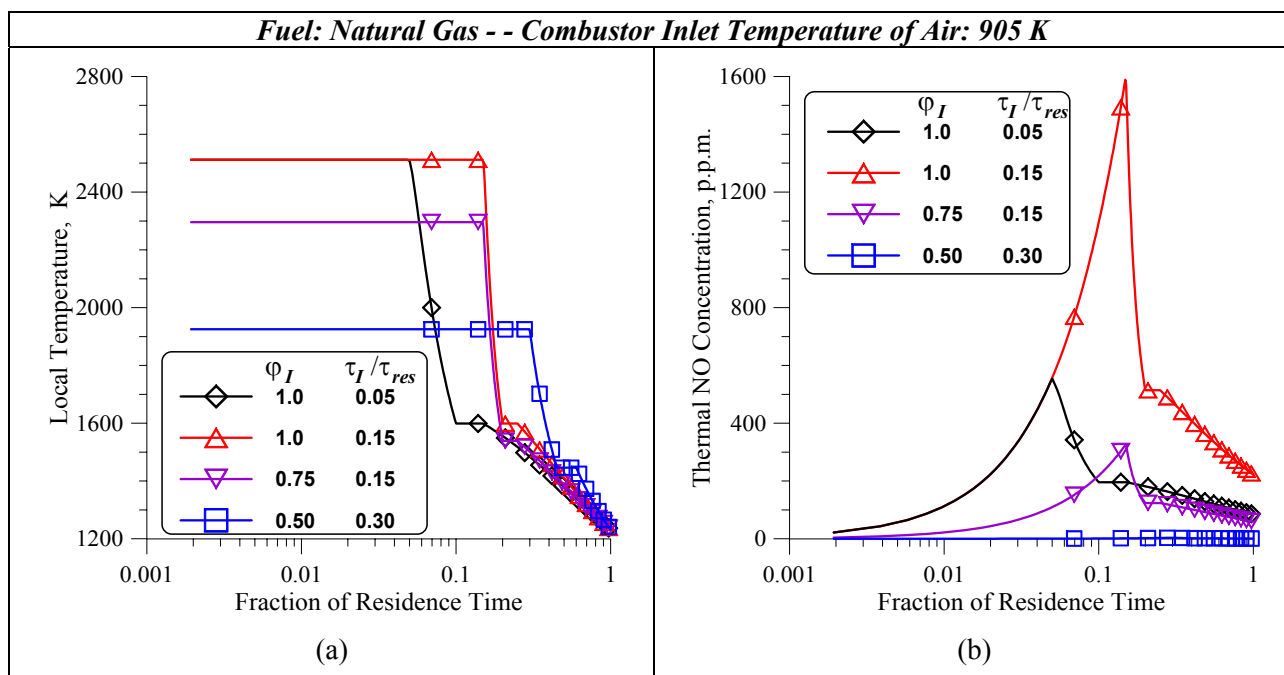


Figure 3.2: Temperature and Thermal NO Profiles in the Time-Domain.

As stated, the results are obtained for a primary stoichiometric fuel/air ratio and the slope of the NO profiles clearly indicates the higher formation rate in the case of the solid-waste derived, hydrogenated fuel. In any case, the final concentration levels are unacceptable for a typical low-NO<sub>x</sub> operation, since also in the natural gas case the predicted NO level is above 80 p.p.m.

Results like those in figs. 3.1 and 3.2 give an useful, preliminary sketch of the situations which would occur for the pollutant formation under given conditions of the combustor entry air and fuel/air ratio distribution throughout the combustion chamber. Both temperature and NO profile could reflect, in a somewhat global appearance, those occurring in a typical diffusive combustor with a stoichiometric flame involving the whole reactants in the primary zone. The unfavourable values of the NO concentration suggest the way to be followed for a better environmental behaviour of the micro-gas turbine and the most widely adopted solution consists of a lean-premixed combustion, with a primary equivalence ratio,  $\phi_p$ , considerably lower than the stoichiometric one.

The combined effect of the primary equivalence ratio,  $\phi_p$ , and of the primary residence time fraction,  $\tau_1 / \tau_{res}$ , is summarized in fig. 3.3. Of course, an increase in this time fraction from 5% to 15% for a stoichiometric fuel/air ratio would significantly augment the permanence of the combustion products at the highest temperatures (fig. 3.3a) and the nitric oxide formation would proceed with an enhanced rate (fig. 3.3b) with a totally unacceptable final concentration. The same time fraction has been considered for a reduced primary equivalence ratio, of 0.75, which probably needs larger times for the flame propagation. Fig. 3.3(a) underlines the temperature decrease in the primary zone while fig. 3.3(b) evidences the relevant attenuation of the NO formation rate. Nevertheless, the final nitric oxide contents – of nearly 60 p.p.m. – are not satisfactory, probably because of the too high air temperature at combustor inlet, and this suggests a further decrease in the primary equivalence ratio. A value of 0.5 for  $\phi_p$  would lead, despite of the necessary increase in the primary residence time, to an almost negligible concentration of thermal nitric oxides.



**Figure 3.3: Effect of the Primary Equivalence Ratio and Residence Time on the NO Mechanism.**

It should be reminded that the results discussed above, although of interest for a preliminary choice of some operating parameters of the combustion chamber, need a deeper investigation mainly because of some key assumption, like the one of thermo-chemical equilibrium of the combustion products, and the absence of any fluid-dynamic approach.

Really, the whole residence time and the relative fractions pertaining to each region are simply hypothesized but the actual values result from the complex flow fields within the combustor. Similarly, the true situation of the combustion progress is fairly far from the equilibrium conditions and the actual rates are depending on both the reaction kinetics and the turbulence levels. In particular the last examined case, referring to a primary equivalence ratio of 0.5, shows encouraging results in terms of NO concentration (less than 1 part per million!) but the combustion activation and progress throughout the lean fuel/air mixture must be accurately checked. A widely diffused solution for aiding the mixture ignition is the employment of a stoichiometric pilot flame of variable intensity in accordance with both the combustor load level and the air inlet temperature. The initial existence of two parallel processes (i.e., the pilot and the lean-premixed ones) is beyond the assumption that led to the results in figures 3.1 – 3.3 and also the actual NO level resulting from a pilot assisted lean-premixed combustion must be expected to be largely higher than in the predictions in fig. 3.3 (b).

Concluding this section requires a summary of the main requirements for a combustion chamber operating within a micro-gas turbine generating or co-generating set:

- The combustor size must fit the dimensions of the other MGT components.
- The chamber should appreciably adapt to a number of different conditions in terms of fuel supplied, load-levels, variable air temperatures.
- An effective compromise must be found between the need of combustion completion and pollutant reduction. In other words the residence times, and the time fraction inside the primary zones, should be limited enough to prevent an excess in thermal NO formation. On the other hand, specially when adopting the lean-premixed fuel/air quality, appropriate conditions must exist for the combustion activation and progress.

- The solution to the above problem seems to be a pilot stoichiometric flame, provided that some conditions do not need an excess of fuel to the pilot line, so inducing high formation rates for both prompt and thermal nitric oxides.

Although the pilot assisted, lean-premixed combustor is the most up-to-dated solution for the emission reduction, a preliminary comparison with other combustor types seems to be likely for deciding the most appropriate choice.

The last consideration is worthy of a clarifying example like that in fig. 3.4. A comparison is shown, with the employment of the thermo-kinetic model again, among the expected behaviours of three different combustor types:

- A typical diffusive combustion chamber (*Diff.*) with a stoichiometric fuel/air ratio in the primary zone;
- A lean-premixed combustor (*LP*) with a primary air excess;
- A rich-quench-lean (*RQL*) combustor with a rich primary mixture followed by the quenching air supply and, finally by air addition for the combustion completion.

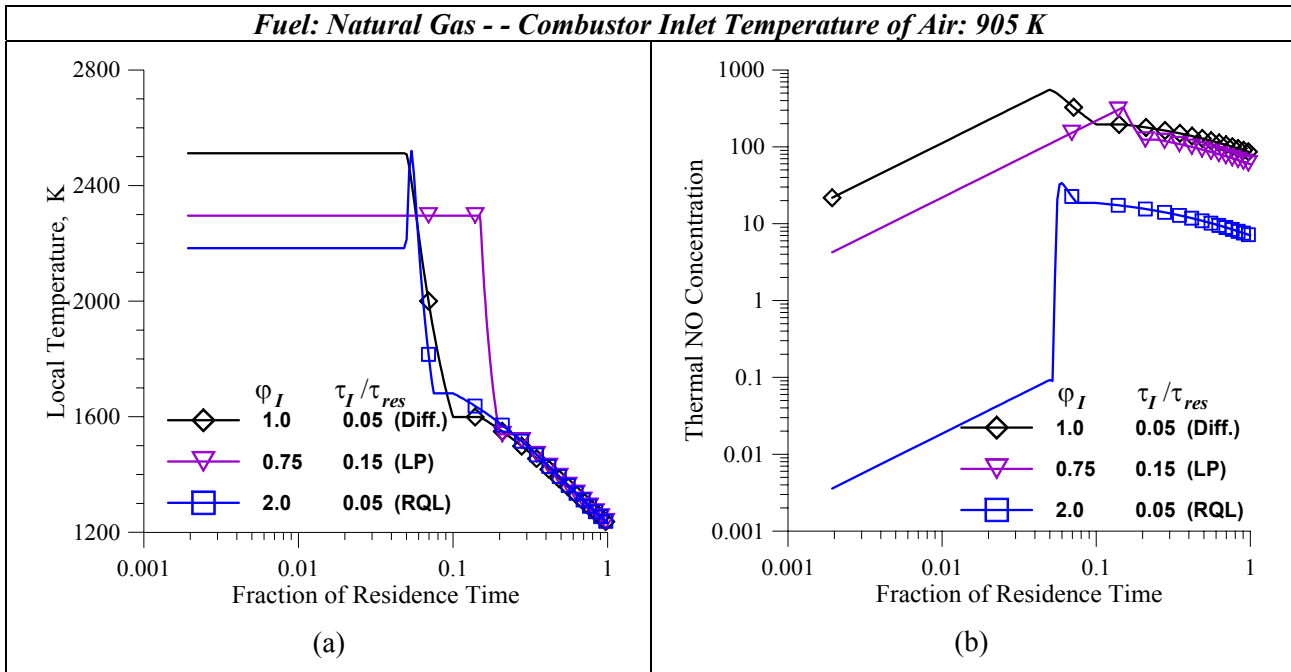


Figure 3.4: Time-Dependent Temperature and NO Profiles for Different Combustor Types.

The first two types have been already compared in the previous figures and they substantially differ because of the rather slower NO formation rate in the LP combustor (fig. 3.4b), which is partially compensated by the necessity of a longer time fraction inside the primary region. A completely different behaviour is exhibited by the RQL chamber. The considerably lower temperature in the primary region (fig. 3.4a) is explained by the incomplete combustion which is due to the air defect. The sudden temperature raise when the first part of the quenching air is supplied produces a faster NO formation, compared with the two other types. The mechanisms is quickly stopped by the quenching effect which involves a steep temperature drop. The final concentration appears therefore to be particularly low, so confirming that attention must be paid to the possible employment of some effective alternatives to the lean-premixed chamber.

On the other hand, some aspects related to the RQL combustor are to be deepened, mainly with regard to the actual combustion progress and to the formation of unburned or partially burned species. This will be the subject of the comparison of the different combustors on a CFD basis, as discussed in the following sections.

**3.2 The MGT Combustors**

The analysis discussed before have been carried out basing on a purely thermo-chemical approach with the purpose of outlining the main characteristic which are required to a combustion chamber operating within a micro-gas turbine concept. Besides of the several proposal made by the numerous researchers in this field and described in section 2, this paragraph aims to a comprehensive description of the different combustor types which could be taken into account, so recalling the considerations at the end of the previous paragraph.

**The Annular Combustor Scaled for MGT Applications.** This combustor geometry originates from a well consolidated configuration in the *GE* experience [35] for aero-derivative gas turbines, and its wide diffusion is supported by a large number of both experimental tests and numerical simulations. In addition, many authors have demonstrated the capability of this combustor to adapt to different conditions, like water or steam injection, shift from the diffusive to the lean-premixed operation, fuelling with different mixtures, etc. In the authors’ experience, this chamber exhibits a satisfactory behaviour also when supplied with hydrogenated fuels or when operated with variable inlet conditions [54, 55].

For the above reasons, the combustor features seem to meet the typical requirements for MGT applications, like those related to the use of bio-mass or solid-waste derived fuels or the suitable response to different conditions of the inlet air. Of course, a resizing is needed and in particular papers [58, 55] propose the scaling of the original combustor (which equips an aero-derivative gas turbine of the 20 MW class) in both span-wise and azimuthal directions. The resulting scaled height and average diameter allow a proper fit of the typical compressor and turbine sizes for the *MGT* application. The cross-section scaling ensures almost the same velocity levels as in the original combustor while preserving the axial length leads to the same order of magnitude for the residence times.

In order to evaluate the appropriate scale factor, the data in table 3.3 were employed. In this way, also the chamber volume is scaled by the area scale factor, say by the inverse volumetric flow rate ratio, and this ensures that also the typical global estimate of the residence time ( $\tau_{res} = V/\dot{V}$ ) leads to the same value for both the original and the scaled combustor.

**Table 3.3: Data for the Annular Combustor Scaling**

<i>Combustor Data</i>	<i>Full-Size Combustor</i>	<i>Scaled MGT Combustor</i>
Inlet Pressure, bar	18.0	3.8
Inlet Temperature, K	698.5	905.3
Inlet Air Density, kg/m <sup>3</sup>	9.24	1.46
Air Mass Flow Rate, kg/s	60.0	0.80
Volumetric Flow rate, m <sup>3</sup> /s	6.49	0.548
Firing Temperature	1550	1250
Fuel Mass Flow Rate, kg/s	1.3	7x10 <sup>-3</sup>
Overall equivalence Ratio	0.350	0.140
Area Scale Factor	11.85	
Linear Scale Factor	3.44	

A schematic view of the original and scaled burner is given in fig. 3.5. In particular, fig. 3.5(a) evidences the scaling of the inlet flow areas and the preservation of the axial length, while fig. 3.5(b) better highlights the annular combustor location around the axis. A peripheral periodicity occurs after 12° according to the periodical arrangement of both 30 inlet air swirlers and 30 fuel injectors with 30° full cone shaped jets from 5 holes.

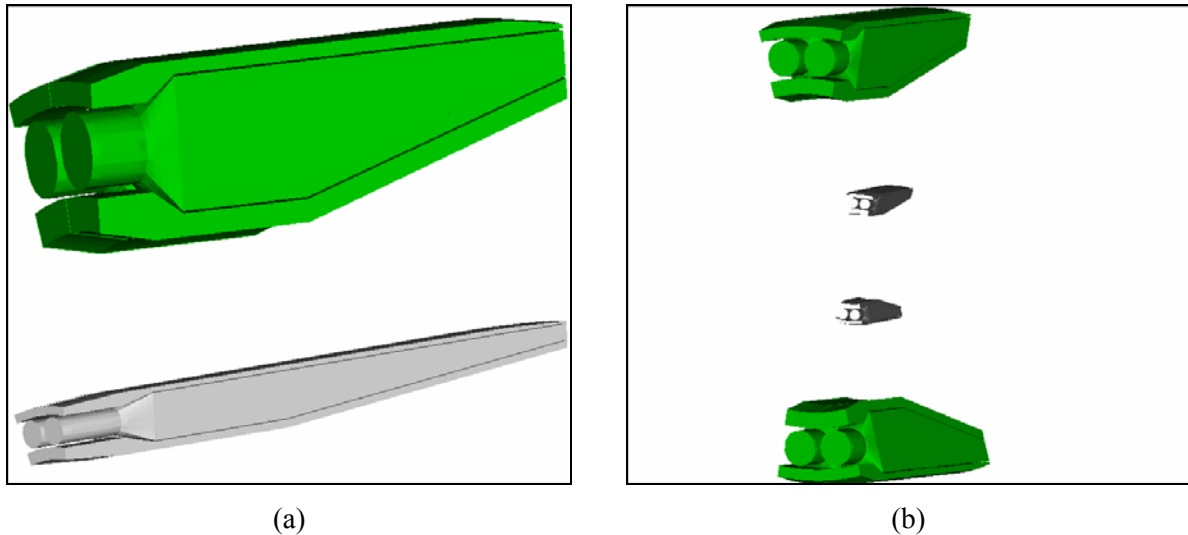
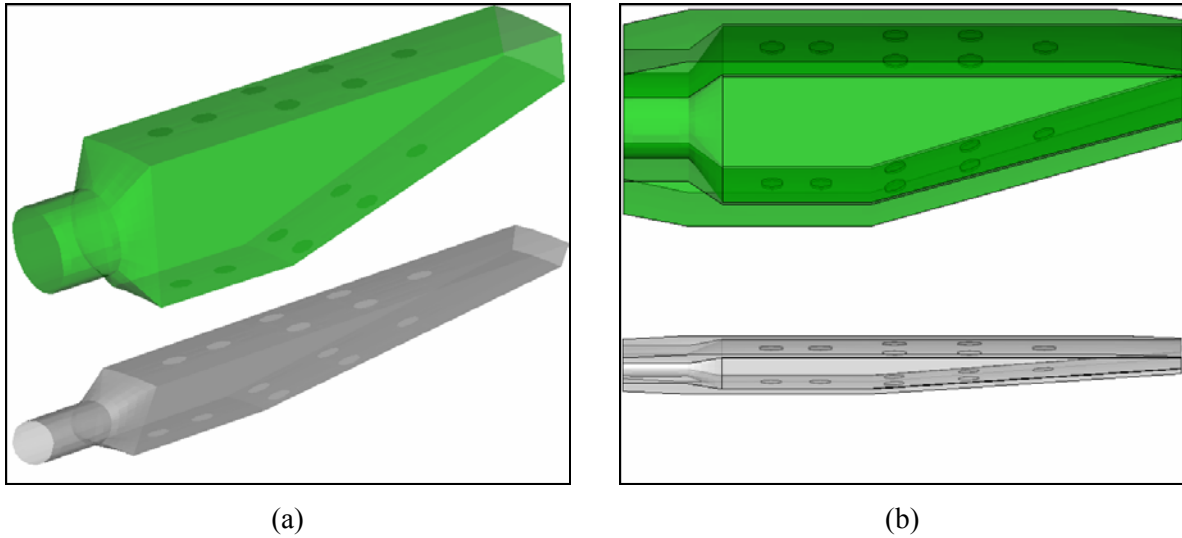


Figure 3.5: Schematics of the Full-Size and Scaled Annular Combustors.

A fairly stoichiometric fuel/air ratio in the primary region results from the air split between the central circular inlet and the external liner ports. This could ensure acceptable conditions for the auto-ignition in a wide operating range but is also responsible, as well known, for the existence of local temperature peaks and therefore for a considerable production of thermal nitric oxides.

Table 3.3 shows that the original and scaled combustor would operate with different overall equivalence ratios, since in the first case the temperature rise through the combustor is much higher. Thus, for obtaining the same unit equivalence ratio in the primary zone different air splitting are required: this could rather automatically obtained since the front inlet flow areas are reduced by the area scale factor, while those of the secondary and dilution holes are decreased only by the linear scale factor. For this reason, most of the inlet air would be addressed, in the scaled combustor, to the external liners and the stoichiometric fuel/air ratio should be obtained in the primary zone.

The above situation can be better examined in fig. 3.6 which gives details of the secondary and dilution holes displacement along the burner walls (fig. 3.6a) and of the axial development of both burner core and external liners (fig. 3.6b).



**Figure 3.6: Secondary and Dilution Hole Location in the Full-Size and Scaled Annular Combustors.**

**The Lean-Premixed Combustor.** This chamber, of the tubular type, consists of a burner, whose primary zone is supplied by a circular bladed swirler, and an external liner which addresses the air flow to both the cooling slices and the dilution holes. The geometry considered was expressly conceived by the Ansaldo Research Center [6, 57, 58] for the *MGT* application and the authors of this paper are contributing to the design of experiments for the test facility which is nearly to be activated. The radial fuel injection takes place immediately downstream of the blade channel through 18 injector with 4 holes each. A complete fuel and air mixing is therefore attained prior to combustion. Operating the primary zone at a lean fuel/air ratio results in both low reaction temperatures and elimination of hot spots within the burner zone, and so in drastically reduced  $\text{NO}_x$  emissions. Major difficulties arise regarding the mixture flammability and self-ignition, due to the strongly reduced equivalence ratio at the primary region inlet, which is of 0.55 at base rating. The mixture ignition must be therefore aided by a pilot stoichiometric flame. The rate of fuel supplied to the pilot line, through 12 single hole injectors, is of nearly 10% at the baseline operation but it should increase both at part-load and at reduced inlet air temperatures. Referring to the combustor size, the length is almost the same as in the annular chamber but an increased height is needed in order to obtain nearly the same average cross section and axial velocity levels.

Fig. 3.7 provides both an overview of the whole combustor geometry and details of the inlet sections. In particular the location of the injectors downstream of the swirling blades and along the central pilot line is detectable in fig. 3.7b.

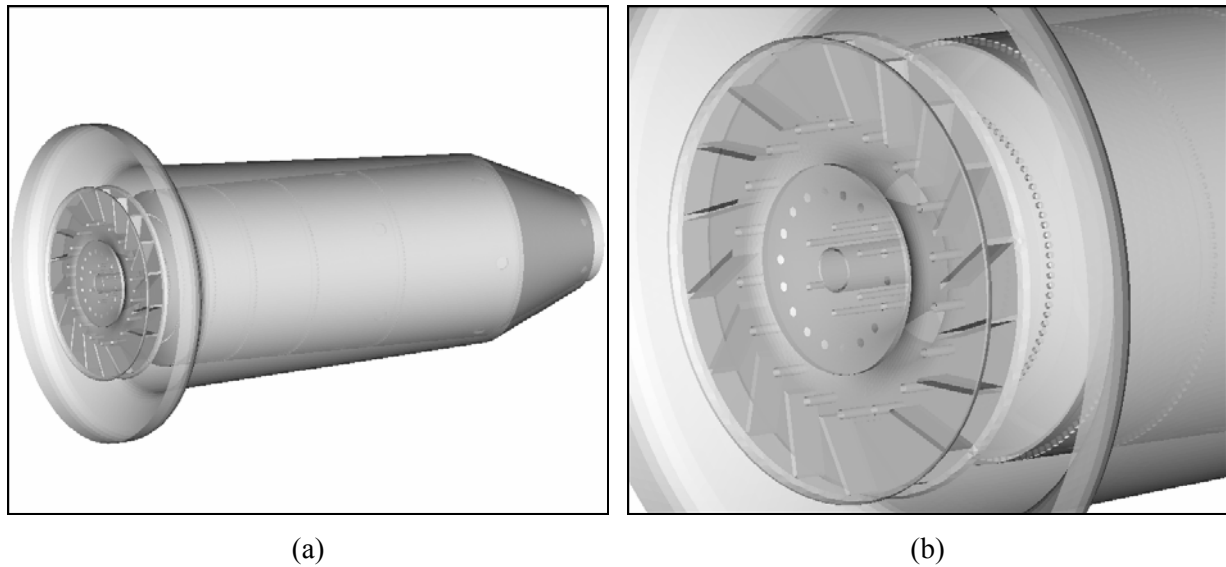


Figure 3.7: Configuration of the Lean-Premixed Combustor.

The axial development of the burner and external liners geometry is shown in the next figure 3.8 which also allows the different inlet channels to be distinguished. The primary region is entered through the radial inlet swirlers and the following elbow shaped channel. Both primary and dilution air enter the chamber through the annular front section and the air flow is split into the different streams. The pilot line has a separate, central axial inlet.

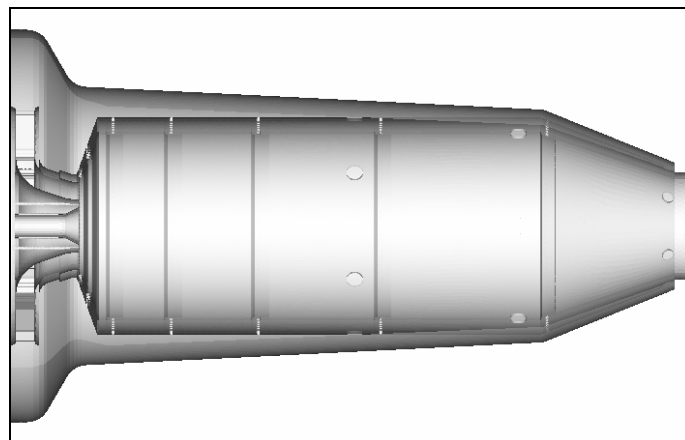
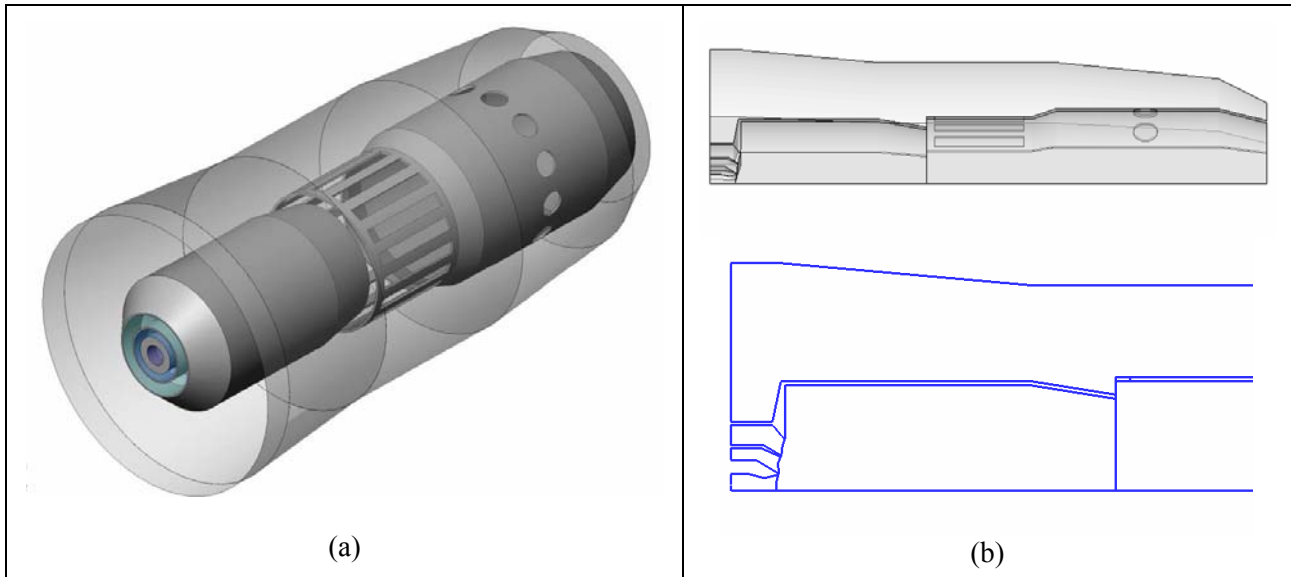


Figure 3.8: Axial Development of the LP Combustor.

**The *RQL* Combustor.** The Rich-burn, Quick-quench and Lean-burn combustor [50, 51, 67, 68, 70] has been considered here for its characteristics of effectively operating in a wide range of overall fuel/air ratios and inlet air temperatures, simultaneously limiting the production of nitric oxides. The technique consists of burning the fuel far above the stoichiometric conditions in a first stage of the combustor (i.e., the rich zone), in order to avoid the simultaneous occurrence of high temperatures and oxygen availability, both responsible for the production of thermal  $\text{NO}_x$ . The CO and unburned hydrocarbons generated in the rich zone will be oxidized under smoother conditions and low temperatures in the lean zone. The transition from “fuel-rich” to “fuel-lean” combustion is obtained through the introduction of air jets which dilute the mixture in the second region of the combustor (quench zone), where the flow is accelerated in order to limit the residence time in this potentially stoichiometric zone.

The combustor configuration in fig. 3.9, must be intended as an authors' attempt to meet the RQL features for the *MGT* application. Really the actual combustor operation is strongly influenced by the effectiveness of the dilution jet penetration at the quench stage and an optimization of the mixing pattern downstream of this zone is therefore required. A key role is played in this sense by the extent and orientation both of the quenching ports and of the holes for the final supply of the diluting air. The length is nearly 60% greater than in the other two combustors and the primary equivalence ratio is close to 2.



**Figure 3.9: Schematics of the RQL Combustor.**

Table 3.4 compares the typical air sharing between the primary flows and those to the secondary and dilution ports. The annular combustor operates with a nearly stoichiometric air, while a strong excess is fixed for the *LP* chamber. This leads to a nearly unit equivalence ratio for the annular diffusive combustor while the premixing line produces a fuel air mixture far below the unit value. The data uncertainty for the RQL combustor indicates that the fuel/air ratio should be more properly evaluated within the fuel injection zone. Therefore, the primary air flow is intended as the one from the inlet air channel which is closest to the injector location.

**Table 3.4: Air and Fuel Distributions**  
(overall fuel/air ratio = 0.00875, overall eqv. ratio = 0.141)

<i>Combustor</i>	<i>Diff.</i>	<i>LP</i>	<i>RQL</i>
Primary Air, %	17	29.6	3 ÷ 10
Sec. and Dil. Air, %	83	69	97 ÷ 90
Pilot Air, %	--	1.4	--
Primary Fuel, %	100	90	100
Pilot Fuel, %	--	10	--
Primary Eqv. Ratio	0.83	0.45	4 ÷ 1.2
Pilot Eqv. Ratio	--	1.09	--

Of key interest is the comparison between the two last combustors because they are based on rather opposite concepts and may, consequently, produce strongly different combustion behaviours. Really, the lean-premixed combustor should avoid problems in terms of NO formation but could also encounter

limitations related to the auto-ignition conditions. The RQL one, on the contrary, should present a more effective behaviour by the latter point of view, but a more accurate investigation of the combustion completion is required, together with a proper selection of the amounts of air to be split among the rich and the quench and lean regions.

The role of the CFD becomes therefore fundamental for identifying the actual flow patterns in terms of mixing rates between the fuel and air jets and to evaluate the actual penetration of the secondary and diluting air flows inside the reacting mixture. Comparing the three combustors under different operating conditions represents, in the authors' opinion, a fundamental step, even if not exhaustive, to assess the main problems related to each configuration, thus providing the way to be followed for either an optimisation or a geometry refinement.

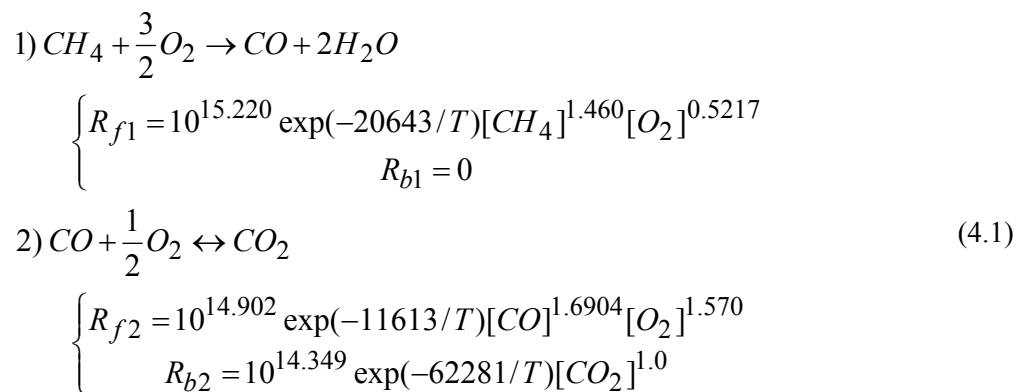
#### 4. CFD SIMULATION

In previous section 2 we have referred to a number of authors who have addressed their studies to the simulation of the combustion development under the typical conditions occurring for the MGT operation. The widely diffused tool for this kind of analysis is the computational fluid dynamics which aims at the solution of the Navier-Stokes equation within a multi-dimensional domain involving reacting species. A proper modelling of the typical phenomena, like the fuel-air mixing the atomisation and evaporation of liquid fuels, the reaction mechanisms and the transport phenomena, can lead to a good predictivity level and therefore to a satisfactory approximation of the real combustor pattern.

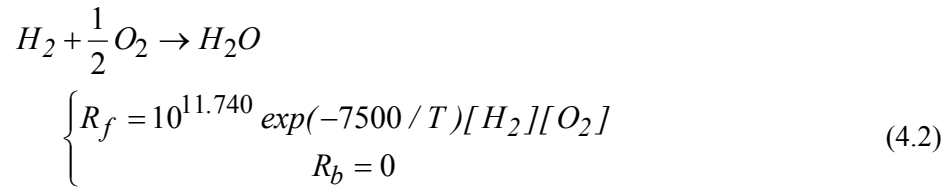
Besides the great number of research experiences in this field which can be found in the technical literature, this section describes the authors' efforts in the CFD based simulation of MGT combustors with examples of reacting flow calculations throughout the three configurations described in section 3. Thus this section should not be intended as an exhaustive discussion of the CFD potentials, but it should rather be considered as an assessment of the procedure to be followed for setting up a numerical simulation and analysing the results.

The flow solver mainly used by the authors was the *KIVA3V* [37], whose main-characteristics are recalled in the following:

- The code performs the solution of the unsteady Navier-Stokes system of equations with an arbitrary Lagrangian-Eulerian method [36]. Viscous flow effects, and the fuel-air mixing and turbulent chemistry rates as well, are approached with a classical two-equation ( $\kappa$ - $\varepsilon$ ) model.
- For estimating the chemical reaction rates, both solvers assume the finite rate – eddy dissipation model. A global two-step methane oxidation mechanism was introduced [38, 39]:



- Regarding to the hydrogen oxidation , a single step reaction was assumed, of the type:



- In terms of kinetically controlled mechanism, the generic kinetic reaction ‘r’ involving *NSP* species proceeds at a rate given by:

$$\omega_{k,r} = R_{fr} - R_{br} = k_{fr} \prod_{m=1}^{NSP} (C_m)^{a_{mr}} - k_{br} \prod_{m=1}^{NSP} (C_m)^{b_{mr}} \quad (4.3)$$

where  $k = C_e T^x e^{-(E_a/T)}$ ,  $E_a$  being the activation energy, and  $a_{mr}$ ,  $b_{mr}$  are integral stoichiometric coefficients. The forward and backward reaction rates,  $R_f$  and  $R_b$ , are those in equations (4.3) and (4.4).

The turbulent mixing-controlled rate,  $\omega_{t,r}$ , is obtained by the Magnussen and Hjertager model [20], namely:

$$\omega_{t,r} = C * \varepsilon / \kappa * \min(x_f, x_{ox}) \quad (4.4)$$

where  $x_f$  and  $x_{ox}$  are the mass fractions of fuel and oxidant,  $\kappa$  and  $\varepsilon$  the turbulent kinetic energy and its dissipation rate,  $C$  is the proportional factor in the mixing-controlled turbulent combustion varying with both flow conditions and fuel composition.

The actual reaction rate is then calculated as:

$$\omega_r = \min(\omega_{k,r}, \omega_{t,r}) \quad (4.5)$$

The set of chemical kinetics equation is completed by those of the extended Zel’dovich mechanism [41] for the prediction of thermal nitric monoxide formation. The equations are simultaneously solved in each computational cell by an algorithm that determines the formation rate of the species involved in the process, as described in section 3.

Two empirical correlations for the auto-ignition delay time of methane are used in some of the test cases presented. The first one has been generated by Spadaccini et al. [52] and the auto-ignition delay is calculated as:

$$\tau = 2.21 \times 10^{-14} \exp(22659/T) [O_2]^{-1.05} [CH_4]^{0.33} \quad (4.6)$$

The validity is limited to temperatures of 1300 K and above. So the correlation by Li and Williams [53], for the low temperatures defined as less than 1300 K, is also introduced:

$$\tau = (2.6 \times 10^{-15} [O_2]^{-4/3} [CH_4]^{1/3}) / T^{0.92} \exp(-13180/T) \quad (4.7)$$

Although the above equations identify the auto-ignition threshold, in this first application they are assumed to be able to establish a flammability criterion since they incorporate information about the local

fuel to air equivalence ratio. The values of  $\tau$  are, in fact, sensitive to the oxidant and fuel concentrations. Either an excess in fuel contents or an oxygen lack would increase the delay times and the mixture ignition could not take place within the computational cell.

The delay time concept is transformed into a spatially delayed ignition by comparing the  $\tau$  values with those,  $\tau'$ , necessary for the mixture to reach each computational cell, say:

$$\tau' = \frac{\sigma}{V'} \quad (4.8)$$

where  $\sigma$  is the distance between the injector location and the cell and  $V'$  is the average velocity along the same direction. The ignition occurs wherever the  $\tau' > \tau$  condition is fulfilled.

Since the code performs the numerical solution of time-dependent equations, the accuracy is ensured by an appropriate choice of the grid size and the time step must meet stability criteria. This condition originates from the fact that each time interval requires the simultaneous solution of the main flow equations and of the several sub-models and a fully-implicit procedure is almost impossible. The solver incorporates therefore a number of stability criteria and the value of each new time step is updated by applying the most restrictive condition.

The time-dependent solution may be addressed to different purposes, say:

- **A steady, reacting flow problem.** In this case, constant boundary conditions are imposed and arbitrary initial conditions within the computational domain are assigned. Since the initial conditions do not match those at boundaries a numerical unsteadiness takes place and the convergence of the *time-marching* process must be reached. Of course, only the converged flow field is of interest.
- **An unsteady, reacting flow problem.** A physical unsteadiness, and therefore an actual transient development, occurs because of a sudden or a continuous change of the boundary conditions with time. In this case the CFD analysis aims at the evaluation of the time-varying flow field and combustion behaviour throughout the combustion chamber.

In both cases, the computation must start with a proper assignment of both boundary and initial conditions. In the authors' experience an effective way for performing a realistic flow analysis of the combustor is to assign both kind of conditions accordance with the results of a preliminary thermodynamic simulation of the gas turbine operation. In particular:

- The inlet boundaries are assumed to be of the velocity inflow type: therefore the inlet axial velocity is calculated, for given thermodynamic conditions, to meet the actual amount of air flow rate entering the combustor, which is automatically split into the primary air and the secondary and dilution air flows through the liner;
- The inlet temperature, in accordance to the recuperator exit levels, must be imposed;
- The static pressure at combustor exit is determined by starting from the inlet total pressure level and evaluating the outlet velocity level and a total pressure loss (nearly 3% of the total inlet pressure) through the combustion chamber;
- A swirled intake air flow is assigned into the primary zone, so concluding the velocity component assignment. For example, to the sake of an uniform comparison of the combustors, the same swirl angle of 45 degrees was hypothesised at the primary burner inlet. The actual computation of the swirled flow through the inlet bladed channel, although possible for the lean-premixed combustor, seemed to be beyond the scope of this work.

- Two turbulence parameters must also be assigned at the inlet boundary, say the turbulent kinetic energy and the dissipation rate. In all cases, the related values were evaluated by assuming a 10% level of turbulence intensity and an appropriate hydraulic diameter in accordance with the inlet channel size.

In the following examples of the CFD based methodology are presented, with reference to a number of general topics about the MGT combustion, as discussed above

### 4.1 Scaled Combustors

In section 3 we have outlined the possibility of adopting an annular combustor in the MGT operating field, by scaling the flow areas and preserving the axial length and thus the residence times. The reason for this choice originates from a preliminary comparison of two different scaling criteria, say:

- 1) Only the flow areas are reduced by a proper scaling ratio.
- 2) Both flow areas and axial length are scaled, the latter by the linear scaling ratio of 3.65.

The second option would better fit the overall MGT dimensions but a reduced residence time is available for the combustion completion.

As stated, the calculations were performed with a time marching procedure and figure 4.1 shows a typical convergence history, in terms of the gas exit mass flow rate. Both computations achieve the convergence after nearly 3000 time steps and the comparison shows that the same level of accuracy is practically obtained. The flow distributions are compared in the mid plane of the computational domain (i.e., a 3D sector of 12°) and they allow estimation of the main differences between the flow pattern throughout the differently scaled combustors. Figure 4.2(a) displays the levels of velocity magnitude which present significant differences which can affect the whole process. First, the combustor with the scaling criterion (1) exhibits a higher velocity level in the central core of the primary zone, while the second one presents a rather slower flow, probably because of the more enhanced shift of the streamlines towards the endwall regions (fig. 4.2. b). This difference could affect the actual residence time of the reactants within the primary zone. Secondly, the interaction of the main flow with those from the secondary and dilution holes results in different developments towards the combustor outlet. In particular, the velocity distribution in the first scaled combustor appears to be much more uniform than in the second one.

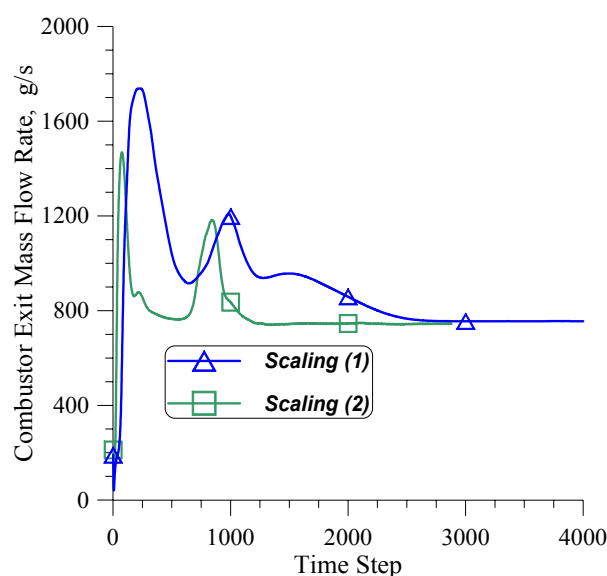


Figure 4.1: Convergence Histories of the CFD Calculations.

Looking at the turbulence parameters in fig. 4.2 (c) and (d), the turbulence intensity in the second combustor is rather higher in the primary zone and also the eddy dissipation rate (in terms of the local  $\varepsilon/k$  ratio) present increased values in correspondence of the first and second rows of the secondary holes. These observations can explain that higher reaction rates can be expected for the fully scaled combustor, so compensating the reduced length and allowing a proper combustion completion.

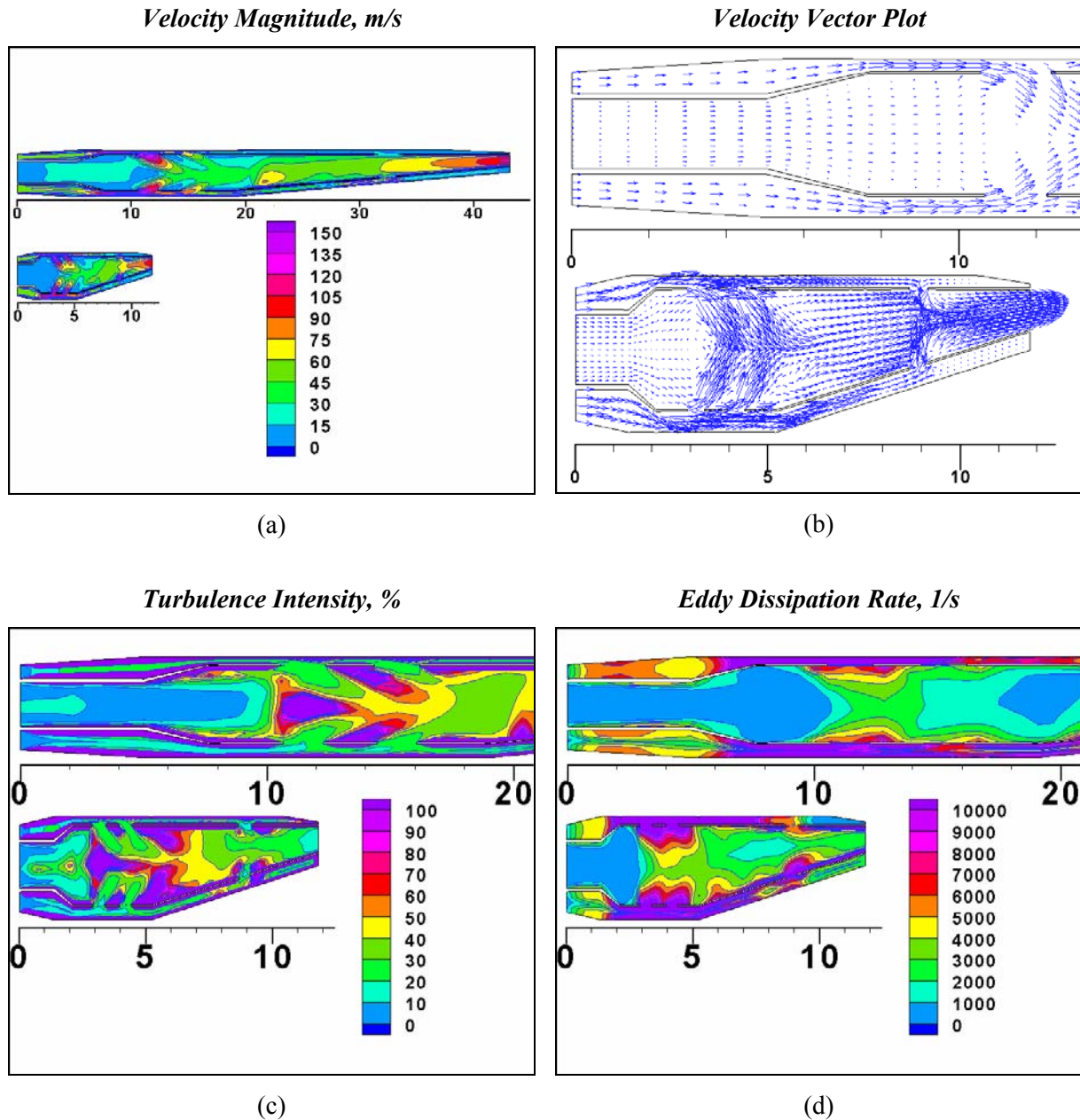


Figure 4.2: Velocity and Turbulence Parameter Distributions in the Combustor Mid-Planes.

Actually, the distributions in figure 4.3 confirm that the fuel consumption is completed within the primary zone (fig. 4.3a) and in both cases the residual carbon monoxide is oxidized in the secondary zone (4.4a). Therefore also the reduced length combustor, which better meets the requirements for MGT applications, could ensure a satisfactory combustion efficiency.

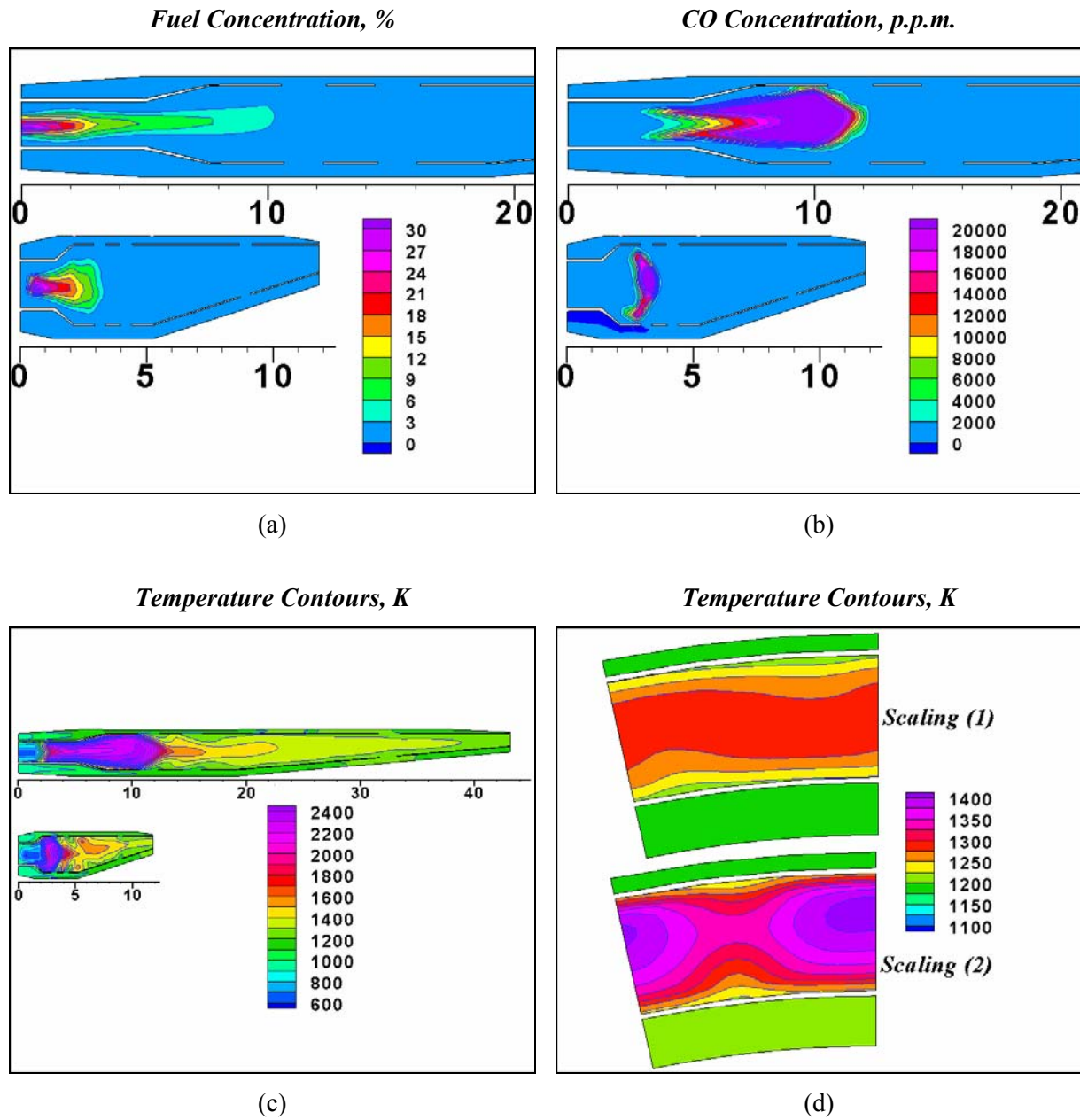


Figure 4.3: Temperature and Species Distributions in the Scaled Combustors.

It should be reminded that the example refers to combustors of the diffusive type, thus with a high fuel concentration in the injection zone and no fuel-air premixing. Consequently the meridional temperature distribution (fig. 4.3c) presents typical peaks of more than 2200K and the radial extension of the high temperature zone is slightly increased in the fully scaled combustor because of the flow field pattern. A less encouraging result is in terms of the temperature uniformity at the combustor outlet. The same figure 4.3(c) shows that the reduced length of the dilution zone prevents an efficient mixing of the exhausts with the diluting air. The consequent temperature distribution in the outlet plane (fig. 4.3d) is much more ineffective in the second combustor, with larger hot spots which are unacceptable for the safe operation of the turbine vanes specially. Really a wide temperature scattering from the expected average firing temperature conflicts with the eventual choice of uncooled blades.

A final comparison is presented in fig. 4.4 on terms of axial development of the temperature profiles and thermal NO concentrations. The first diagram (fig. 4.4a) confirms the existence of relevant peaks within the primary region and of the quick temperature drops because of the air addition through the secondary and dilution holes. The outlet temperatures are nearly the same but the temperature distributions in the previous figure 4.4d highlight that relevant hot spots may still exist in the exit plane, specially for the second combustor. In the latter case, the thermal NO development in fig. 4.4 (b) seems to be smoother because the reduced residence times play a favourable role under this point of view: the nitric oxide formation is clearly slower and the related peak is considerably shifted forward and the kinetic mechanism is promptly stopped by the air addition. This last consideration is the most encouraging for adopting the reduced length combustor, even if the final NO concentration is above the typically acceptable limits.

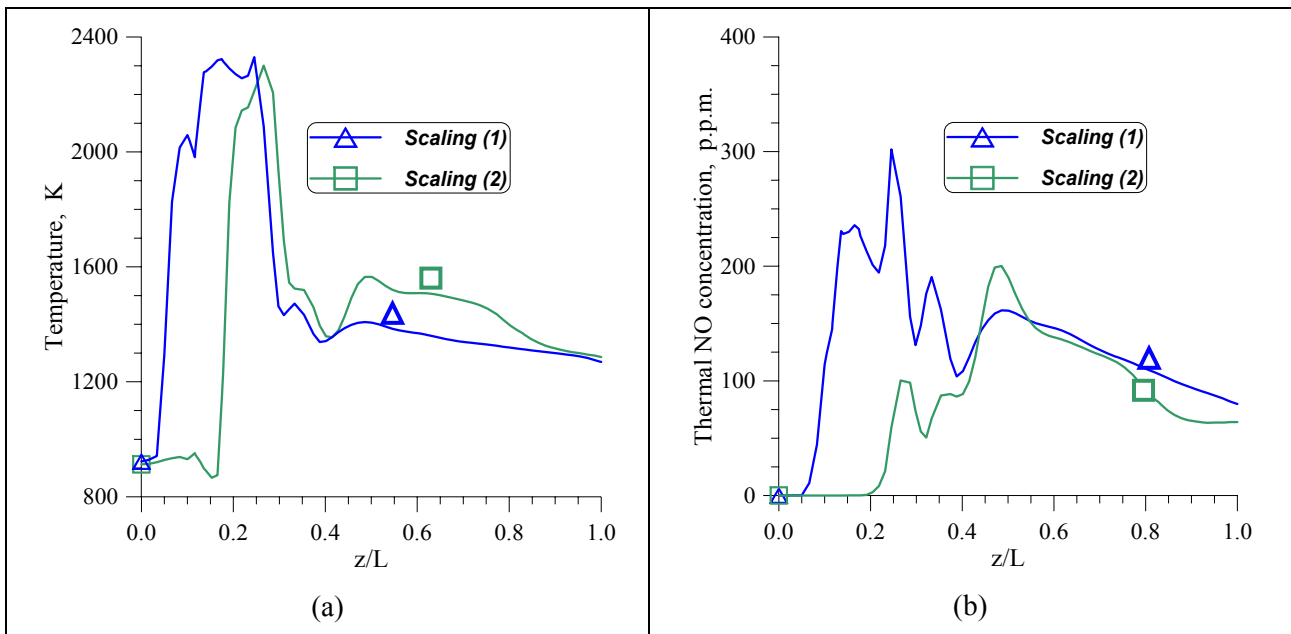


Figure 4.4: Axial Distribution of Temperature and Thermal NO in the Scaled Annular Combustors.

Summarizing the comparison of the two scaled combustors, it may be concluded that in the case of a diffusive combustion chamber the major obstacle to the adoption of a reduced length is represented by the unfair temperature distribution in the exit plane, since no relevant residual of carbon monoxide or unburned species is observed. More challenging problems could arise with lean-premixed combustors and this suggests the comparison of different concepts, like those listed in the previous section 3.2.

## 4.2 Comparing the Different Combustors

This section summarizes an authors' work aiming at the comparison of the fluid-dynamic behaviour of the three combustors described in sect. 3.2 [58]. The solution is obtained in periodical computational domains and details of the block-structured meshes are given in figure 4.5.

Although the technical literature is almost definitely oriented to the lean-premixed concept, a proper evaluation of the potential of different combustor concepts is helpful for the ultimate choice of the optimal solution. The purpose of this analysis was therefore an assessment of the several problems which may take place in terms of combustion development and completion, pollutant formation and part-load operation as well. The off-design conditions induced by either the recuperator by-pass or the low BTU fuel supply were also examined.

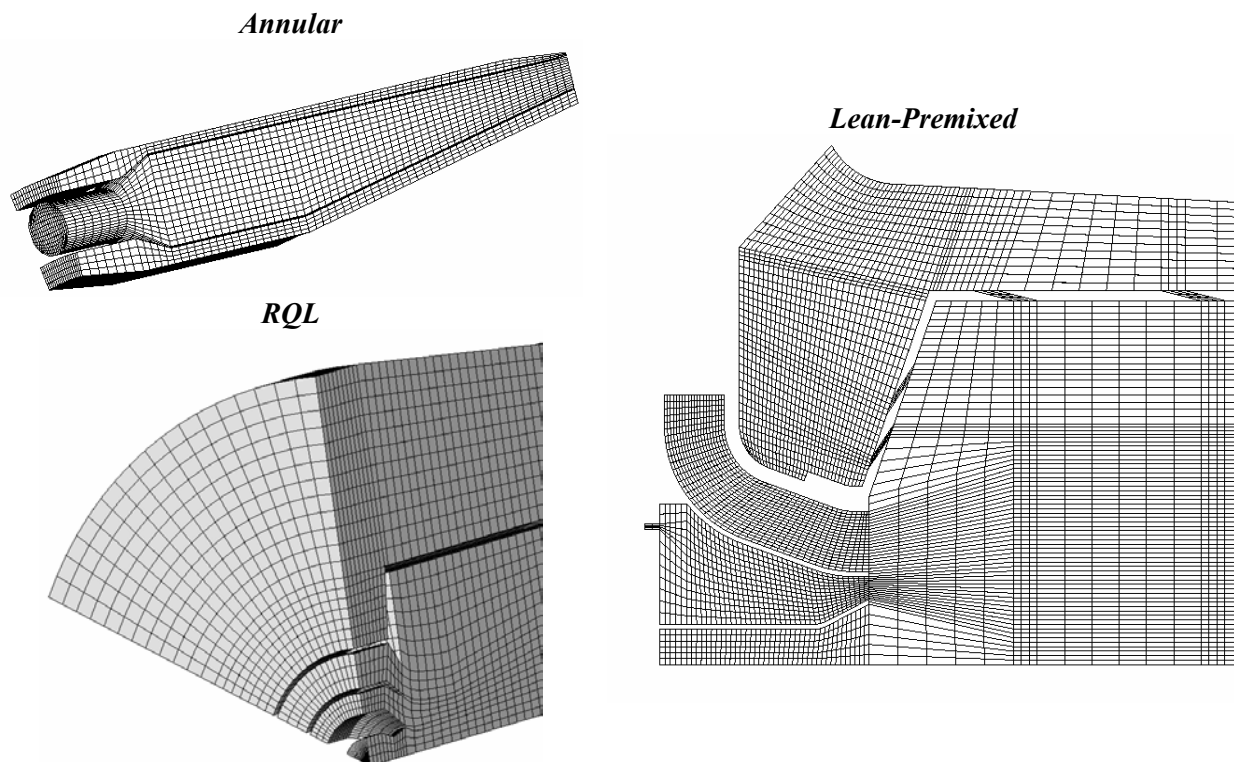


Figure 4.5: Details of the Computational Grids.

Table 4.1: Mean Time Steps and Average Values at Combustor Exit

	<i>COMBUSTOR</i>	$\bar{\Delta t}$ s	$\bar{T}_{ex}$ K	[NO] p.p.m.	[CO] p.p.m.
<i>Nat. Gas,</i> $X_b = 0$ <b>Full Load</b>	<i>Annular</i>	$6.5 \times 10^{-6}$	1268	66.9	.003
	<i>Lean-Premixed</i>	$4.3 \times 10^{-6}$	1217	26.4	4.42
	<i>RQL</i>	$4.0 \times 10^{-6}$	1247	149.6	1526
<i>Nat. Gas,</i> $X_b = 0.9$ <b>Full Load</b>	<i>Annular</i>	$5.0 \times 10^{-6}$	1286	10.5	.005
	<i>Lean-Premixed</i>	$3.7 \times 10^{-6}$	1194	32.6	157.0
	<i>RQL</i>	$3.8 \times 10^{-6}$	1198	55.7	865
<i>BIOM(O),</i> $X_b = 0$ <b>Full Load</b>	<i>Annular</i>	$7.5 \times 10^{-6}$	1269	87.6	5.5
	<i>Lean-Premixed</i>	$4.4 \times 10^{-6}$	1244	36.3	8.5
<i>Nat. Gas,</i> $X_b = 0$ <b>Part Load</b>	<i>Annular</i>	$7.3 \times 10^{-6}$	1072	42.4	--
	<i>Lean-Premixed</i>	$3.1 \times 10^{-6}$	1047	17.4	0.27
	<i>RQL</i>	$4.4 \times 10^{-6}$	1083	132.0	1218

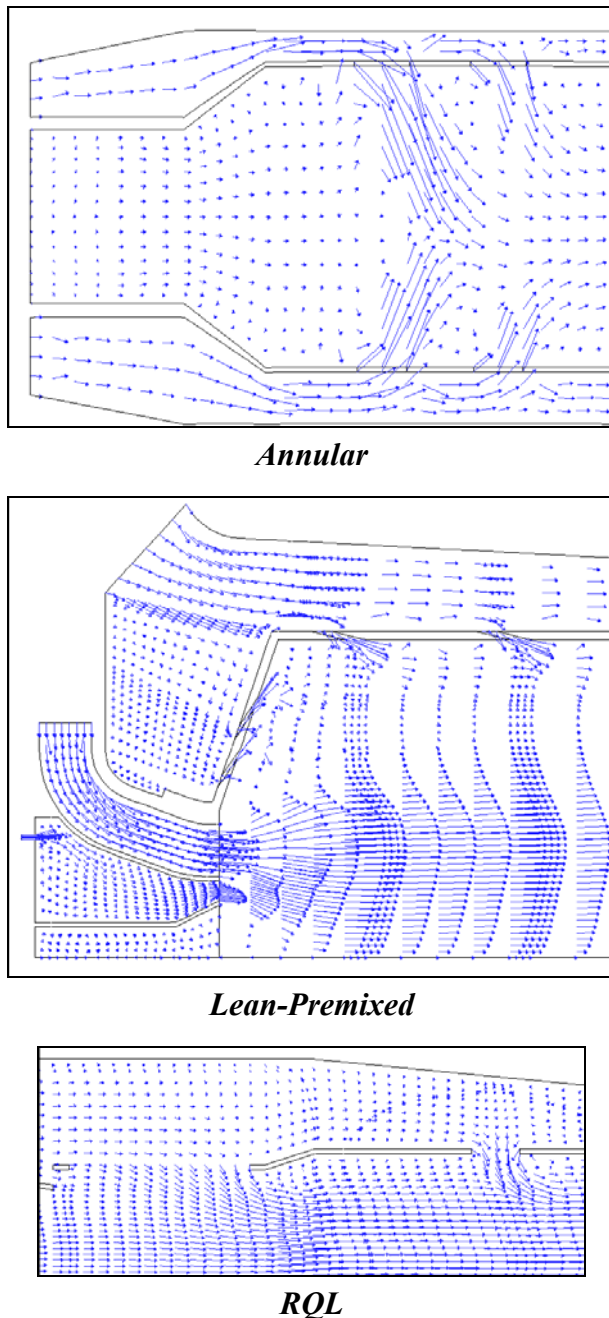


Figure 4.6: Details of Velocity Vector Fields.

combustor presents a good penetration of the secondary air within the primary flow so that an early combustion completion can be expected. The lean-premixed combustor can be examined in the primary region, with reference to the interaction between the flow from the pilot and the premixed line, which is responsible for the mixture ignition.

Regarding to the RQL chamber, it must be recalled that a satisfactory dilution jet penetration at the quench stage is required. A preliminary analysis of the flow distribution in the quench zone (fig. 4.6) highlights that the intensity of the flow vorticity is not sufficient to decrease the combustion temperature of the flow from the primary region.

A synopsis of the final results is given in table 4.1, which reports the average computational time step,  $\overline{\Delta t}$ , and the weight-averaged values of the combustor exit temperatures and pollutant concentrations at computation convergence. It is worth-noting that the differences in the exit temperatures depend on the actual combustion completion (thus on the presence of unburned or partially-burned species) and on the different heat transfer rates which were evaluated by assuming the same wall temperature (of 1000 K at full-load and 900K at part-load conditions) in all cases. Under this point of view, the greater penalty affects the lean-premixed chamber.

The latter exhibits, as expected, the most favourable behaviour in terms of thermal NO concentration which remains at acceptable levels even in the case of the hydrogenated *BIOM(o)* fuel. When lower air inlet temperatures occur, the lean-premixed combustor shows a CO increase, certainly due to the greater amount of fuel supplied to the pilot line. The annular combustor is the most effective one in terms of combustion efficiency, as confirmed by the lowest contents in carbon monoxide, but the NO production is higher than in the lean-premixed chamber. The RQL combustor presents unfair results in terms of outlet pollutant concentrations, so suggesting that the arrangement of the several regions would need a further optimisation.

The flow fields and property distributions are discussed only in the baseline case, i.e., natural gas fuelling at full load and  $X_b = 0$ .

Figure 4.6 provides some details of the velocity vector fields in the most representative regions of each combustor. For instance the annular

Consequently, the temperature distributions in fig. 4.7 exhibit an adequate uniformity at the combustor outlet in the case of the annular chamber, while a poor interaction of the primary jet with the diluting air is observed in the lean-premixed one, thus producing a relevant span-wise temperature gradient. As expected, the quenching effect in the RQL chamber is not properly accomplished. In this way, a longer lean zone could be needed as to complete the combustion (fig. 4.8). A further effect of the fuel concentration in fig. 4.8, is given by the relevant CO contents at the outlet of the same chamber (see table 4.1) as a typical result of an incomplete combustion. Both the annular and the lean-premixed chamber exhibit, on the contrary a more regular fuel consumption and the CO production is satisfactorily bounded.

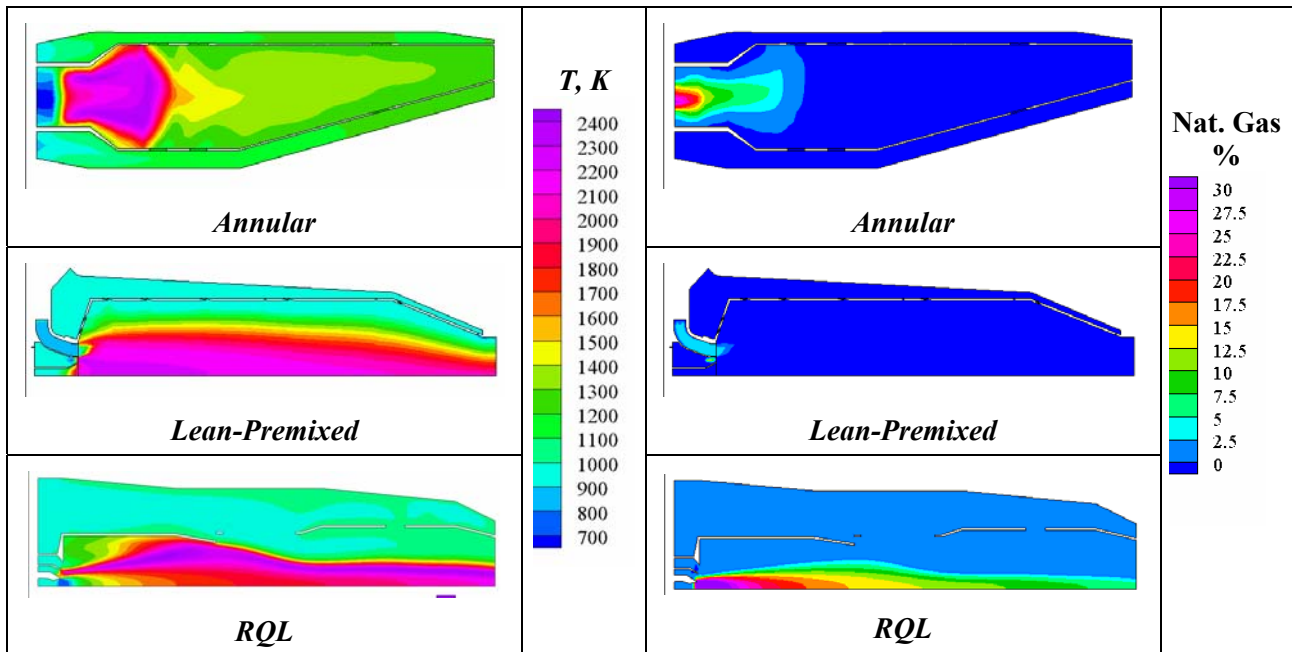


Figure 4.7: Comparison of Temperature and Fuel Distributions in the Combustor Meridional Plane (full load,  $X_b = 0$ ).

The curves in figure 4.8, which refer to axial distributions evaluated along straight lines intersecting the outlet section at mid-span. In particular, figures 4.8 (a) and (c) show the axial trends of the temperature and NO values and the highest values are attained in the secondary and dilution zones by the RQL chamber. In the latter combustor the tail of the combustion development produces a restart in both CO and NO productions closely to the outlet station.

The response of the annular combustor is that typical of a primary stoichiometric combustion and the related peaks are suddenly cut-off by the secondary air supply. A more progressive behaviour can be observed in the lean-premixed chamber with a smoother decrease of all values to the final levels.

Figures 4.8 (b) and (d) are an attempt to establish a relationship between the turbulent reaction rate ( $TRR$ , evaluated by eq. (4)) and the natural gas consumption. The turbulent mixing rate, and the  $TRR$  levels, appears to be sufficiently high in the case of both the annular and the lean-premixed combustors, and this results in a satisfactory combustion completion within the early region of the burner. On the contrary, poor  $\varepsilon/\kappa$  and  $TRR$  levels are achieved in the RQL combustor and this is in accordance with the inefficiency detected for the quenching and lean zones.

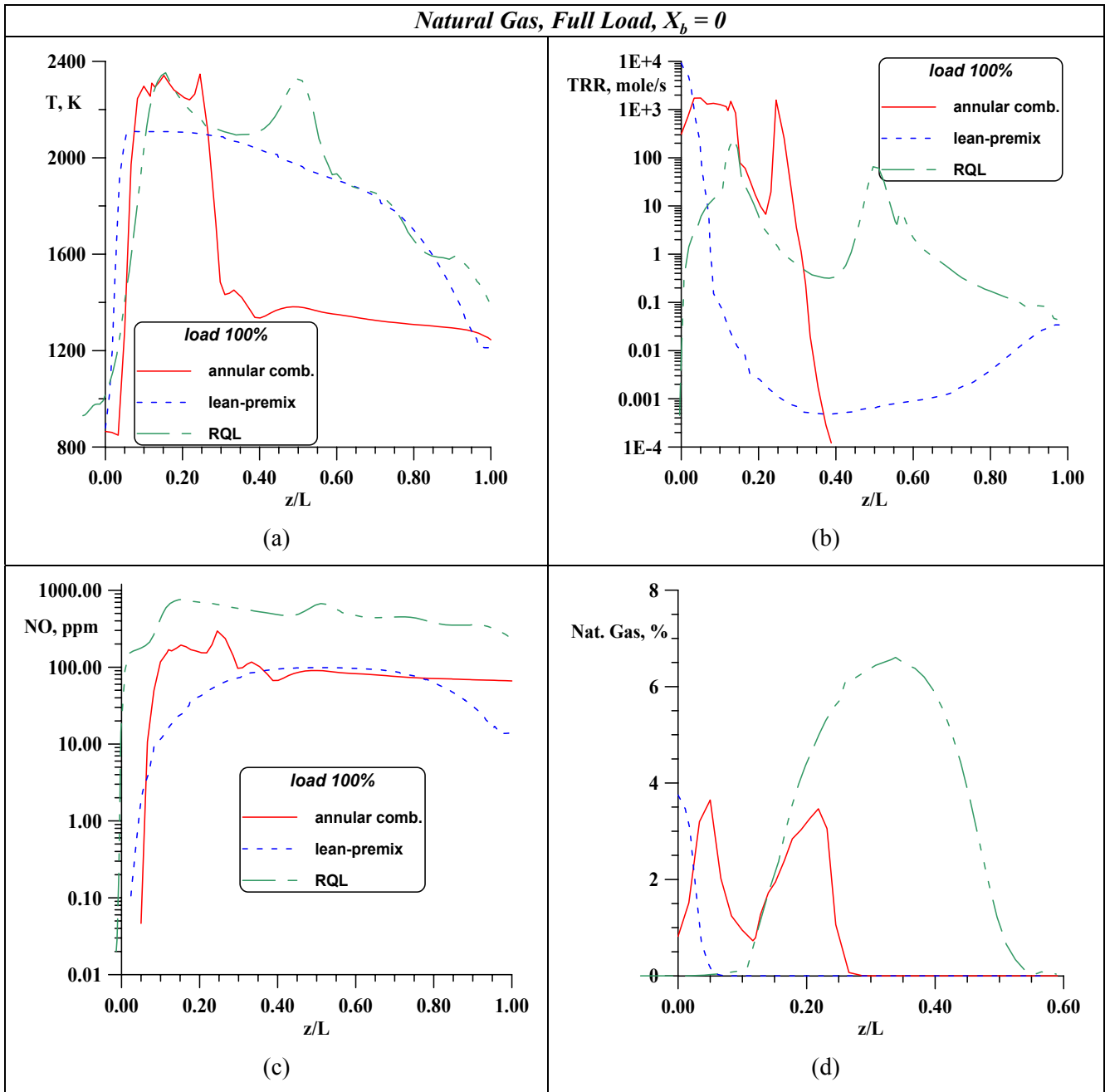


Figure 4.8: Axial Distributions of Temperature, Nitric Oxide and Combustion Rates.

### 4.3 A Fully 3D Analysis of the LP Combustor

The above section leads to the general conclusion that the widely employed solution of the lean-premixed combustor seems to be the one that most properly fits the requirements for the combustion process within the MGT operating conditions. On the other hand the previous analysis was conducted within reduced computational domains and a number of aspects have been left poorly investigated. For instance:

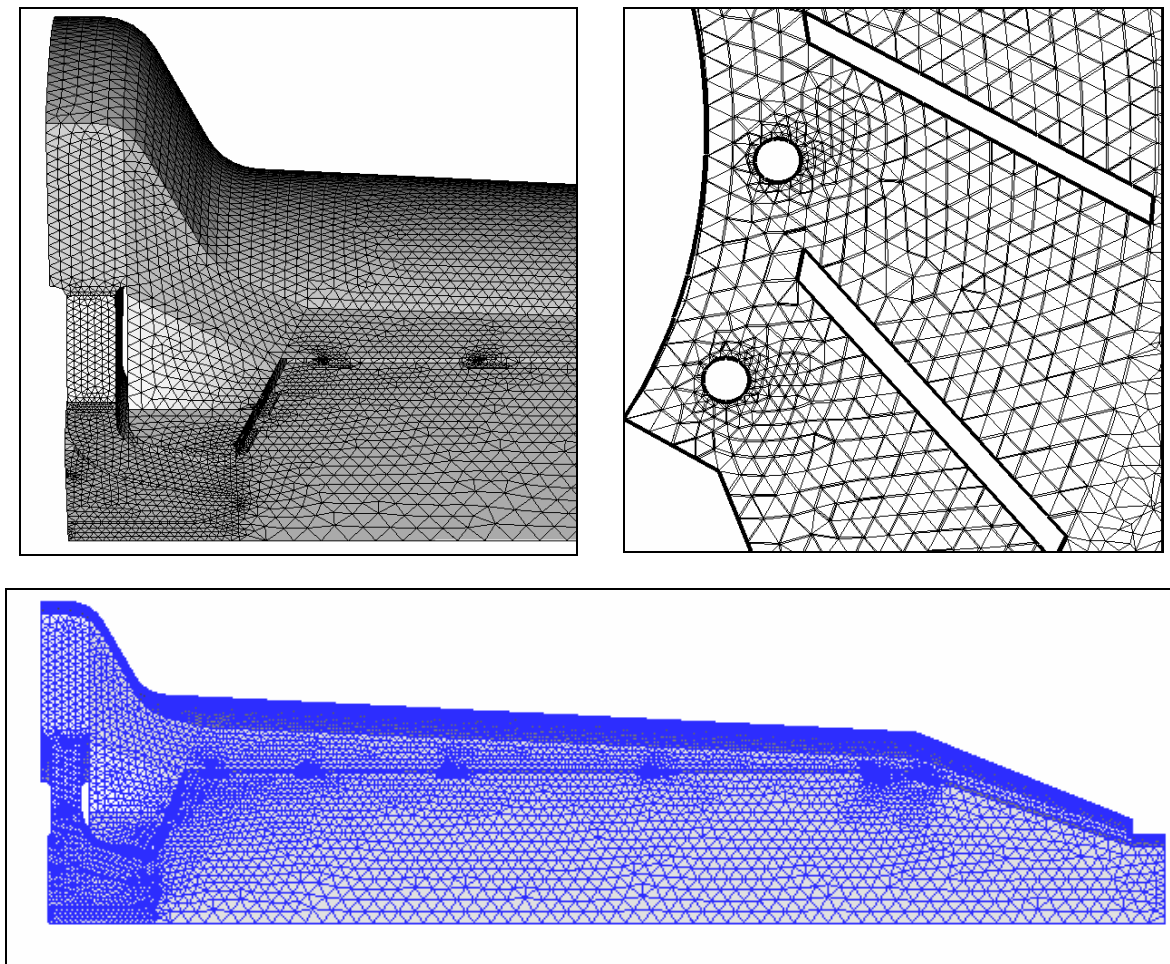
- The air splitting between the premixing line and the external liner was assigned. Really, the air flow rate to the different combustion regions originates from the flow entering the same combustor inlet area. The amount of air which is addressed to each region results from the whole flow

distribution throughout the combustor, so including the flow trough both the swirling vanes and the cooling and dilution ports.

- Similarly, the actual swirl angle of the flow entering the primary region must be properly assigned as a result of the velocity conditions downstream of the radial vanes (fig. 3.7b). The flow evaluation in this zone also requires a particular care because it directly precedes the air and fuel mixing process.

For these regions, at least a limited number of fully 3D computations within a well resolved domain are needed: besides the obvious purpose of an accurate CFD analysis of the combustor, a proper post-processing of the flow data may provide the boundary conditions for faster calculations within less refined domains like those employed for obtaining the results in section 4.2.

The fully 3D computations were performed with the *FLUENT*® flow solver within a computational domain referring to a 60° periodical sector. The accuracy is ensured by an unstructured grid of 765000 cells which allows a proper resolution of the most critical zones in the flow field (fig. 4.9).



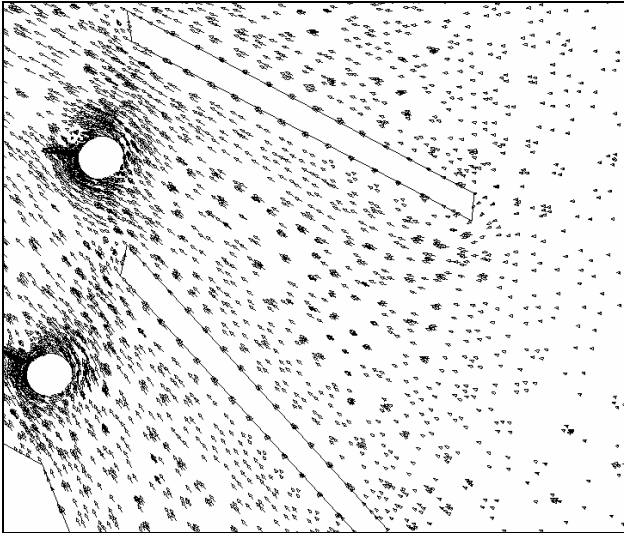
**Figure 4.9: Details of the Unstructured Mesh in the 3D Periodical Sector.**

Fig. 4.10 presents the flow distribution in a plane of the swirling blade cascade. The flow field interaction with the sharp blades and the injectors just downstream may be appreciated in fig. 4.10(a) while fig. 4.10(b) gives details of the velocity intensities. The flow angle distribution reaches a fairly uniform

pattern past the injectors (fig. 4.10c) and the fuel jet past the injectors begins the mixing process with the air (fig. 4.10d).

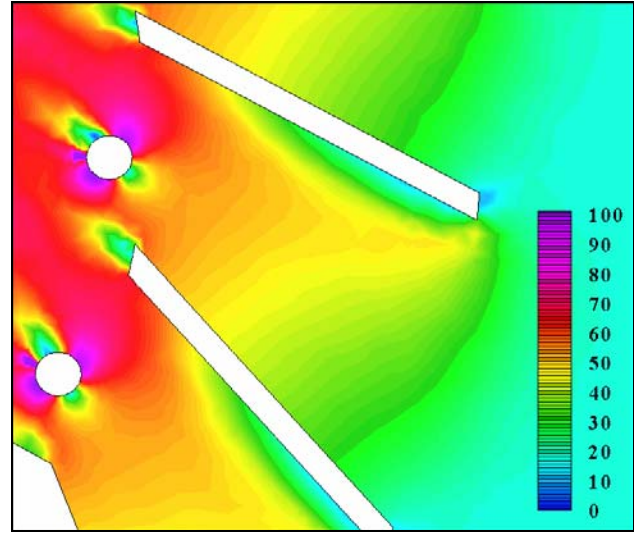
*Natural Gas, Full Load,  $X_b = 0$*

*Velocity Vector Field*



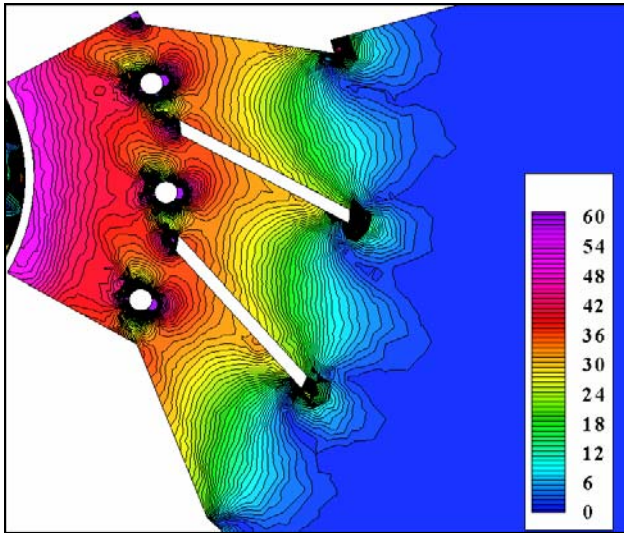
(a)

*Velocity Contours, m/s*



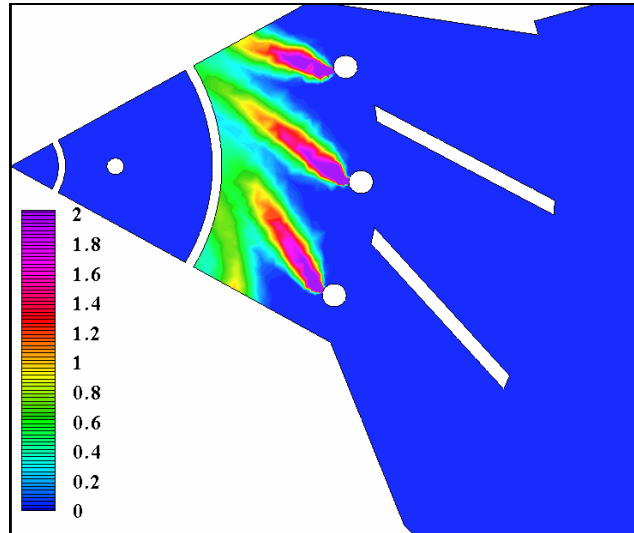
(b)

*Flow Angle, deg*



(c)

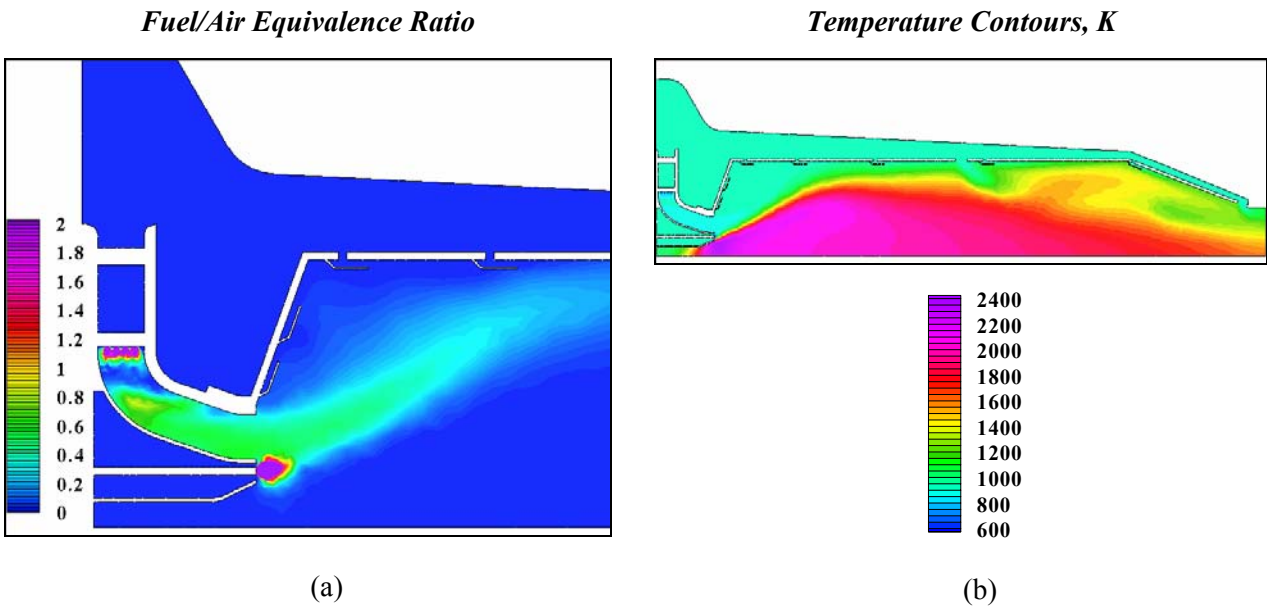
*Fuel/Air Equivalence Ratio*



(d)

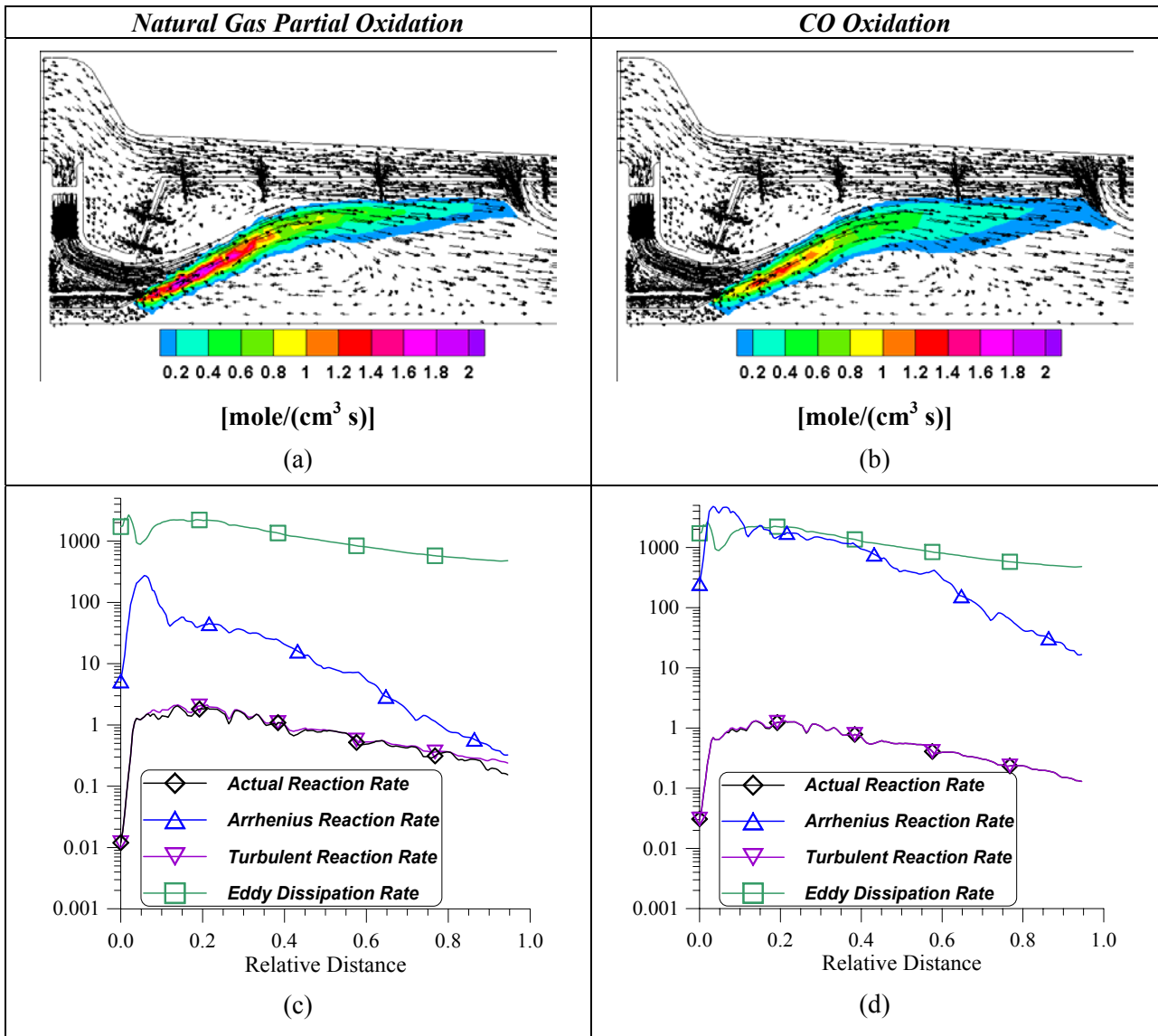
**Figure 4.10: Flow and Fuel Distributions in the Swirling Vane Plane.**

Fig. 4.11(a) confirms that a uniform lean mixture is obtained at the primary zone inlet and it also allows identification of the main directions of the reaction mixture transport. Accordingly, the direction of the flame front can be clearly detected in fig. 4.11(b). The temperature peak is however located in proximity of the pilot flame, originated by the almost stoichiometric mixture from the axial injector (fig. 4.11(a)).



**Figure 4.11: Fuel and Temperature Distribution in a Meridional Plane.**

The interaction of the flow field with the combustion development is displayed in figures 4.12 (a) and (b). The region of the maximum reaction rates is bounded by the two counter-rotating vortices. The higher one also interacts with the air addition from the cooling and diluting holes, and the main effect is the temperature limitation near the liner walls as demonstrated by figure 4.11(b). Figures 4.12 (a) and (b) also show that the reactions are strongly slowed down by the air flow from the diluting holes as confirmed by the temperature distribution in fig. 4.11(b). An interesting analysis of the combustion process is allowed by the figures 4.12 (c) and (d) that display the trend of both the reaction rates and the eddy-dissipation rate along a line inside the region of maximum combustion activity. These diagrams confirm that the overall process is mainly governed by the turbulence, since the actual reaction rate is practically coincident with the one estimated by eq. (4.4) for the turbulent mixing-controlled rate [27]. The methane oxidation is faster than the one of carbon monoxide which extends in a wider region (fig. 4.12(b)).



**Figure 4.12: Reaction Rate Contours ((a) and (b)) and Identification of the Combustion Mechanism ((c) and (d)).**

The distributions in fig. 4.13 are estimated along an axial line intersecting at mid-span both the primary zone inlet and the combustor outlet. The mass fraction behaviour confirms the considerations already made about the different speeds of consumption for natural gas and carbon monoxide. In particular a 36 p.p.m. contents is observed at the outlet station. The temperature distribution in fig. 4.13(b) is typical of a combustion development from lean-premixed reactants with a smoother decrease from the peak of nearly 2100K to the final temperature level. The same figure allows comparison of the axial distribution resulting from the CFD analysis in the fully 3D domain with the one obtained from calculation of a simplified 2D domain. The qualitative accordance is acceptable and the peak location and level are in good agreement. Such a results indicates a basic role which can be played by a hierarchic computational approach, say:

- The fully 3D calculation leads to a correct estimation of some input data, like the mass flow rate subdivision, the swirl angles, the inlet turbulence parameters, etc.
- The 2D analysis may be more extensively applied to parametric studies, optimizing procedures and comparison of many operating conditions with reduced computational costs.

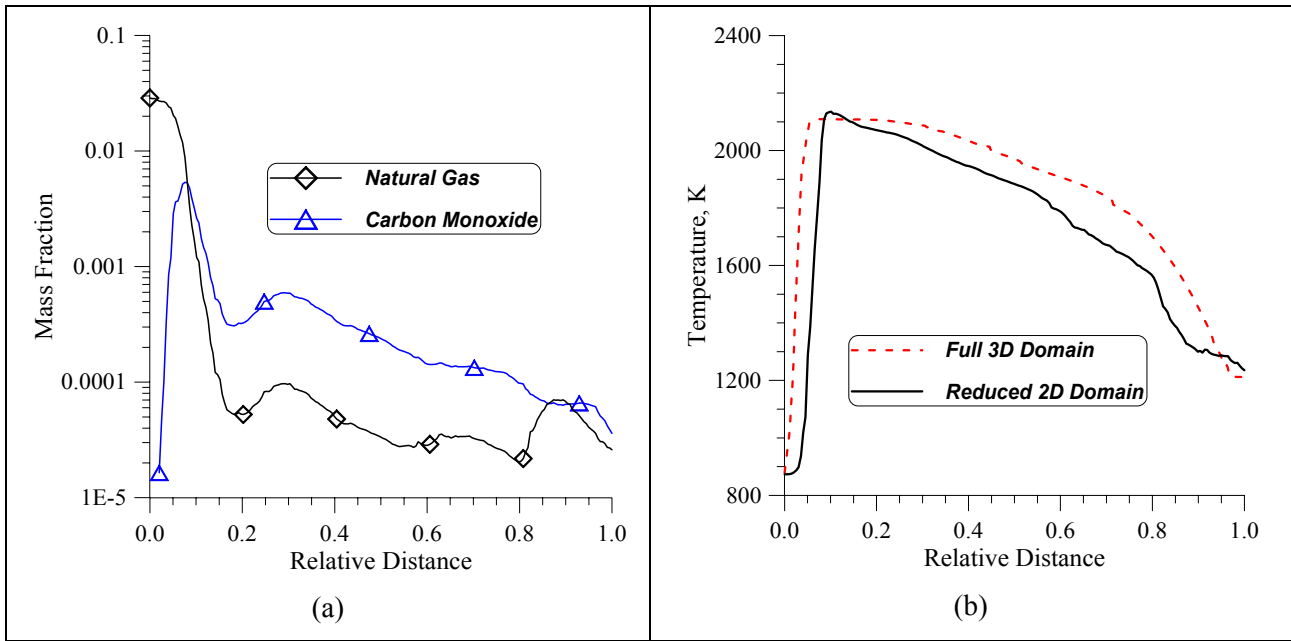


Figure 4.13: Axial Distribution of Burning Species and Temperature.

Such a hierarchic approach has been employed for the final results presented in the following.

#### 4.4 Off-Design Analysis

Basic on the previous assumption, a wide variety of cases may be examined by fast-computations in a 2D domain, for instance if an extensive analysis of part-load conditions must be carried out.

The first example refers to the comparison of the full-load with the 60% load behaviour of the lean-premixed combustion chamber. The data in table 4.2 are employed for assigning the boundary conditions. In addition, the part-load example employs a different partition of the fuel between the pilot and the main fuel line, with an increase of the fuel from the main injector from 10% to 50% of the whole fuel flow rate.

Table 4.2: Computational Cases Considered for the CFD Based Combustor Analysis

	$\dot{m}_a$ kg/s	$\dot{m}_f$ kg/s	$T_{in}$ K	$p_{in}$ bar	$T.I.T.$ K
<i>Nat. Gas, <math>X_b = 0</math> Full Load</i>	.8076	.0069	905.3	3.86	1239.6
<i>Nat. Gas, <math>X_b = 0.9</math> Full Load</i>	.8075	.0146	513.0	3.84	1239.6
<i>Nat. Gas, <math>X_b = 0</math> 60% Load</i>	.8120	.0056	802.0	3.67	1068.7

The effect of the increase of the pilot fuel plays a fundamental role in the temperature distribution (figs. 4.14 (a) and (b)): really, despite a reduced average outlet temperature, the part-load case exhibits a wider region with the temperature peaks. Consequently the NO production, although with a retarded activation of the mechanism, is substantially increased at part-load operation (figures 4.14 (c) and (d)).

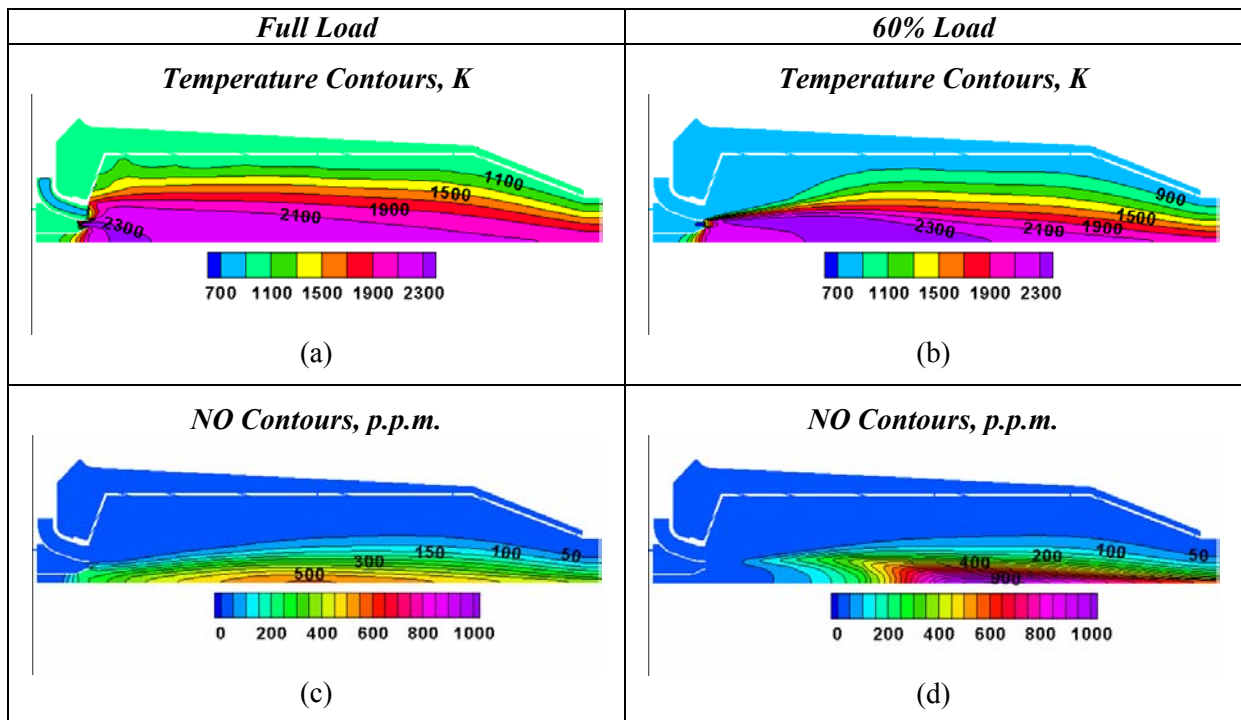


**Figure 4.14: Comparison of Temperature and NO Distributions at Different Load Levels.**

A second example compares the combustor operation with the fully recuperated cycle ( $X_b = 0$ ) with the one with the by-pass opening ( $X_b = 0.9$ ). The latter strongly reduces the combustor inlet temperature (table 4.2) and requires an increased fuel addition for reaching the same firing temperature. Also in this case the fuel to the pilot line must be raised up to the 30% of the total fuel flow rate.

In fig. 4.15 the axial distributions of temperature and thermal NO are compared. The lower combustor inlet temperature results in a more delayed combustion activation so that the peaks of both temperature and NO concentration are shifted forward. At the same time, both peaks are higher than for the normal operation with fully recuperated cycle and, in particular, a reduced path is left for the thermal NO reduction towards the combustor outlet.

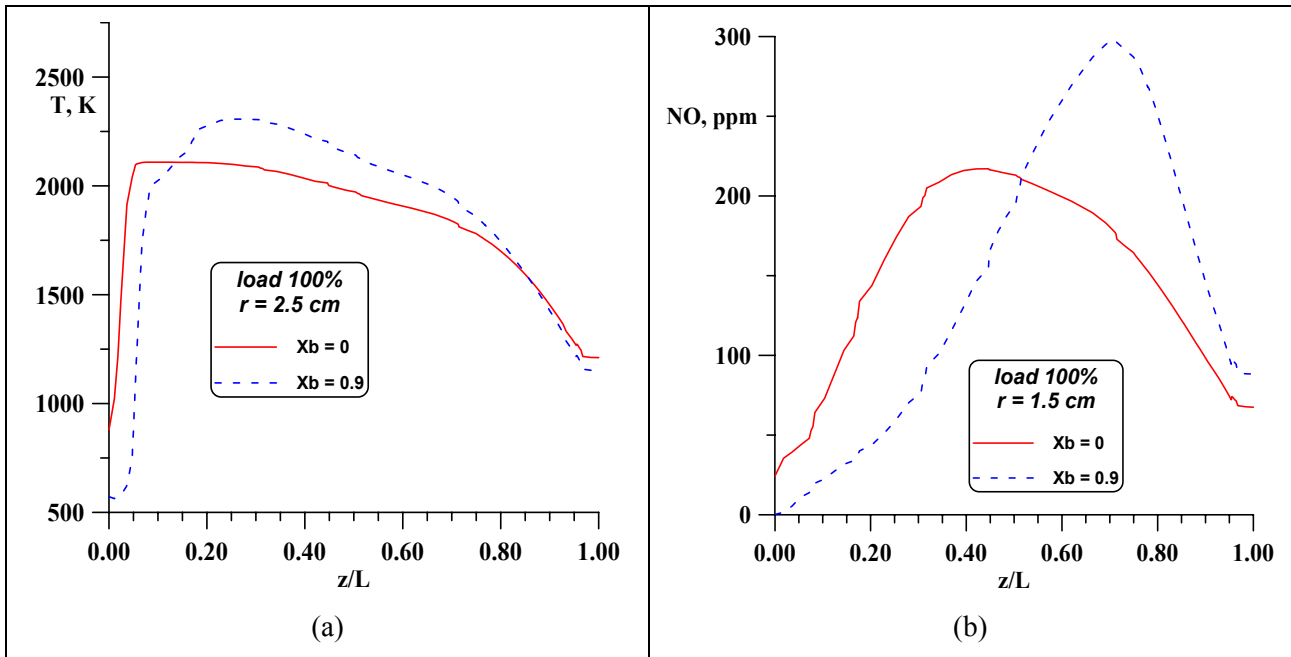


Figure 4.15: Comparison of Temperature and NO Axial Distributions for Fully and Partly Recuperated Cycles.

The more relevant effect of the change in the operating conditions appears clearly to be the dramatically increased CO production. Two concurring causes contribute to the situation displayed in fig. 4.16: the first one is due to the oxygen defect along the flow paths from the pilot line and the second reason is the delayed activation of the methane partial oxidation in the  $X_b = 0.9$  case, so that the full oxidation to carbon dioxide is prevented in a larger zone of the combustor.

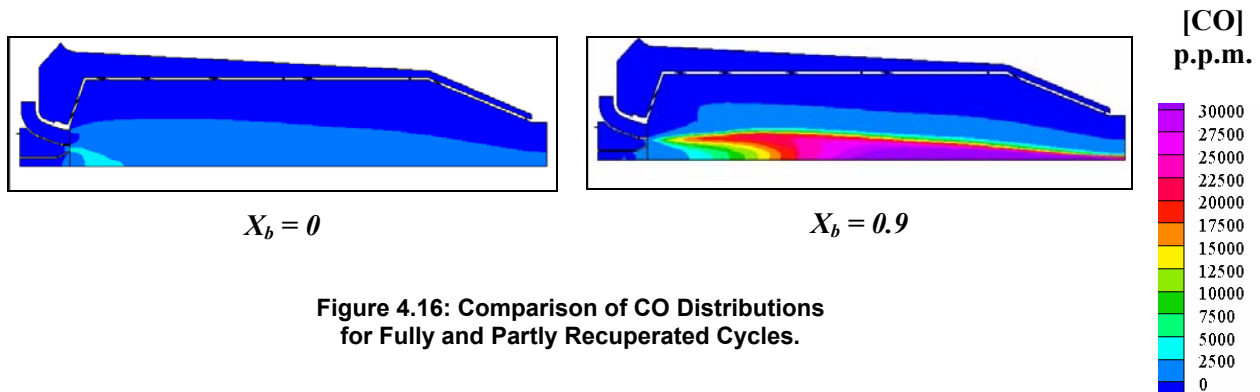


Figure 4.16: Comparison of CO Distributions for Fully and Partly Recuperated Cycles.

#### 4.5 Comparing the Combustor Behaviour with Different Fuels

The preliminary thermo-kinetic analysis in section 3 indicated that employing bio-mass or solid-waste derived fuels may involve a different combustion behaviour. The gaseous fuel composition itself can be responsible for different pollutant production: for instance the *BIOM(O)* and *SW* fuels in table 3 present non-negligible hydrogen contents and the higher flame temperature can enhance the mechanism of thermal NO formation. Generally, if looking at the C/H ratio of the burning species in these alternative fuels, the relative carbon contents is higher than in the natural gas, so that an inefficient combustion development may lead to an increased CO production.

When the gasified fuel has a too limited calorific value the related mass addition could be excessive, so avoiding an easy adaption of the injection system to different fuels. Furthermore, fuels like the *BIOM(a)* one exhibit poor flammability properties, so that a mixture with the natural gas appears to be more appropriate. The comparison of the lean-premixed combustor operation with a conventional natural gas and with a 50% mixture with the *BIOM(a)* fuel in terms of temperature distribution (figs. 4.17 (a) and (b)) shows that an almost similar behaviour can be obtained so encouraging the employment of such alternative energy sources. In this case, the CO production (figs. 4.17 (c) and (d)) undergoes a slight decrease, since a reduced core of formation in the early combustion region can be observed and therefore a longer flow path is available for the complete oxidation.

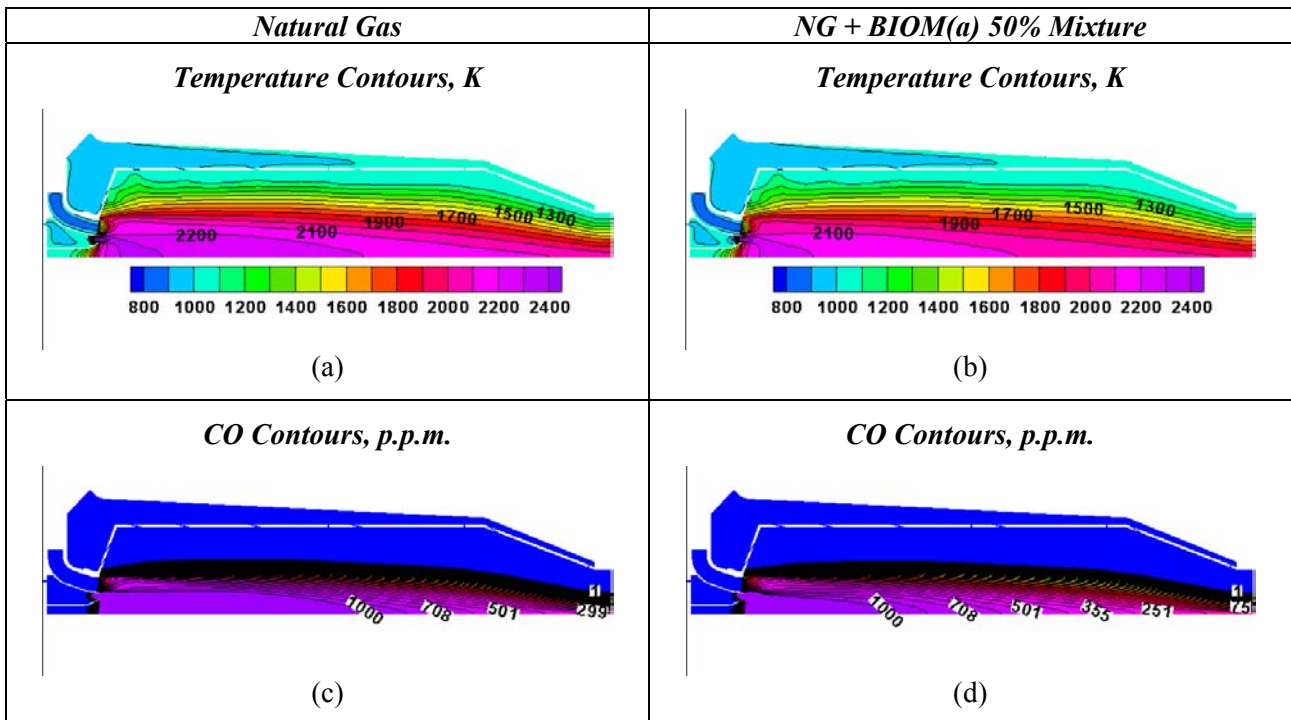


Figure 4.17: Comparison of Temperature and CO Distributions for Different Fuels.

When employing a medium LHV fuel, like the *BIOM(O)* one obtained from the oxygen based gasification of bio-masses, the effect of the hydrogen contents is clearly observed along the straight axial path coming from the pilot line. Really, the almost stoichiometric mixture reaches higher flame temperatures than in the natural gas case (fig. 4.18(a)) and this actually corresponds to a faster rate of NO formation in fig. 4.18(b) close to the pilot location. This slightly conflicts with the preliminary thermo-kinetic analysis but the final concentrations of nitric monoxides are in qualitative accordance with those predicted in fig. 3.2, so indicating a fairly lower production in the *BIOM(O)* case.

The trend of the carbon products is displayed in the following figures 4.18 (c) and (d) and confirm that the main source of CO formation is the stoichiometric region for the pilot line, with a higher concentration resulting from the employment of the *BIOM(O)* fuel. Examining the concentration pattern of CO<sub>2</sub> is of interest for appreciating the satisfactory behaviour of the whole oxidation process, since along a flow path from the premixed line a complete oxidation of the carbon monoxide is obtained.

As a concluding consideration, the response of a lean-premixed combustion chamber to both conventional and alternative fuels is generally suitable with the MGT operation. This results from the acceptable levels of pollutant species in all cases examined at the nominal conditions. Major problems arise in terms of

temperature uniformity at the combustor outlet, since all the distributions in the previous figures have presented a remarkable span-wise gradient around the average level of firing temperature. This results is inconsistent with the need of operating the micro-gas turbine with reduced costs for the cooling system and it is worthy of a further deepening in order to comply with the simultaneous requirement of an efficient combustion within a reduced size device.

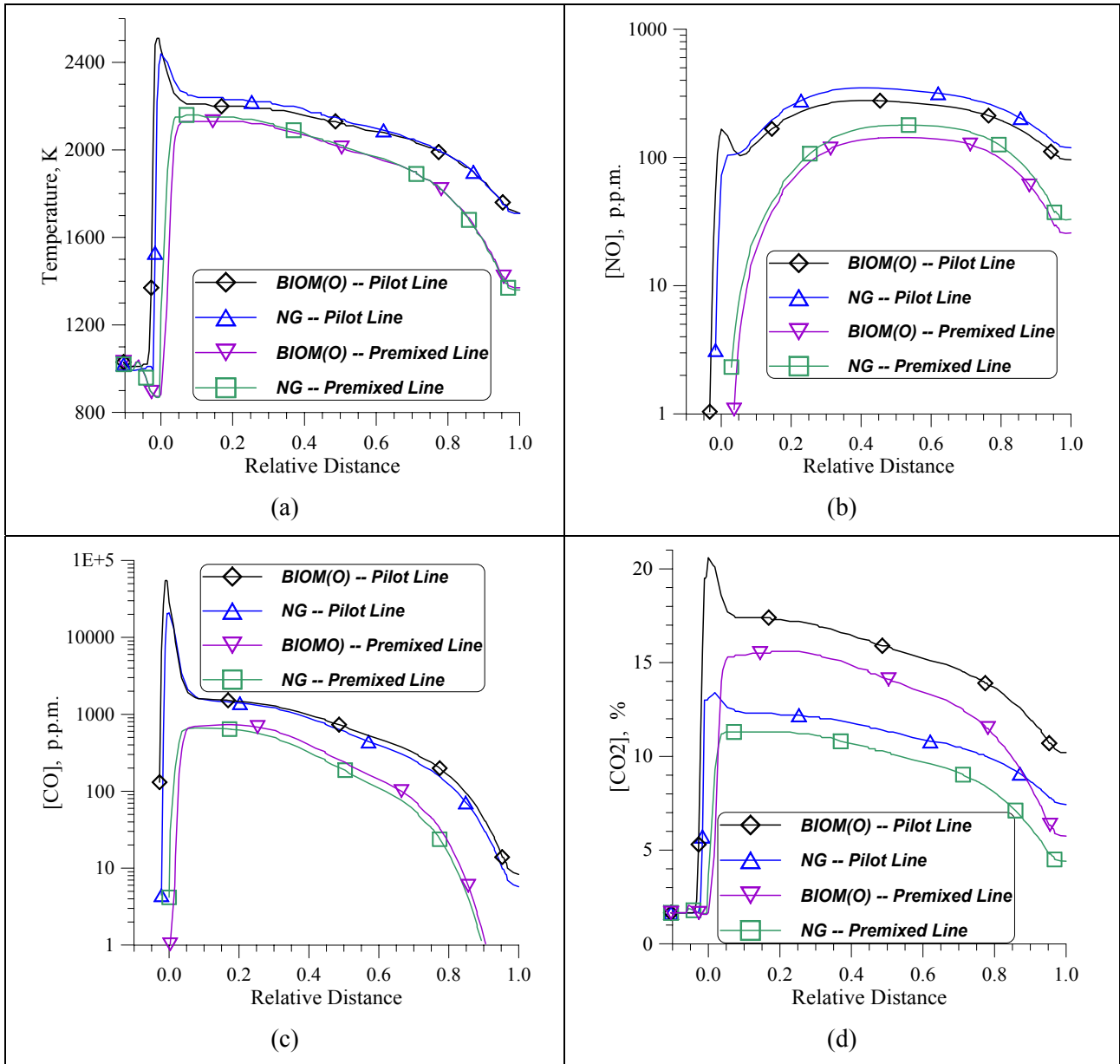


Figure 4.18: Comparison of Axial Distributions for Natural Gas and BIOM(O) Fuels.

## 5. CONCLUSION

This paper has provided a synopsis of the numerous existing examples of MGT combustors as well as of the matters concerning the micro-combustion which are presently only partly solved and are therefore worthy of more deepened studies.

The partial fulfilment of the several requirements can be generally explained by some conflicting situations which arise from both the possible introduction of fuels with different composition and properties and the wide range of mechanical and electrical loads that a MGT based plant should cover. This aspect addresses the efforts of both the researchers and the manufacturers to a multi-objective optimised design and in this sense a fundamental role is played by the CFD simulation as an aiding tool for performing both parametric analyses and optimising procedures.

Looking at more detailed problems involving the combustion process inside small-size combustors, the examples in the final section of this papers have demonstrated that the present technology level is able to satisfy a fast development of the process within limited flow paths: in particular the pilot-assisted, lean-premixed combustion operates with satisfactory levels of both pollutant and unburned species, at least at the base rating conditions. As stated, a greater attention must be paid to some unacceptable temperature gradients through the outlet section and this appears the most challenging problem to be dealt with in terms of combustor fluid-dynamics.

The part-load operation results still effective even if some pollutant increase takes place mainly because of the necessity of sustaining the premixed flame through a stronger contribution of the pilot line. The same practice appears to be less efficient when operating with partially recuperated cycles which involve a larger fuel addition but with a decreased inlet air temperature. The CFD based analysis has shown in this case a simultaneous increase of nitric and carbon monoxides so indicating that the combustor design should be improved, at least in terms of a more reliable concept for the fuel injection system.

As announced, the purpose of this lecture can be considered as achieved if the previous assessment of the MGT combustor problems stimulates the future researchers' work to find the ultimate effective solution.

## **ACKNOWLEDGMENTS**

The researches described in sections 3 and 4 have been carried out also in the course of a cooperation with the *Ansaldo Ricerche* s.p.a. ("Micro-Cogen" research project) that is acknowledged for providing data on the LP combustor.

The author's researches in the micro-gas turbine field have been supported by the Italian Government within a research project on the dynamics of energy conversion systems (*PRIN 2002*).

## **REFERENCES**

- [1] Jeong Jung Yoon and Heon Seok Lee, 2004, "The study on development of low nox combustor with lean burn characteristics for 20kW class microturbine", ASME paper GT2004-53200.
- [2] Satoshi Dodo, Tomoaki Inoue, Masaya Ichinose, Manabu Yagi, Kuniyoshi Tsubouchi, Kazuyuki Yamaguchi, Yasushi Hayasaka, 2004, "Development of an advanced microturbine system using humid air turbine cycle", ASME paper GT2004-54337.
- [3] O. Ibrahim, P. Zimmermann, C. Hirsch\*, T. Sattelmayer, B. Gerhard, C. Steinbach, 2004, "A microturbine operating with variable heat output", ASME paper GT2004-53011.
- [4] Andrei Colibaba-Evulet, Michael J. Bowman, Anthony R. Brand, 2004, "Design and evaluation of the AIMS combustor", ASME paper GT2004-53150.
- [5] Tsutomu Wakabayashi, Koji Moriya, Shonosuke Koga et al., 2004, "Performance of A Dry Low NOx Gas Turbine Combustor With An Improved Innovative Fuel Supply Concept", ASME paper GT2004-53338.

- [6] Joao Parente, Giulio Mori, Viatcheslav V. Anisimov, Giulio Croce, 2004, “Micro Gas Turbine Combustion Chamber Design and CFD Analysis”, ASME paper GT2004-54247.
- [7] Yoichiro Ohkubo, Osamu Azegami, Hoshinori Idota, Hiroshi Sato, Shinichiro Higuchi, 2001, “Development of Dry Low-NO<sub>x</sub> Combustor for 300 Kw Class Gas Turbine Applied to Co-Generation Systems”, ASME paper 2001-GT-0083.
- [8] Dieter Bohn, Joachim Lepers, 2003, “Effects of Biogas Combustion on the Operation Characteristics and Pollutant Emissions of a Micro Gas Turbine”, ASME paper GT2003-38767.
- [9] M.C. Mkpadi, G.E. Andrews, I. Khan, M.N. Mohd Jaafar, M. Pourkashanian and Y. Yang, 2001, “Lean/Lean Staged Low NO<sub>x</sub> Combustion for Near Stoichiometric Gas Turbine Primary Zone Conditions”, ASME paper GT-0082.
- [10] Tsutomu Wakabayashi, Seiichi Ito, Shonosuke Koga, Masamichi Ippommatsu, Koji Moriya, Kazuo Shimodaira, Yoji Kurosawa, Kazuo Suzuki, 2001, “Performance of a Dry Low-NO<sub>x</sub> Gas Turbine Combustor Designed with a New Fuel Supply Concept”, ASME paper GT-0050.
- [11] Ruud L.G.M. Eggels, Christopher T. Brown, 2001, “Comparison of Numerical and Experimental Results of a Premixed DLE Gas Turbine Combustor”, ASME paper GT-0065.
- [12] O. Liedtke, A. Schulz, and S. Wittig, 2003, “Emission Performance of a Micro Gas Turbine LPP-Combustor with Fuel Film Evaporation”, ASME paper GT2003-38697.
- [13] Sato, H., Amano, T., Iiyama, Y., Mori, M., and Nakamura, T., 1999, “Development of a Three-Stage Low Emissions Combustor for Industrial Small-Size Gas Turbines,” ASME paper 99-GT-236.
- [14] Smith, K.O., Holsapple, A.C., Mak, H.K., and Watkins, L., 1991, “Development of a Natural Gas Fired, Ultra-Low NO<sub>x</sub> Can Combustor for 800 kW Gas Turbine Engines,” ASME 91-GT-303.
- [15] Solt, J.C., and Tuzson, J., 1993, “Status of Low NO<sub>x</sub> Combustor Development,” ASME 93-GT-270.
- [16] V.M. Phi, J.L. Mauzey, V.G. McDonell and G.S. Samuelsen, 2004, “Fuel Injection and Emissions Characteristics of a Commercial Microturbine Generator”, ASME paper GT-2004-54039.
- [17] Steele, R.C., Jarrett, A.C., Malte, P.C., Tonouchi, J.H., and Nicol, D.G. (1997), “Variables Affecting NO<sub>x</sub> Formation in Lean-Premixed Combustion,” *Journal of Engineering for Gas Turbines and Power*, Vol. 119. pp. 102-107.
- [18] Quang-Viet Nguyen, 2002, “Measurements of Equivalence Ratio Fluctuations in a Lean Premixed Prevaporized (LPP) Combustor and its Correlation to Combustion Instability”, GT-2002-30060.
- [19] O. Liedtke, A. Schulz, and S. Wittig, 2002, “Design Study of a Lean Premixed Prevaporized Counter Flow Combustor for a Micro Gas Turbine”, GT-2002-30074.
- [20] Dutta, P., Gore, J.P., and Sojka, P.E., 1997, “Emissions Characteristics of Liquid-Fueled Pilot Stabilized Lean Premixed Flames in a Tubular Premixer-Combustor”, ASME Journal of Engineer for Gas Turbine and Power, Vol. 199, pp. 585-590.
- [21] Lee, J.C.Y., Malte, P.C., and Benjamin, M.A., “Low NO<sub>x</sub> Combustor for Liquid Fuels: Atmospheric Pressure Experiments using a Staged Prevaporizer- Premixer”, ASME 2001-GT-81.

- [22] C.M. Spadaccini, J. Lee, S. Lukachko, I.A. Waitz, A. Mehra, X. Zhang, 2002, "High Power Density Silicon Combustion Systems for Micro Gas Turbine Engines", ASME paper 2002-GT-30082.
- [23] G. Riccio, P. Adami, F. Martelli, D. Cecchini, L. Carrai, 2002, "Improvement of Gas Turbine Injection Systems by Combined Experimental/Numerical Approach", ASME paper GT-2002-30101.
- [24] Hitoshi SHIOTANI, Toshimi TAKAGI, Tatsuyuki OKAMOTO, Shinichi KINOSHITA and Hironobu, 2002, "Teraoka Construction of Low Nox and High Stability Flames Aiming at Micro Gas Turbine Combustion", ASME paper GT-2002-30463.
- [25] Jeffery A. Lovett and Kevin T. Uznanski, 2002, "Prediction of Combustion Dynamics in a Staged Premixed Combustor", ASME paper GT-2002-30646.
- [26] Lefebvre, A.H., 2000, "Gas Turbine Combustion", ed. Taylor & Francis.
- [27] Peters, N., 2000, "Turbulent Combustion", Cambridge University Press.
- [28] Shuji Tanaka<sup>1</sup>, Takashi Yamada<sup>1</sup>, Shinya Sugimoto<sup>1</sup>, Jing-Feng Li<sup>2,4</sup> and Masayoshi Esashi<sup>3</sup>, 2003, "Silicon nitride ceramic-based two-dimensional microcombustor", in *Journal of Micromechanics and Microengineering*, Vol. 13, pp. 502-508.
- [29] Bozza, F., Cameretti, M.C., Tuccillo, R., "Performance Prediction and Combustion Modelling of Low-CO<sub>2</sub> Emission Gas Turbines", *ASME paper no.* 2001-GT-0066.
- [30] Bozza, F., Fontana, G., and Tuccillo R., 1994, "Performance and Emission Levels in Gas Turbine Power Plants," *ASME Transactions - Journal of Engineering for Gas Turbines and Power*, Vol. 116, pp. 53-62.
- [31] Bozza, F., Cameretti, M.C., Marro, A., and Tuccillo, R., 2000, "Performance and emission analysis of a variable load operated gas turbine," in *Advanced Energy Systems*, Vol. 40, pp. 400-415, ed. ASME.
- [32] Bozza F., Rizzo G., and Tuccillo R., 1998, "Identification of a Model for Monitoring Nitric Oxide Emissions in a Gas Turbine Power Plant," in "*Theory and Practice of Control and Systems*", World Scientific Publishing Ltd. London UK, pp. 437-442, ISBN 981-02-3668-9.
- [33] Mc Bride, B.J., and Gordon, S., 1994, "Computer Program for Calculation of Complex Equilibrium Composition and Applications", *NASA RP* 1311, parts I and II.
- [34] Tolpadi, Anil K., Prakash, C., Hura, H., and Mongia, H.C., 1998," Advanced Combustion Code: Overall Description Prediction of a Jet diffusion Flame and Combustor Flowfields," *ASME paper* 98-GT-229.
- [35] Price, G.R., Botros, K.K., and Goldin, G.M., 2000, "CFD Predictions and Field Measurements from LM1600 Gas Turbine during Part Load Operation," *ASME paper* 2000-GT-350.
- [36] Hirt, C.W., Amsden, A.A., Cook, J.L., 1974, "An Arbitrary Lagrangian-Eulerian Computing Method for All Flow Speed", *Journal of Computational Physics* 14, 227-253.
- [37] Amsden A.A., 1997, "KIVA-III v: Block structure KIVA program Engine with vertical or canted valves", *LA – Los Angeles* 13313 – MS, Los Alamos.

- [38] Nicol, G.D., Malte, P.C., Hamer, A.J., Roby, R.J., and Steele, R.C., 1998, "A Five-Step Global Methane Oxidation – NO Formation Mechanism for Lean Premixed Gas Turbine Combustion," *ASME paper* 98-GT-185.
- [39] Miller, J.A., and Bowman C.T., 1989, in *Prog. in Energy and Combustion Science* 15:287.
- [40] Magnussen, B.F. and Hjertager, B.H., 1977, "On Mathematical Modeling of Turbulent Combustion with Special Emphasis on Soot Formation," 16<sup>th</sup>. *Symposium on Combustion, The Combustion Institute*, Pittsburgh.
- [41] Zel'dovich, Y.B., Sadovnikov, P.Y., Frank-Kamenetskik, D.A., 1947, "Oxidation of Nitrogen in Combustion," *Academy of Science of SR, Institute of Chemical Physics*, Moscow-Leningrad.
- [42] Crocker, D.S., Nickolaus, D., and Smith, C.E., 1998, "CFD Modeling of a Gas Turbine Combustor from Compressor Exit to Turbine Inlet," *ASME paper* 98-GT-184.
- [43] McGuirk, J.J., and Spencer, A., 2000, "Coupled and Uncoupled CFD Prediction of the Characteristics of Jets from Combustor Air Admission Ports," *ASME paper no.* 2000-GT-0125.
- [44] Roy, C.J., Moran, A.J., and Thomas, G.O., "Autoignition Characteristics of Gaseous Fuels at Representative Gas Turbine Conditions", *ASME paper no.* 2001-GT-0051.
- [45] Malecki, R.E., et al., "Application of an Advanced CFD-Based Analysis System to the PW6000 Combustor to Optimize Exit Temperature Distribution. Part A", *ASME paper no.* 2001-GT-0062.
- [46] Snyder, T.S., et al., "Application of an Advanced CFD-Based Analysis System to the PW6000 Combustor to Optimize Exit Temperature Distribution. Part B", *ASME paper no.* 2001-GT-0063.
- [47] Eggels, R.L.G.M., "Modelling of NO<sub>x</sub> Formation of a Premixed DLE Gas Turbine Combustor", *ASME paper no.* 2001-GT-0069.
- [48] Mc Bride, B.J., and Gordon, S., 1994, "Computer Program for Calculation of Complex Equilibrium Composition and Applications", *NASA RP* 1311, parts I and II.
- [49] Fantozzi, F., Di Maria, F., Desideri, U., 2002, "Integrated Micro-Turbine and Rotary-Kiln Pyrolysis System as a Waste to Energy Solution for a Small Town in Central Italy – Cost Positioning and Global Warming Assessment –", *ASME paper no.* GT-2002-30652.
- [50] Diers, O., Koopman, J., Fischer, M., Hassa, C., 2001, "Investigation of two advanced cooling mixing concepts for a rich quench lean combustor", *ASME paper* GT-2001-0085.
- [51] Anacleto, P., Heitor, M.V., Moreira, L.N., 1996, "The mean and turbulent flowfields in a model RQL gas-turbine combustor", *Experiments in Fluids* 22(1996) 153-164.
- [52] Spadaccini, L.J., and TeVelde, L.J., 1982, "Autoignition Characteristics of Aircraft Type Fuels", *Comb. & Flame*, 46:283-300.
- [53] Li, S.C. and Williams, F.A., 2000, "Reaction Mechanism for Methane Ignition", *ASME paper no.* 2000-GT-145.
- [54] Bozza, F., Cameretti, M.C., Tuccillo, R., 2002, "The Employment of Hydrogenated Fuels from Natural Gas Reforming: Gas Turbine and Combustion Analysis" *ASME paper* GT-2002-30414, in *ASME Jrnl. of Engineering for Gas Turbines and Power*, Jan. 2004.

- [55] Bozza, F., Cameretti, M.C., and Tuccillo, R., 2003, “Adapting the Micro-Gas Turbine Operation to Variable Thermal and Electrical Requirements”, *ASME paper* GT 2003-GT-38652, to be published in *ASME Transactions*.
- [56] Cameretti M.C., and Tuccillo R., 2000, “Three-Dimensional Mixture Formation Modeling for Liquid Fuel Spray in a Gas Turbine Combustor”, proc. of 16<sup>th</sup>. *ILASS Europe Conference*, pp. IV.3.I – IV.3.VI, ed. Technical University of Darmstadt.
- [57] Croce, G., Mori G., and Parente, J., 2003, “Assessment of traditional and flamelets models for micro turbine combustion chamber optimisation”, *ASME paper* GT-2003-38385.
- [58] Cameretti, M.C., and Tuccillo, R., 2004, “Comparing Different Solutions for the Micro-GasTurbine Combustor”, *ASME paper* GT 2004-GT-53286.
- [59] Bozza, F., and Tuccillo, R., 2004, “Transient Operation Analysis of a Cogenerating Micro-Gas Turbine”, *ASME paper* ESDA-2004-58079.
- [60] Davison, C.R., Birk, A.M., 2004, “Steady State and Transient Modeling of a Micro-Turbine with Comparison to Operating Engine”, *ASME paper* GT-2004-53378.
- [61] Turrell, M.D., Stopfod, P.J., Syed, K.J., Buchanan, E., 2004, “CFD Simulation of the Flow Within and Downstream of a High-Swirl Lean Premixed Gas Turbine Combustor”, *ASME paper* GT-2004-53112.
- [62] Duwig, C., Fuchs, L., 2004, “Study of a Gas Turbine Combustion Chamber: Influence of the Mixing on the Flame Dynamics”, *ASME paper* GT-2004-53276.
- [63] Koutsenko, I.G., Onegin, S.F., Sipatov, A.M., 2004, “Application of CFD-Based Analysis Technique for Design and Optimization of Gas Turbine Combustors”, *ASME paper* GT-2004-53398.
- [64] Mongia, C., Held, T., Hsiao, G., Pandalai, R., 2003, “Challenges and Progress in Controlling Dynamics in Gas Turbine Combustors”, *Journal of Propulsion and Power*, Vol. 19, No. 5, 2003, pp. 822-829.
- [65] Shuji Tanaka<sup>1</sup>, Takashi Yamada, Shinya Sugimoto, Jing-Feng Li, and Masayoshi Esashi, 2003, “Silicon nitride ceramic-based two-dimensional microcombustor”, in *J. Micromech. Microeng.* **13** (2003) 502–508.
- [66] ZWLi<sup>1</sup>, S.K. Chou, C. Shu and W.M. Yang, 2005, “Effects of step height on wall temperature of a microcombustor”, in *J. Micromech. Microeng.* **15** (2005) 207-212.
- [67] T.J. Rosfjord and F.C. Padget, 2001, “Experimental Assessment of the Emissions Control Potential of a Rich/Quench/Lean Combustor for High Speed Civil Transport”, *NASA/CR – 2001-210613*.
- [68] Clarence T. Chang and James D. Holdeman, 2001, “Low Emissions RQL Flametube Combustor Test Results”, *NASA/TM – 2001-211107*.
- [69] Robert R. Tacina, Changlie Wey, and Kyung J. Choi, 2001, “Flame Tube NOx Emissions Using a Lean-Direct-Wall-Injection Combustor Concept”, *NASA/TM – 2001-211105 AIAA–2001–3271*.
- [70] Christopher O. Peterson, William A. Sowa, and G.S. Samuelsen, 2002, “Performance of a Model Rich Burn-Quick Mix-Lean Burn Combustor at Elevated Temperature and Pressure”, *NASA/CR – 2002-211992*.

- [71] V.G. McDonell and G.S. Samuelsen, 2000, “Measurement of fuel mixing and transport processes in gas turbine combustion”, in Meas. Sci. Technol. **11** (2000) 870–886.
- [72] Christopher Stone and Suresh Menon<sup>1</sup>, 2003, “Open-loop control of combustion instabilities in a model gas turbine combustor”, in Journal of Turbulence, March 2003.
- [73] Tuccillo, R., 2005, “Performance and Transient Behaviour of MGT based Energy Systems” in VKI LS on “Micro Gas Turbines”, March 2005.